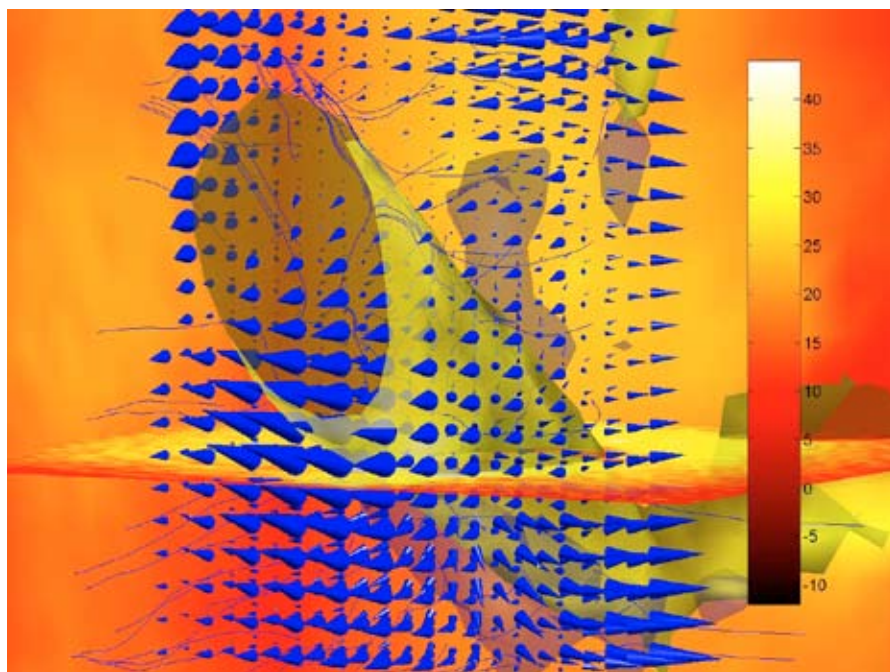


Analysis of drying wood based on nondestructive measurements and numerical tools



Jonas Danvind

Luleå University of Technology
Department of Skellefteå Campus, Division of Wood Technology

Analysis of drying wood based on nondestructive measurements and numerical tools

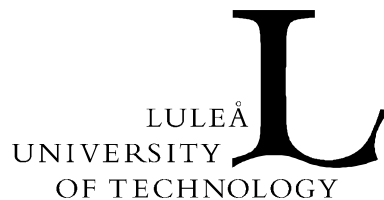
Jonas Danvind



Valutec AB

P.O. Box 709, SE-931 27 Skellefteå, Sweden

E-mail: jonas.danvind@valutec.se



Luleå University of Technology

Skellefteå Campus

Division of Wood Technology

Skeria 3, SE-931 87 Skellefteå, Sweden

2005

Cover page: Calculated three-dimensional moisture flux around a knot. The flux was assumed to be governed by Fick's laws, and the calculations were based on moisture content and strain measurement methods developed in this thesis. The scale on the right is moisture content in %. The same knot was studied in Paper III in this thesis.

ABSTRACT

Improved understanding of moisture and mechanical behaviour is a general objective for wood drying research. The main objective of this doctoral thesis was to develop nondestructive experimental methods suitable for collecting valuable response data related to the moisture behaviour and mechanical behaviour of drying wood and to refine this information into modelling parameters.

A method for simultaneous noncontact measurement of two-dimensional surface deformations and interior densities was developed. This was done using Digital Speckle Photography (DSP) and X-ray Computed Tomography (CT). Displacements and densities were used for calculation of strain and of moisture content. Experimental tests of the measurement method were done on cross sections of Scots pine. The following accuracy was stated for different properties:

- A typical calculated displacement error of approximately 10 μm was found.
- Strains derived from the displacements had a maximal error of 1.11 mstrain.
- Moisture content measuring accuracy was estimated to $\pm 1.8\%$ moisture content at a significance level of 0.05 in a measuring volume with the approximate size $2 \times 2 \times 1.5 \text{ mm}^3$.

A similar noncontact technique based only on X-ray CT scanning was developed. Displacements were then estimated from boundary movements of an object in CT images. The estimated standard deviation of the measured moisture content error for this method was 0.04% moisture content. The mean error was unknown.

Two different approaches to determining moisture diffusion coefficients from the studied data were presented. The first was based on minimizing the difference between measured and computed values through an optimization scheme. This approach required an initial assumption of the functional form of the diffusion coefficient. The second approach calculated diffusion and mass transfer coefficients through direct finite difference calculations on measured moisture content data. Results on Norway spruce showed interesting local variations of the diffusion coefficient, especially near the evaporation surface. Comparisons between measured and FEM simulated data showed good results.

An example showed that a multivariate method of analysis could be an effective and easy-to-use tool for untangling relationships between variables and for generating information from data.

Finally, it could be stated that the methods presented will be of use to improve the understanding of the behaviour of drying wood, with the focus on moisture and mechanical properties.

Keywords: wood, drying, nondestructive measurements, x-ray computed tomography, speckle photography, displacement, strain, density, moisture content, diffusion, mass transfer, FEM, multivariate, PLS

PREFACE

I realised during my Master's Thesis work, at Forest Research in New Zealand, the importance of good fundamental information for materials modelling. The aim of the work at that time was to measure as many parameters as possible for wood deformation modelling based on the parameters used in the licentiate thesis of Sigurdur Ormarsson, Chalmers University, Sweden. I soon understood that many parameters were needed due to the complexity of wood. Later I also discovered the complexity of measuring them. The success was not great; quite good measuring of shrinkage and deformation of small wood sample pieces, but very poor results on measuring longitudinal Modulus of Elasticity and Poisson's ratios. I had learnt what so many already knew: wood is a material with a lot of variations and it is not easy to retrieve information from it. This can be summarised by a quotation of the always-helpful Birger Marklund, technician at Luleå University of Technology:

-What have I always said? One should not work with wood.

After my Master's project I started working as an industrial PhD student at the Swedish sawmilling company Grånge Skog & Trä AB in combination with the Division of Wood Technology, Luleå University of Technology. After 18 months I was employed by Valutec AB, a Swedish-Finnish wood drying kiln manufacturer, and continued the same project. I did not hesitate to start the research on "Response analysis of pine and spruce to air convective drying". I knew from earlier experience that this was a challenge, and this thesis that you now hold in your hand is the result thereof.

This work was supported by the wood dry kiln manufacturer *Valutec AB*, the *Swedish Agency for Innovation Systems (Vinnova)* through the *Skewood* research program, the *Swedish Foundation for Strategic Research (SSF)* through the *Wood Technology* research program, *Kempestiftelsen* and the *Swedish Foundation for Technology Transfer*. Up to May 2000 it was also supported by *Grånge Skog & Trä AB*, where I was employed before my present employment at *Valutec AB*.

Many people have contributed to my work over the years. First, I wish to thank my supervisor, Professor Tom Morén, for his engagement in the research and for the will to let me grow as a researcher. I thank my co-authors (in chronological order) Per Synnergren, John Eriksson, Håkan Johansson and Mats Ekevad for valuable co-operation that has improved the quality of the research and of our mutual knowledge. Thanks to my colleagues at the university and in the Wood Technology and Skewood research programmes for valuable discussions, contributions to my work and friendship. Thanks to Brian Reedy for proofreading some of the text in this thesis. Thanks to my colleagues at Valutec and my former colleagues at Grånge Skog & Trä for focusing my mind on other things than research and seeing industrial applications of research. Special thanks go to the

owners and management of Valutec, who have supported this research. I also wish to thank family and friends for supporting me in my work and making my spare time full of experiences.

Skellefteå, August 12, 2005

A handwritten signature in black ink, reading "Jonas Danvind". The script is cursive and fluid, with the first letter 'J' being particularly large and stylized.

Jonas Danvind

LIST OF PAPERS

This thesis is based on work in the following papers, referred to by roman numerals:

- I. Danvind, J.; Synnergren, P. 2001. Method for measuring Shrinkage Behaviour of Drying wood using Digital Speckle Photography and X-ray Computerised Tomography. In: Proceedings of 7th International IUFRO Wood-drying Conference. July 9–13, 2001, Tsukuba, Japan. pp 276–281
- II. Danvind, J. 2002. Measuring strain and moisture content in a cross section of drying wood using Digital Speckle Photography and Computerised X-ray tomography. In: Proceedings of 13th International Symposium on Nondestructive Testing of Wood. 19–21 August 2002, Berkley, California, USA.
- III. Danvind, J.; Morén, T. 2004. Using X-ray CT-scanning for moisture and displacement measurements in knots and their surroundings. In: Proceedings of EU COST 15 Wood-Drying Conference. April 22–23, 2004, Athens, Greece.
- IV. Danvind, J.; Eriksson, J.; Johansson, H. 2004. Calibration of a constitutive model for diffusive moisture transport in wood using data from X-ray CT-scanning and Digital Speckle Photography. In: Proceedings of EU COST 15 Wood-Drying Conference. April 22–23, 2004, Athens, Greece.
- V. Danvind, J.; Ekevad, M. 2005. Local water vapour diffusion coefficient when drying Norway spruce sapwood. Accepted for publication in Journal of Wood Science.
- VI. Danvind, J. 2002. PLS prediction as a tool for modelling wood properties. Holz als Roh- und Werkstoff 60:130–140

TABLE OF CONTENTS

ABSTRACT	I
PREFACE	III
LIST OF PAPERS	V
TABLE OF CONTENTS	VII
1 INTRODUCTION	1
2 MATERIAL AND METHODS	6
2.1 MATERIAL	6
2.2 METHODS	8
2.2.1 X-RAY COMPUTED TOMOGRAPHY	8
2.2.2 DIGITAL SPECKLE PHOTOGRAPHY, MEASUREMENT OF DISPLACEMENT	9
2.2.3 DISPLACEMENT CALCULATIONS, ESTIMATION OF DISPLACEMENT	11
2.2.4 EXPERIMENTAL EQUIPMENT	12
2.2.5 COMBINATION OF X-RAY CT AND DSP FOR MEASUREMENT OF DENSITY, DISPLACEMENT, STRAIN AND MOISTURE CONTENT	13
2.2.6 COMBINATION OF X-RAY CT AND DISPLACEMENT CALCULATIONS FOR MEASUREMENT OF DENSITY, DISPLACEMENT, STRAIN AND MOISTURE CONTENT	14
2.2.7 MULTIVARIATE STATISTICS	15
2.2.8 DIFFUSION THEORY	17
2.2.9 SURFACE MASS TRANSFER	18
2.2.10 METHODS FOR ESTIMATION OF DIFFUSION COEFFICIENTS	18
3 RESULTS	20
4 DISCUSSION	25
5 FUTURE RESEARCH	28
6 CONCLUSIONS	29
7 REFERENCES	30

1 INTRODUCTION

In the research field of Wood Physics, the branch related to the drying of sawn timber is of great importance. This is due to the significant values that are generated by drying wood to moisture content levels and other drying responses appropriate to the end user's needs. There are also costs related to the drying of wood, such as the energy that is needed to evaporate water and the quality loss costs caused by drying defects. Many factors influence drying results, all the way from the forest to the end customer who uses the manufactured wood product. In order to achieve the best drying results, one has to control all the steps. For example, cracks in sawn timber can be caused by such different sources as the harvester of the trees, too long storage of logs or sawn timber prior to artificial drying, unfavourable sawing pattern, inappropriate artificial drying, severe material characteristics, and so on. The wood drying group of the International Union of Forest Research Organisations, IUFRO, arranges an international conference every second year focused on different aspects of artificial wood drying. During the first conference, which was held in Skellefteå in 1987, some ideas for future work in the research field of wood drying were stated (Söderström 1996):

- I. Develop a better understanding of moisture movement.
- II. Provide more information on mechanical behaviour properties, especially mechanosorptive creep.
- III. Optimize drying schedules to obtain minimal degradation.
- IV. Establish techniques for continuous monitoring of moisture content and stress development in the kiln.
- V. Put the technology already developed into practice.
- VI. Standards of wood drying quality.

Over the years, a lot of work has been put into these topics in the form of experimental tests, modelling of responses, development of new drying, measuring and control techniques, and so on. In Scandinavia, the dominant artificial drying technique is air convective drying of Norway spruce and Scots pine, which has also been the interest of this thesis.

In order to develop a better understanding of moisture movement (point I), there is a need for good experimental information on moisture behaviour during drying. Then this information can be studied using qualitative and/or quantitative analysis; for example, by inspecting moisture information using common sense to reveal relationships, or by deriving modelling parameters based on already existing fundamental assumptions, or by a combination of both. In many studies the moisture information during drying is acquired through destructive testing wherein samples are cut into smaller pieces and the moisture content is determined by weighing and drying. At the division of Wood Technology at Luleå University of Technology there is a medical X-ray Computed Tomography (CT)

scanner, Siemens Somatom AR.T. In the wood science field, this type of equipment can be used for nondestructive evaluation of, primarily, density. Wood density information reconstructed from X-ray CT scanning can be used in many ways in research, and examples are presented by several authors (Ekevad 2004; Nordmark & Oja 2004; Sepúlveda et al. 2002; and Chiorescu & Grönlund 2000). Lindgren (1992) presents methods for deriving density and moisture content data from X-ray CT data. When retrieving moisture content based on density data, small wood regions within CT images prior to and after drying are compared in order to calculate the mass differences within the wood. To be able to compare the same regions, it is important to know how they are displaced and deformed during drying. For estimating the displacement and deformation of wood in CT images, different image-analysis methods have been presented (Lindgren et al. 1992; Lindgren & Lundqvist 2000; and Danvind & Morén 2004). Another way is to assume linear volume shrinkage and calculate moisture content based on the measured density and a calibrated oven-dry density. By using two linear relations between density and moisture content, one below fibre saturation point (FSP) and one above, the moisture content in a local image region can be estimated (Lindgren 1992) if the local oven-dry density is known. Due to the latter requirement, there is a need for calibration of local oven-dry density, and if that is done in a CT image captured later in the drying sequence than the one where the moisture content is to be determined, then the displacements and deformations of evaluation regions also have to be known. Hence for this method also it is important to know the local displacements for acquiring local moisture content. However, the larger the evaluation regions are, the smaller are the inaccuracies due to displacement errors. Also, if the studies are made on wood above FSP, then the deformation of the wood is less, and thus the moisture content errors are smaller. Often when qualitative analyses of moisture are of interest, it is sufficient to study the changes in density without deriving moisture content, as done by Fromm et al. (2001) and Wiberg and Morén (1999).

A common way to provide experimental moisture and mechanically coupled data on wood (points I and II above) is to do one-dimensional loading tests in a temperature- and humidity-controlled environment (see Håkansson (1998), Svensson (1997) and Hanhijärvi (1995)). Also two-dimensional mechanical properties can be acquired by measuring two-dimensional strains on specimens under one-dimensional loading as done by Jernkvist and Thuvander (2001), who measured elastic and shear modulus within the annual ring of a wood sample. They used a digital image correlation technique called Digital Speckle Photography (DSP) to measure two-dimensional displacement fields. However, they did not control the environment of the experiment. The DSP algorithm they used was developed by the Division of Experimental Mechanics at Luleå University of Technology (Sjödahl 1995), and it was also used in this work for displacement measurements. Another example in which a digital image correlation technique is applied to wood is presented by Choi et al. (1991). Thanks to the development of computational capacity, the DSP method can quickly measure displacement by the use of computers. Earlier, this types of image correlation demanded many more hands-on operations, such as the method used by Benckert (1992).

The work presented in this thesis has partly focused on finding good methods for determining local displacements in CT images in order to derive local moisture content and strain data, which can contribute to an improved understanding of moisture movement and strain behaviour in drying wood (points I and II above). For this purpose,

a method for simultaneous measurement of two-dimensional strain fields and moisture content distribution in a cross section of a drying wooden board was developed. The method is partly based on the Computed Tomography (CT) scanning technique, which Wiberg (1996) used earlier, and on the surrounding equipment that he used in order to create a drying environment. The displacements from which the strain fields were derived were measured using the DSP technique mentioned above (see papers I and II). When using the DSP technique for surface measurement of displacements, the region that was studied with CT scanning had to be near the sample's surface, since measured surface displacements were assumed to agree with the displacement in the CT image. Hence, the measurements were restricted to one cross section, i.e., two-dimensional measurement, and the end surfaces had to be sealed thoroughly. The latter proved difficult (see paper IV). In order to estimate displacements in scans further away from the end surfaces of the scanned piece and to perform three-dimensional analyses of moisture content, a method for estimating displacements in the CT images was developed (paper III). This is a similar approach to the one used by Lindgren et al. (1992) and Lindgren and Lundqvist (2000), but there are some differences that will be further discussed in the method section.

A quantitative way to develop better understanding of wood, based on experimental data, is to do material modelling and fit the results to the measured data. Here, this approach has been used to study the diffusion of moisture below fibre saturation point (FSP). Many researchers studied this problem over the years; for example, Rosenkilde and Arfvidsson (1997), Simpson and Liu (1997), Hukka (1999) and Koc et al. (2003). It is well accepted that moisture movement below FSP is governed by diffusion. This means that moisture flow is negatively proportional to the spatial moisture content gradient, through the diffusion coefficient, often called D , according to Fick's law (refer to paper V). In this work, D was solved by inverse finite difference methods in two ways (paper V) and by a more sophisticated, so-called inverse Finite Element Modelling method (paper IV). Also the mass transfer coefficients, β , at the surface were estimated (paper V). The estimations of D and β in this work were not extensive studies in different external drying conditions using varying wood sample sizes and different wood species. Hence, this is more a presentation of different methods for deriving these moisture-modelling parameters below FSP.

During the last decade there have been some major improvements in the understanding of moisture movement in the capillary regime of drying, i.e., above FSP. These improvements have also lead to improvements in industrial drying. Morén (2001), Larsson and Morén (2003) and Larsson and Morén (2004) describe a technique for rapid industrial drying of Norway spruce sapwood, in particular, based on an assumption of high moisture flow in the capillary regime, which was experimentally verified by Wiberg et al. (2000). The drying technique is adaptive to the moisture state in the capillary regime of drying wood through measurement of the temperature drop across the wood load, and it was implemented in an industrial control system developed by Valutec AB (2005) in 1995. Wiberg and Morén's (1999) experimental studies show that the water flow in wood well above the FSP, i.e., in the capillary regime, does not have a diffusion-controlled behaviour, which often has been applied in wood drying. The findings (Wiberg et al. 2000) show that the evaporation of water in the capillary regime is controlled by the transferred heat to the evaporation front. This is an example of how points I, III and V above have been applied at Luleå University of Technology in Skellefteå.

Wiberg and Morén (1999) and Wiberg et al. (2000) also study the behaviour of the evaporation front that recedes just below the wood surface until the so-called irreducible saturation (IS) point is reached. At IS the capillary communication between pores is assumed to break, and the expression has long been used in the drying of porous media, for example, by Norman (1970). Due to the resolution of the CT scanner used (Wiberg & Morén 1999 and Wiberg et al., 2000) for studying the evaporation front, its accuracy could be questioned. Rosenkilde and Glover (2002) measured surface moisture content data in the outer “dry shell” of wood using Magnetic Resonance Imaging (MRI), with a better spatial resolution. They also find the “evaporation front” behaviour. However, their measurements were almost too detailed, and Rosenkilde et al. (2004) suggest using MRI at a lower spatial resolution to be able to follow the evaporation front further into the material than 500 μm . This matter of surface heat and mass transfer has been the subject of many discussions in the wood drying field, since the mass transfer is higher theoretically than what is found experimentally. Often this is compensated for by using a correction factor as done by, for example, Hukka (1999). The experimental information on drying behaviour near the wood surface has other consequences for the material description in modelling, where partly new modelling approaches are needed. Salin (2002) describes an example of this based on experimental work by Wiberg et al. (2000). In the work presented here, the moisture content variations in the surface layer have not been studied, since they were assumed to be on the limit of the measuring accuracy for moisture content using the measuring methods presented here. The edge filtering problems of the CT reconstruction algorithm are one reason for lower accuracy near to an object’s edges in a CT image. However, the methods developed here can be of use in higher resolution scanning techniques for this kind of surface moisture measurement.

Wood material modelling has today become accepted in many applications of wood utilization both in research and in industry. Today there are two Swedish commercial wood drying simulation tools available on the market, ValuSim from Valutec AB and Torksim from SP Träteck. These models are based on modelling of moisture and stress in Scots pine (*Pinus sylvestris*) and Norway spruce (*Picea abies*), depending on interior and exterior parameters. The latter are temperature, humidity and velocity of surrounding air. Both models originate from work done at the Technical Research Centre of Finland, VTT, and have been further developed by the two parties. These tools can be used for training of personnel, generating schedules and online simulation of moisture content and stress. ValuSim is integrated in Valutec’s industrial drying kiln control system. They are good examples of the technology transfer from research to industry, points III and V above. It is not only in Finland and Sweden that the use of industrial simulation tools is increasing. A similar development is taking place on the international level. Thanks to the increase of computational speed, it has become easier to perform large computations. As a consequence, it is possible to set up more advanced wood material descriptions; for example, the three-dimensional Finite Element Model (FEM) presented by Ormarsson (1999). Ormarsson’s model has proven useful in describing how stable structural timber members can be manufactured by splitting and gluing pieces together (Ormarsson et al. 2001). More information on the modelling of wood drying can be found in the comparison of wood drying models by Kamke and Vanek (1994) and the wood drying textbook by Keey et al. (2000).

Wood drying response data can be analysed in a more qualitative way by using multivariate calibration, which developed strongly in the field of chemometrics during the 1970s. Multivariate methods are suitable for finding relationships among many correlated or uncorrelated variables, which is often the case when working with wood. Oja (1999) uses Projection to Latent Structures by means of Partial Least Squares (PLS) to predict properties of logs scanned in a CT scanner. Johansson (2001) calibrates a model on two-dimensional microwave data for simultaneous moisture and density determination in wood. Nyström and Hagman (1999) present how compression wood can be detected by multivariate image analysis on spectral images. The last paper in this thesis shows an example of PLS as a tool for modelling wood properties. It is intended that this method of analysis will be used for future qualitative evaluation of extensive data collected using the measurement methods presented here. This might yield important information on influencing parameters that could be applied in more fundamental physical and mechanical assumptions to be used in quantitative models.

The original objective for this research was to study responses of pine and spruce subjected to air convective drying. This more general objective was later broken down to develop two- and three-dimensional methodologies for estimating displacements and moisture content of drying wood pieces; i.e., to develop methods for the acquisition of response data. Another objective was to develop methods for estimating moisture diffusion coefficients of measured data.

The following chapters describe the CT and DSP methods and the measuring methods whose development was based on them both. Also, a short description of multivariate methods, Principal Component Analysis (PCA) and PLS, and diffusion theory is given. Some results are presented and discussed, and suggestions for further work are made. Six papers are enclosed; the first three describe the experimental methods developed, the following two describe methods for deriving diffusion coefficients from measured data, and the last one presents an example of PLS modelling on wood.

2 MATERIAL AND METHODS

2.1 Material

The purpose with the wood materials that have been tested in papers I, II, III and VI was to test the experimental measuring methods that were developed and to provide an example of a multivariate analytical method. The wood materials tested in papers IV and V were used to test the algorithms for estimating diffusion coefficients.

Samples used for the evaluation of the measurement method in papers I and II were of Scots pine (*Pinus sylvestris*) with the sizes $90 \times 40 \times 18 \text{ mm}^3$ and $150 \times 50 \times 18 \text{ mm}^3$. These samples were end-coated with a varnish, “Celco Golvlack” (no. 10133) from Nordsjö, to prevent longitudinal drying, and then the end surfaces were coated with white high-temperature-resistant spray paint. On the white surface, a randomized speckle pattern was manually applied using black spray paint. During measurement the samples were mounted on a polyamide screw which was securely tightened to a steel fixture.

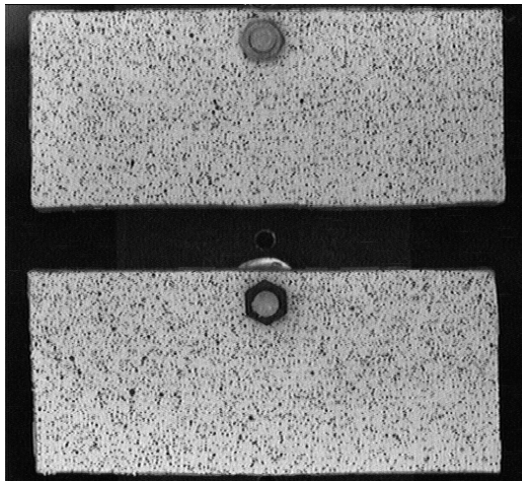


Figure 1. DSP image of two $90 \times 40 \times 18 \text{ mm}^3$ samples.

In the study in paper III, a $54 \times 59 \times 200 \text{ mm}^3$ sample of Scots pine (*Pinus sylvestris*) with several interior defects was dried for 40 hours at the dry and wet temperatures of approximately 50°C and 30°C respectively, and the air speed was approximately 4 m/s. The sample was end-coated using the varnish mentioned above.

In paper IV, five samples were dried simultaneously, but only one Norway spruce (*Picea abies*) sample was used in the presentation. This is the second sample from the top in Figure 2. X-ray CT scanning was used in combination with the DSP method to study radial drying. Therefore, all surfaces except the tangential surfaces were coated with the varnish mentioned above, and the end surfaces were also sprayed with randomized

speckles, as in papers I and II. The studied sample had the approximate size of $130 \times 20 \times 20 \text{ mm}^3$.

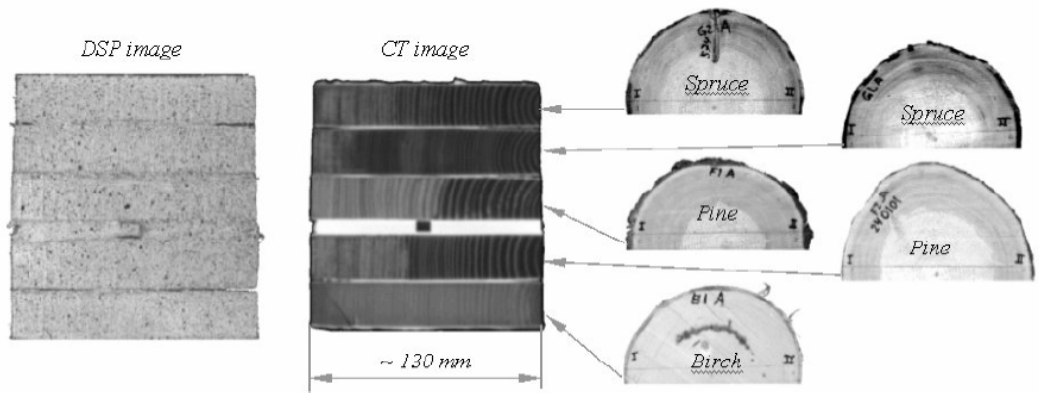


Figure 2. DSP and CT images of samples in paper IV.

In paper V, approximate one-dimensional drying was studied by sealing five surfaces of a Norway spruce (*Picea Abies*) sample using polyurethane glue (Cascol 1809 from Casco) and aluminium foil and then drying it. The coated surfaces were also thermally insulated using Styrofoam. The sample had the green dimensions of $42 \times 31 \times 205 \text{ mm}^3$, in approximately tangential \times radial \times longitudinal direction. During drying, the humidity and temperature of the circulating air were approximately constant at 43% RH and 50°C . The air speed was approximately 4 m/s.

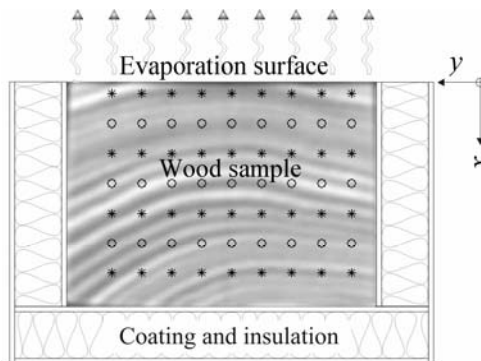


Figure 3. Norway spruce sample studied in paper V.

Tests on several samples with the sizes $20 \times 20 \times 300 \text{ mm}^3$ and $10 \times 10 \times 300 \text{ mm}^3$ from one slab of Radiata pine (*Pinus radiata*) provided data for the prediction modelling in paper VI. These samples were tested in an earlier study done by the author at Forest Research, Rotorua, New Zealand, (refer to Danvind 1999 where the material is described further).

2.2 Methods

Nondestructive Testing (NDT) is preferable when studying the dynamic behaviour of wood. One such example can be taken from wood drying in which several factors interact: the thermal, chemical, moisture and mechanical behaviour of the wood. The two latter have been studied here using a combination of two known nondestructive techniques, namely X-ray CT scanning and DSP, as mentioned earlier. These two techniques are briefly described here, as well as the experimental equipment used and the way the two methods were combined.

Two drawbacks with the DSP technique proved to be the sealing of the end surface and the limitation to two dimensions. Therefore, an alternative displacement estimation to the DSP method was developed, which is called “displacement calculations” here. This method is also described here as well as its combination with X-ray CT scanning.

In paper VI, an example of how a multivariate method can be applied to predict responses in wood is presented. A short description of two multivariate methods is given.

Last in this chapter a brief description of diffusion theory is given. In papers IV and V, diffusion theory is used in methods for estimating diffusion coefficients. These methods are summarised here.

2.2.1 X-ray Computed Tomography

In tomography based on radiation, a series of images is taken of the object under study by sending radiation through the object and receiving it on the other side. The radiation could be, for example, ultrasound, microwaves or x-rays; the last-named was used here. By using a reconstruction algorithm, the different images are put together to form an image of the interior of the object; see for example Cormack (1963), who received the Nobel Prize for his tomography algorithm. Most tomography algorithms are based on a transformation of the received signals into a Fourier series that describes the signal with waves of different frequency and amplitude. The edges of the studied object give a very sharp difference in the received signals and are problematical to describe with Fourier series. Finding edge-filtering techniques for tomography applications has therefore been an important field of research. One example is Shepp-Logan edge filtering (Herman 1980) that was implemented in the equipment used here, which was a Siemens Somatom AR.T medical X-ray CT scanner.



Figure 4. Part of the experimental setup: a digital camera and an X-ray CT scanner.

Different materials and densities absorb the radiation differently. If the constituents, their density and the porosity of the wood being studied are known, the so-called x-ray attenuation coefficients and the CT numbers can be calculated, a process which is further described by Lindgren (1992). CT numbers are strongly correlated to density, and from them a good estimation of the interior density of the object can be achieved. Lindgren (1992) shows that density accuracy in a CT scanner similar to the one used here is ± 2 kg/m³ for dry wood and ± 6 kg/m³ for wet wood with moisture content ranging from 6%–100%. This accuracy is estimated for a $2 \times 2 \times 1.5$ mm³ volume at a significance level of 0.05. The larger the measuring volume is, the more accurate is the density measurement. In the trials done here, larger measuring volumes have been used, and therefore the measurement accuracy is assumed to be slightly better than that stated above. However, a larger measuring volume affects the spatial resolution, which is at best approximately three times the pixel size according to a rule of thumb stated by Lindgren (1992). Due to low spatial resolution, Lindgren (1992) recommends not using this type of medical CT scanner for separating densities within annual rings. The SIEMENS CT scanner used here outputs two-dimensional images with the size 512 x 512 pixels, where the intensity level of each pixel corresponds to the measured density in that measuring volume. The measuring volume, which is also called voxel, is limited by the scan width in the direction perpendicular to the image plane. Scan widths can be 2, 5 or 10 mm thick.

2.2.2 Digital Speckle Photography, measurement of displacement

At the Division of Experimental Mechanics at Luleå University of Technology, research has been done on the development and use of Digital Speckle Photography (DSP) algorithms (Sjödahl 1995; Synnergren 2000; Johnson 1998; and Andersson 2000). Here, cooperation took place with Per Synnergren (see paper I), who made a DSP algorithm coded in C++ available for use in this application.

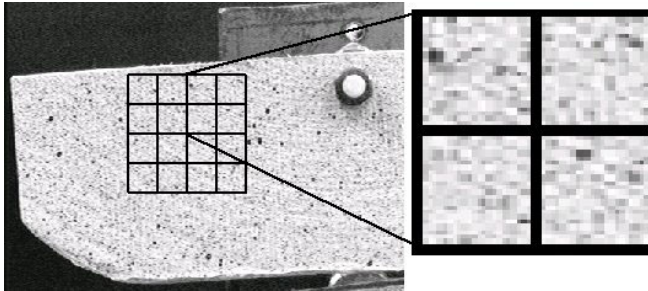


Figure 5. Surface with randomized speckle pattern and 32 x 32 pixels subimage regions.

A simple description of the method can be given by assuming that an image of a surface is captured before deformation. The surface has a randomized speckle pattern that can be artificially applied or be a natural variation in the surface. The surface is divided into so-called subimage regions, where each region has its own identity pattern for later recognition. Then a deformation of the surface takes place, and the subimage regions move and/or become distorted. Now the idea is to find each subimage region in the deformed image by recognizing their patterns using a mathematical cross-correlation algorithm. Each subimage region is a matrix with the same size as its pixel size in the image. For example, a 30 x 30 pixels subimage region corresponds to a 30-rows-by-30-columns matrix. By moving this matrix over the deformed image and calculating the correlation for each position, the position with the highest correlation gives the new position of the subimage region. DSP measurements are dependent on sufficient speckle density, contrast and mean speckle size for good measurement accuracy (see paper I). The DSP algorithm is further described by Sjödahl (1995).

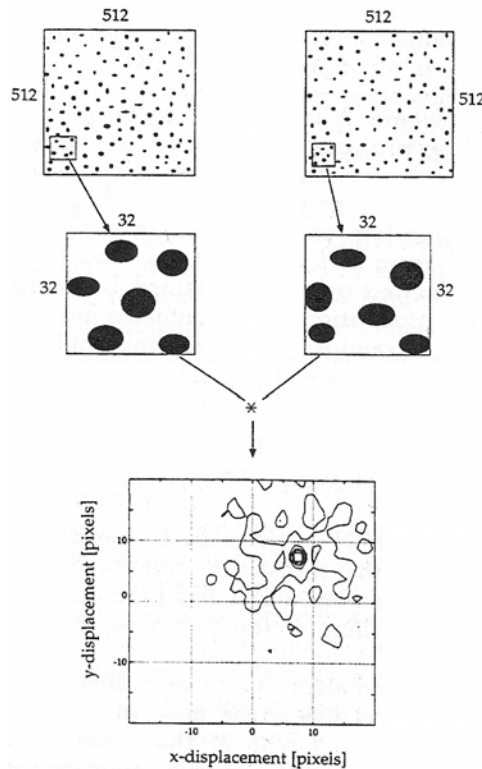


Figure 6. Original figure text: “Figure 6. Principle of the algorithm; * indicates the cross-correlation of two subimages 32 x 32 pixels in size.” (Sjödahl 1995). Published with permission of Mikael Sjödahl, Division of Experimental Mechanics, Luleå University of Technology.

2.2.3 Displacement calculations, estimation of displacement

Since the DSP method described above was limited to measuring displacement at the end surface of the studied sample, a method for estimating displacement in CT images was developed. In theory, DSP could be used on CT images, but here the contrast and density changes of the interior density pattern are too large when wood is dried from the green state. Instead, a method based on the boundary shape of the scanned object was developed. Each CT image was processed into a binary image so that object pixels were set to one and background pixels were set to zero. The relative position of a pixel in the undeformed object was calculated by studying the CT image from four corners. Then the position of that pixel was assumed to be found at the corresponding relative position in the deformed image. This method is unable to measure local interior displacement correctly, since it is based on the object’s boundary shape. The method is presented in paper III.

2.2.4 Experimental equipment

A drying environment was created by circulating air with controlled humidity and temperature through the gantry of the CT scanner using flexible tubing connected to a climate-controlled chamber. The sample being studied was placed inside the gantry mounted on a polyamide screw that was fixed to a rigid steel fixture. A box with glass windows was also made in order to make it possible to capture images of the end surface. DSP images were captured using a digital camera connected to a PC, and CT images were captured at set intervals by a computer connected to the CT scanner. At the beginning of the studies, the images were captured manually, but later this was done automatically. Wiberg (2001) used somewhat similar setup, and he states that temperature could be controlled from -5°C to 115°C and that humidity could be controlled between 15% RH and 98% RH in the temperature range from 25°C to 80°C .

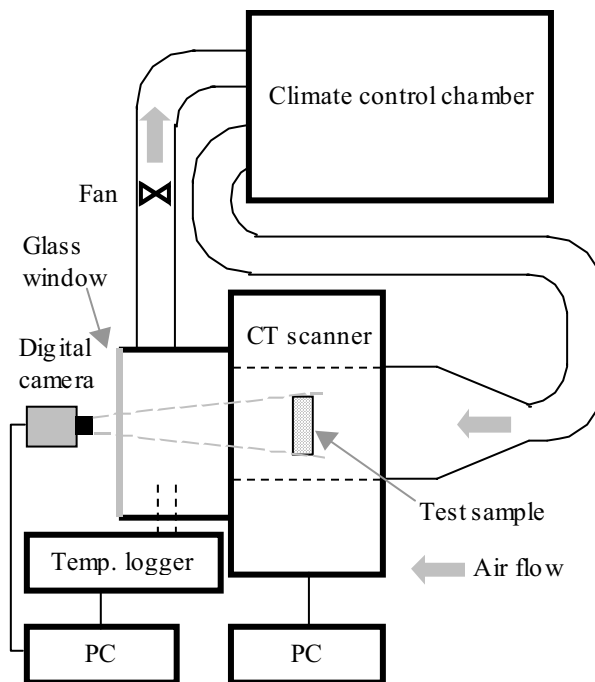


Figure 7. Experimental setup in papers I, II and IV.

2.2.5 Combination of X-ray CT and DSP for measurement of density, displacement, strain and moisture content

As stated in the introduction, it was of interest to combine density and displacement data to provide two-dimensional information on both moisture and mechanical behaviour. When doing this, it is necessary to recognize the same measurement volume during the drying or wetting process. Lindgren et al. (1992) present a method that measures density in CT images and interpolates the deformation using five reference points. However, the deformations are probably more locally orientated than their method can handle, especially when studying “full” drying cycles from green to oven dry. Here the movements of each subimage region were measured with DSP and coupled to the same measurement volume in the corresponding CT images. Lindgren et al. (1992) use their transformation to position pixels from “drier” CT images in “wetter” images, and then they do subtractions to calculate the moisture difference. Since the number of pixels of the object being studied is smaller in the “drier” CT image, there will be missing pixels when it is overlapped onto the “wetter” image. They replace these missing pixels with an average of the neighbouring pixels, which actually will add nonexistent material and thereby result in an underestimation of the moisture difference.

Lindgren and Lundqvist (2000) present an improvement of the transformation used by Lindgren et al. (1992) for which they state the measuring accuracy of moisture content to less than $\pm 1.0\%$ at a 0.05 significance level for measuring regions of $3 \times 3 \text{ mm}^2$. However, this accuracy can be questioned due to the addition of nonexistent material as mentioned above. In this work, the mass and deformation of each subimage region was calculated from the measured densities and displacements. Then masses from different time steps were compared. In this way no extra material was added. From displacements and masses, the strains and moisture contents could be derived.

DSP and CT images contain a lot of information, and it is tedious work to do the necessary operations to derive the resulting parameters. Therefore, several custom-made computer applications were programmed to simplify the procedure. Most of the programming was done in Matlab (Mathworks 2005), and Graphical User Interfaces (GUIs) were set up to make the applications user friendly. In Figure 8 one can see how the different applications are coupled to each other. The way the different applications work is further explained in papers I and II. However, the application of subimages is not explained in any of the papers. In that application, the user can mark a region in which the subimage regions are generated. The subimage can be either square or rectangular, but so far only square regions have been used. It can be of more interest in future use to use rectangular ones when studying behaviour near the surface. All applications that have been programmed in Matlab were developed by the author. The calculation of displacements in C++ was done by Per Synnergren, Division of Experimental Mechanics, Luleå University of Technology.

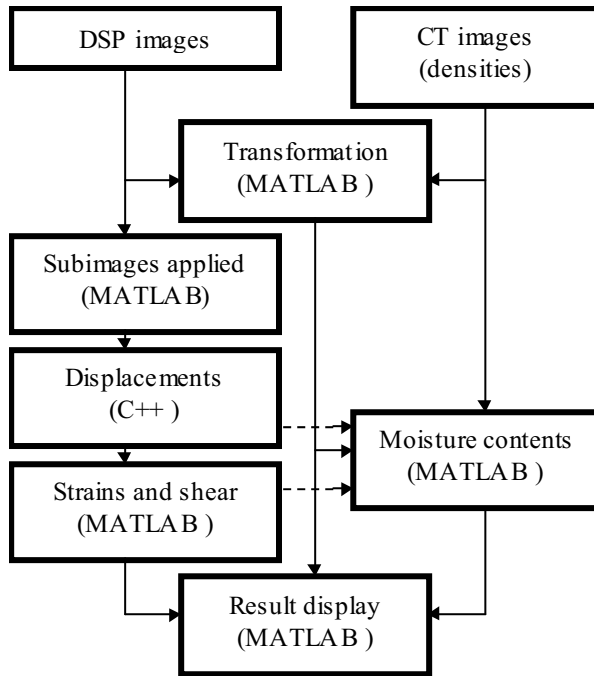


Figure 8. Flow for calculating strain, shear and moisture content distribution from image data in papers II and IV.

It can be seen in Figure 8 that the calculation of moisture content is dependent on information from several sources; hence, it is sensitive to errors in these sources. This matter is further described in the result section. Results from the calculations contain a lot of data and are difficult to interpret when presented in, for example, tables. Since data are collected from two-dimensional images of an object, it is also suitable to visualize the resulting displacements, densities, strains and moisture contents overlapped on the collected images. This is done in the “Result display” application, and it is possible to save stacks of images with a desired result parameter in a movie that can be played on a PC.

2.2.6 Combination of X-ray CT and displacement calculations for measurement of density, displacement, strain and moisture content

This method is similar to the one presented in the previous section. The difference lies mainly in how the displacements are estimated. Here the method in section 2.2.3 was used. This way to estimate displacement had some similarities to the methods developed by Lindgren et al. (1992) and Lindgren and Lundqvist (2000), since they are all based on reference points of the object, and displacements are interpolated between these points. However, when comparing original and deformed images in this work, no extra material was added, since a compensation for strain was made. For this method also a number of Matlab routines were setup to deal with data and present results. The method is further described in paper III.

2.2.7 Multivariate statistics

As mentioned earlier, results from the measurement methods presented here are very data rich. In order to extract valuable information from such extensive information, suitable methods have to be used. One way would be to use multivariate statistics to untangle important relationships in data sets and to predict responses based on the collected data. Principal Component Analysis (PCA) is an analytical tool for describing multivariate data in X space. X is the block of independent variables, also called prediction variables, and the Y block is the set of dependent variables, also called response variables. Another multivariate method is PLS, which stands for Projection to Latent Structures by means of Partial Least Squares, and it is useful for its ability to analyse data with many noisy, collinear and incomplete variables in both X and Y according to Eriksson et al. (2001). In paper VI, an example of how PLS can be used for modelling wood shrinkage and deformation properties in Radiata pine (*Pinus radiata*) is presented.

Since the acceptance for publication of paper VI in September 2000, many publications have been presented on these subjects. One informative source describing principles and applications is published by Umetrics AB (Eriksson et al. 2001), who also have released new versions of the SIMCA software that was applied in paper VI.

Here follow two brief descriptions of PCA and PLS.

2.2.7.1 Principal Component Analysis (PCA)

When studying data sets with many variables and many observations, it can be difficult to see possible relationships between variables when looking at data in a table. In the field of chemometrics, new measuring instruments appeared around 1970 that generated more information than existing chemical data analysis could handle. This accelerated the development of multivariate statistical methods. One of these was PCA, which proved to be useful for describing multivariate data and for classifying data in X. PCA works by finding latent variables, Principal Components (PCs) that explain the systematic variation in the X data block. The first PC is fitted by the least squares method to the observations in order to explain as much of the systematic variation in X as possible. Then the second PC is fitted to explain as much as possible of the systematic variation that is left orthogonal to the first PC. In this way, a set of latent variables, PCs, is fitted that can model the variation in X. The number of PCs is smaller than the number of variables if there are many variables. In this way the method can handle more variables than observations, which is not possible with more traditional statistical methods. The variables can also be dependent on each other, i.e., collinear variables. For the first PC, the systematic variation consists mostly of information, but for later PCs, the variation contains more and more noise. A limit is set to avoid overfitting of the PCA model, since too many PCs leads to overfitting. Both PCA and PLS models can be overfitted and thereby explain not only information, but also noise, which is not desirable. Therefore, validation of models is of importance. Some means for validation are further discussed in paper VI. From the PCA analysis one can identify outliers and find correlated variables. A common area of use is for process monitoring, where deviating process behaviour can be detected if online process variables are continuously fed into a PCA model. The results from PCA models can easily be interpreted in graphical form.

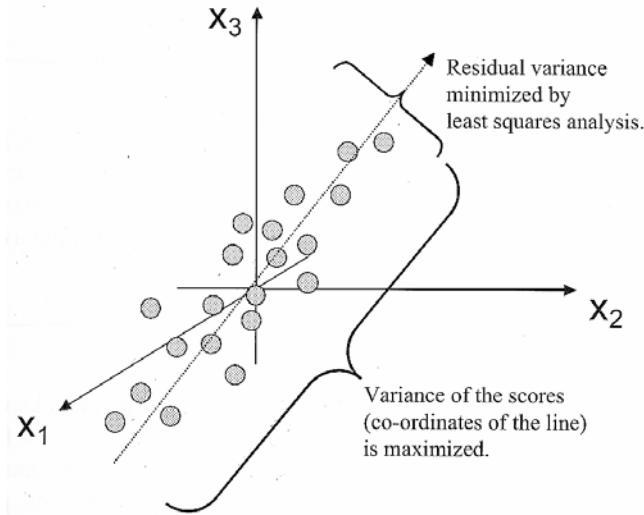


Figure 9. Fitting of a PC in X-space. Original figure text: “Figure 3.2: PCA derives a model that fits the data as well as possible in the least-squares sense. Alternatively, PCA may be understood as maximizing the variance of the projection co-ordinates.” (Eriksson et al. 2001). Published with permission of Umetrics AB.

2.2.7.2 Projection to Latent Structures by means of Partial Least Squares (PLS)

PLS is similar to PCA in the sense that it is based on finding latent variables, PCs, that describe the information in the data being studied. However, in PLS the data set is divided into predictors (X data) and responses (Y data), and both of these sets are considered when the PCs are derived. The relations between PCs in X and in PCs in Y are found through a PLS algorithm that maximizes the correlation between PCs in X and Y through the so-called inner relation (see paper VI). The output gives a prediction model of the Y responses from the X factors. It is possible to study scores, loadings and residuals for relationships among variables, identifying outliers, etc. (see paper VI). In addition, the SIMCA software used in paper VI also outputs predictive power, goodness of fit, variable importance and an estimation of the validity of the prediction model. In total, PLS can be considered to be a useful multivariate analytical tool.

2.2.7.3 Future use of PLS on data from the presented measurement method

PLS can be used when analysing multivariate data on wood, such as the data collected with the measurement method that has been developed and is presented in this thesis. Data collected with this method are extensive, with many variables that change in time and space, such as temperature, humidity, density, moisture content and strain. Fundamental understanding of wood drying behaviour has not fully attained in this research field, but several good modelling approaches based on physical and mechanical laws have been presented, as mentioned in the introduction of this thesis. Here PLS can be a

complementary tool to help find important relationships between variables as well as empirical quantitative models.

2.2.8 Diffusion theory

In this study only the diffusion regime was analysed for estimating modelling parameters. In wood drying, the mass/moisture flux, g , is most often modelled by modified versions of Fick's first and second laws. In equations (1) and (2) these equations for one-dimensional mass flux and mass conservation are shown as presented in paper V. u was moisture content (in [kg/kg]), D was the diffusion coefficient, x was the space variable and ρ_0 was the dry density of wood (dry mass of wood per green volume).

$$g = -D \frac{du}{dx} \quad (1)$$

$$\dot{u} = -\frac{1}{\rho_0} \frac{d}{dx} \left(D \frac{du}{dx} \right) \quad (2)$$

It should be noted that Fick's laws are based on concentrations as the driving potentials, and here both moisture concentration and moisture content were used. The moisture concentration, ω , in paper IV had the unit [kg/m³], and the moisture content, u , in paper V was [kg/kg]. Also, D in Fick's law should be constant, but in wood drying D , is often a function of moisture content and temperature. Here D also varied with distance from the evaporation surface. Hence, it is not wholly correct to refer to the equations presented above as Fick's laws, but that is done in this thesis.

A common functional form for D is the Arrhenius' equation with a dependency on moisture content and temperature. This was used in paper IV in the following form:

$$D(p, \omega) = p_1 e^{p_2 \omega} \quad (3)$$

where ω was the moisture concentration (in [kg/m³]) and $[p_1, p_2]$ were two constant parameter values which were to be determined. In the pieces studied in paper IV, nearly isothermal conditions were found; hence no temperature dependency was included. In paper V, two different sets of D values based on experimental evaluation were used in a Finite Element Model. These two sets are shown in Figure 10.

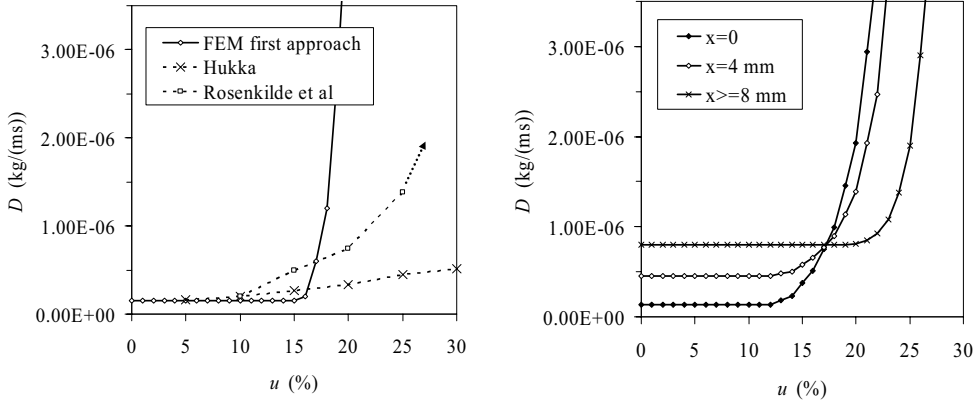


Figure 10. Left: $D(u)$ used in the first approach of FEM calculations in paper V. Comparison with Hukka's (1999) values for Norway spruce heartwood and Rosenkilde and Arfvidsson's (1997) values for Scots pine sapwood. Right: $D(u,x)$ used in the second approach of FEM calculations in paper V. Linear interpolation of D for $0 < x < 8$ mm using the curves for $x = 0$ and $x \geq 8$ mm.

In paper V it was found experimentally that u was a better way than ω to express amount of moisture in our case where ρ_0 varied in space.

2.2.9 Surface mass transfer

A problem that is often discussed in wood drying is how to deal with the mass flux from the surface. In paper IV this problem was avoided altogether by setting the outermost measured ω values in the studied wood sample as boundary values for the calculations.

In paper V the mass transfer at the surface, g_{surf} , was assumed to be driven by the difference between surface moisture content, u_{surf} , and the equilibrium moisture content of the ambient air, u_∞ , through the mass transfer coefficient, β .

$$g_{surf} = \beta \cdot (u_{surf} - u_\infty) \quad (4)$$

u_{surf} was extrapolated through linear or parabolic fit to interior u values near the surface. This was done because the measuring methods could not evaluate moisture content in the surface layer.

2.2.10 Methods for estimation of diffusion coefficients

One of the main objectives of this work was to develop methods for estimating D of measured data. In papers IV and V, three different methods to estimate D and a method to estimate β were presented.

In paper IV a finite element approach was used to describe the material. An iterative procedure was used to minimize the difference between measured and computed data in an objective function. Through that procedure, radial D values were optimized and $[p_1, p_2]$ values (eq. 3) were achieved. It should be noted that the author provided experimental

data for paper IV and participated in the writing of the paper. However, the author is not well acquainted with the computational routines used. These were mainly developed by Håkan Johansson and John Eriksson, Chalmers University.

In paper V, D values were estimated through direct numerical calculations using finite difference schemes on measured data. The calculations were based on equations (1), (2) and (4). In addition, the calculations were extended to two-dimensional mass flux. For this approach, no initial guess of the functional form of D had to be made. Since there were many numerical derivatives of u in this approach, the result was sensitive to small errors in u . Also, β was determined using measured values and equation (4).

3 RESULTS

A measurement method combining X-ray CT scanning and DSP has been developed, and some results regarding measurement accuracy are briefly presented here. Further results on measurement accuracy can be found in papers I and II.

- Displacements measured with DSP could be measured with a random error down to 0.01 pixel if there was a good combination of speckle density, contrast and mean speckle size. Table 1 in paper I shows a calculated displacement error of approximately 10 μm .
- Strains derived from the displacements, measured using DSP, had a maximum error of 1.11 mstrain in an experimental test in paper II.
- Moisture content measurement accuracy was estimated by simulations in paper II, which resulted in a measurement accuracy of $\pm 1.8\%$ moisture content at a significance level of 0.05 in a measurement volume with the approximate size $2 \times 2 \times 1.5 \text{ mm}^3$.

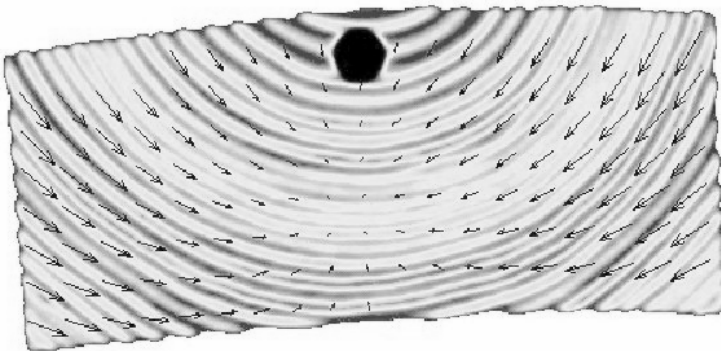


Figure 11. Displacements of subimage regions, measured with DSP, overlapped on the density image, captured with X-ray CT scanning. An example of results from the measurement method developed in papers I and II. Displacements of subimage regions are represented by arrows that are scaled by a factor of three.

A similar measurement method combining X-ray CT scanning and displacement calculations based on image analysis has also been developed (paper III). This method could measure displacement, strains, mass and moisture content. The errors in this method were less thoroughly investigated. However, an estimation of the error in paper V showed that the estimated error standard deviation of the moisture content was as small as 0.04% moisture content in a measurement area of $31 \times 3.9 \text{ mm}^2$, when the mean moisture content was around 20%.

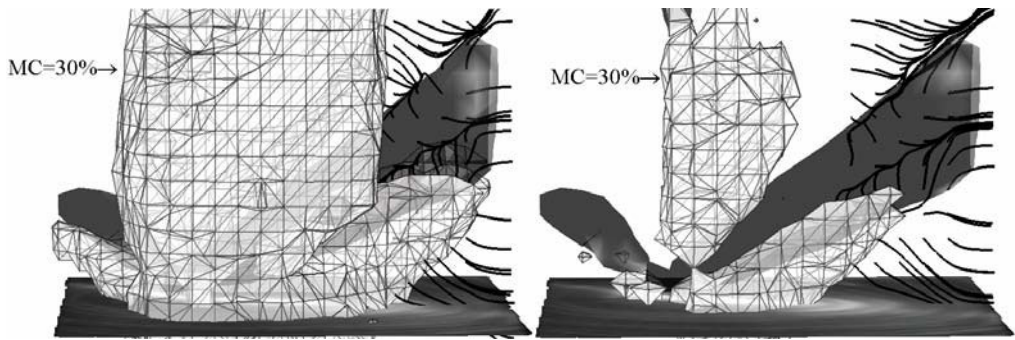


Figure 12. An example of measurements made using the measuring method presented in paper III. Original figure text: “MC iso-surfaces at 30 % MC near two knots, left: 2nd stack, right: 3rd stack. Black lines starting from points within and near the right-hand knot are so called stream-lines orientated along negative MC gradient direction.”

In paper IV the following D formulation for spruce was found:

$$D(\omega) = (7.76 \cdot 10^{-9})e^{(7.63 \cdot 10^{-3}) \cdot \omega}$$

D had the unit [m^2/s] and ω was the moisture concentration in [kg/m^3]. However, it was found that the varnish used for sealing was permeable by water, and therefore the calculated D values were not reliable in paper IV. The comparison between measured and simulated data can be seen in Figure 13.

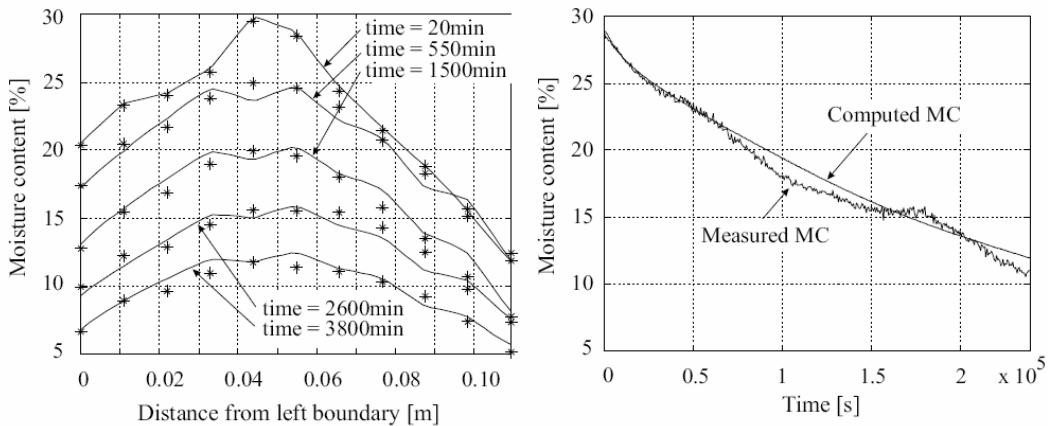


Figure 13. Original figure text in paper IV: “Measured (★) and computed (–) moisture content distribution (left) in space at certain time (right) at $x = 0.0547$ m during drying.”

D and β calculated in paper V are shown in Figures 13 and 14. In Figure 16 a comparison between computed and measured moisture content data is shown.

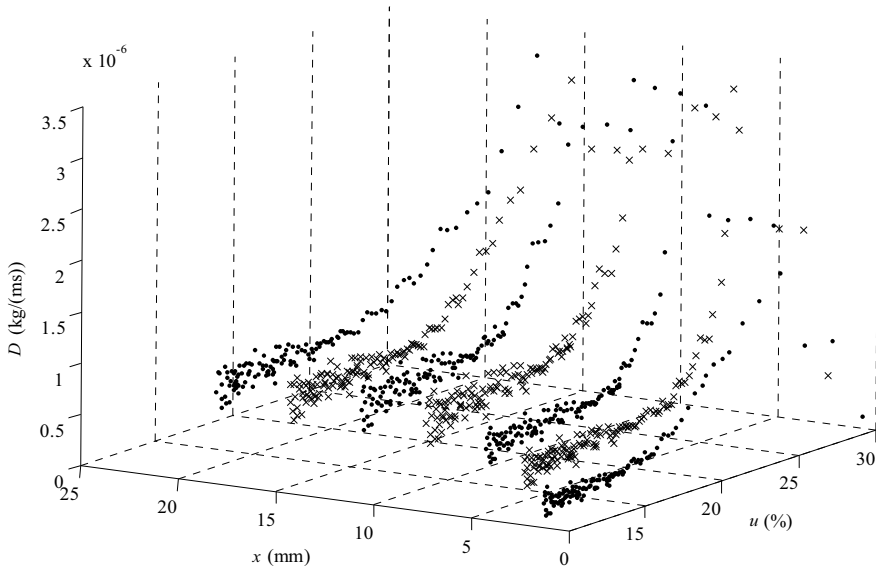


Figure 14. $D(u,x)$ evaluated in paper V using the “2D method”. x was the distance from the evaporation surface and u was the moisture content in the unit [kg/kg].

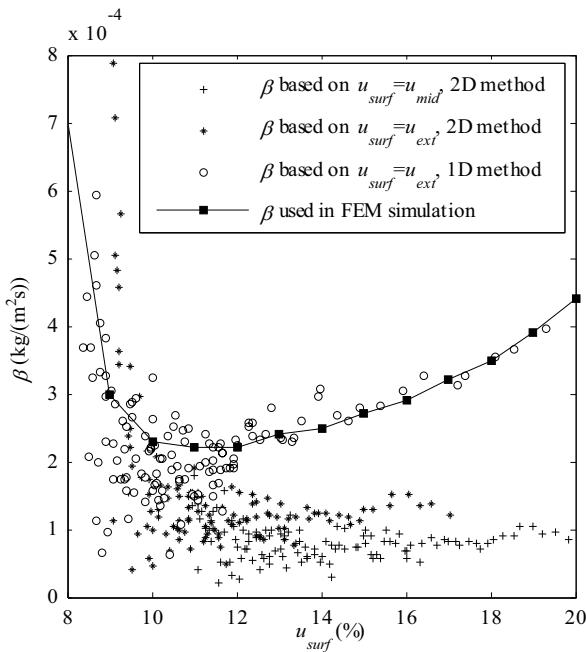


Figure 15. β calculated in paper V. Original figure text: “Fig.6. $\beta(u)$ evaluated with the 1D and the 2D method with alternative surface MCs; u_{ext} –linear extrapolation from two adjacent u values or parabolic extrapolation from three adjacent u values, u_{mid} – mean value of the surface cell, i.e. $u_{mid} = u(x_{i=1}, t^k)$.”

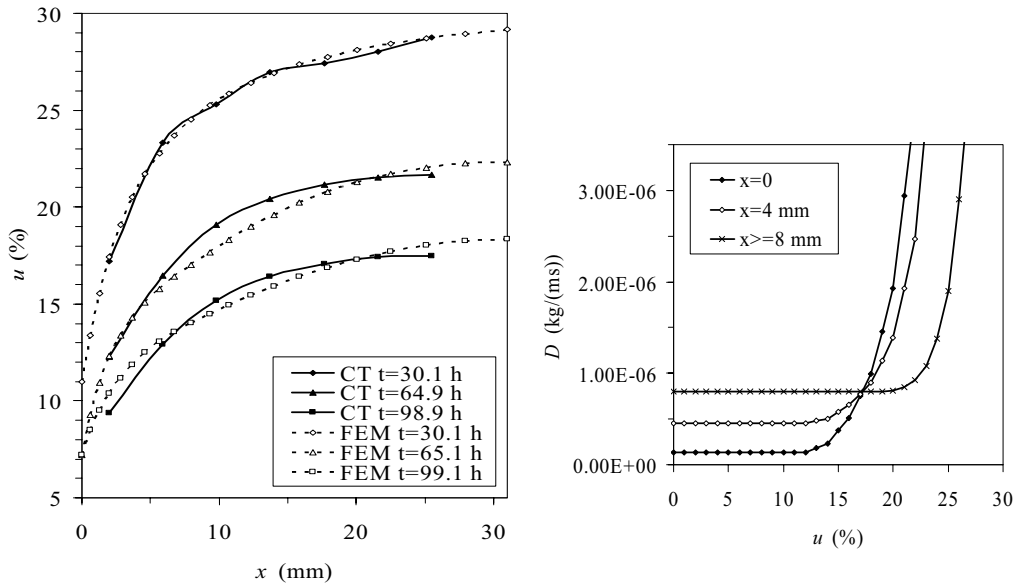


Figure 16. Left: Moisture content $u(x)$ at different times t , measured with CT and calculated with FEM, where β as in Figure 15 and $D=D(u,x)$. Right: $D=D(u,x)$ used in the FEM simulation in the figure to the left.

In paper VI, results showed PLS prediction models of radial, tangential, longitudinal and volumetric shrinkage for the studied samples from one slab of radiata pine. The models were valid in the moisture range between 0% and 22% moisture content. Coefficients of the model are presented in Table 1.

Table 1. R^2 , Q^2 and coefficients for shrinkage prediction model between 0% and 22% moisture content. The response is a linear combination of the coefficients. For example: $\text{Shrink, rad} = 1.6865 - 0.00874703 \cdot (\text{Transit time}) + 0.0037914 \cdot (\text{Density}) - 0.142256 \cdot (\text{M.C.}) + 0.112405 \cdot (\text{Distance from pith}) + 0.217513 \cdot (\text{No. of rings})$.

Y	R²	Q²
Shrink, rad	0.867	0.856
Shrink, tan	0.878	0.868
Shrink, lon	0.674	0.649
Shrink, vol	0.931	0.926

Coefficient	Shrink, rad(%)	Shrink, tan(%)	Shrink, lon(%)	Shrink, vol(%)
Constant	1.6865	2.70692	0.208958	4.52734
Transit time (ms)	-0.00874703	-0.0142319	0.00238886	-0.0202903
Density (kg/m ³)	0.0037914	0.00583206	-0.000157909	0.00919087
M.C. (%)	-0.142256	-0.210658	-0.0153544	-0.354452
Distance from pith	0.112405	0.172795	-0.0043954	0.272613
No. of rings	0.217513	0.331857	-0.0019475	0.53049

4 DISCUSSION

By improving the spatial resolution of the nondestructive measurement of density, it should be possible to measure differences within the annual ring, i.e., separate early and late wood. For this purpose, a CT scanner with a better spatial resolution could be used, or any other technique capable of measuring density at sufficient resolution, for example Nuclear Magnetic Resonance (NMR) equipment. In such an application, the optical magnification of the DSP equipment has to be increased, which can be achieved by using a microscope.

Strain and shear strains measured with the DSP method were very sensitive to rigid body rotation of the object, since a rotation introduced erroneous strains due to the way they were calculated from the displacements. Rigid body rotation was initially not expected to be a problem in the measurement of two-dimensional deformation of a wood cross section firmly secured to a screw. After trials of strain calculation from measured displacements, the deformed subimage regions far from the screw proved much more deformed than what was reasonable (Figure 17). Then it was clear that the orthotropic shrinkage of wood with its radial and tangential shrinkage imposed a rotation of subimage regions in the xy plane of the image. A new way of calculating strains based on rotation of local coordinate axes and differentiations of displacements is proposed in paper II. This has since been implemented, but without thorough comparison of the improvement of the method, and therefore it has not been presented.

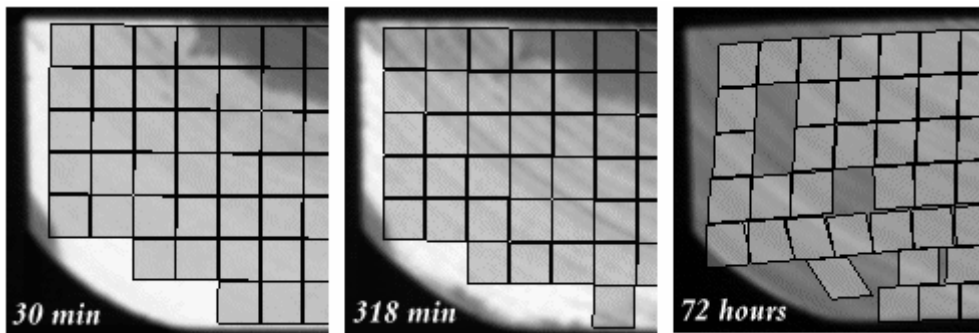


Figure 17. Radial and tangential shrinkage imposed a rotation of subimage regions. This caused erroneous strains, and the calculated shapes of subimage regions were thus exaggerated. It can be seen especially in the image to the right. Some subimage regions were missing, since they were considered erroneous by the filtering routine, as described in Paper II. Drying time is given in the lower left corner of each image above.

DSP with white light as the type of illumination and manually applied speckle pattern was used here. This method is often called white light speckle photography, and it was chosen due to its appropriate accuracy and to the robustness and ease of use of the equipment. DSP can also be used in combination with laser speckles, which results in greater measuring accuracy. However, the deformation of the wood surface studied may in many cases be too large for laser speckles.

A problem that developed during the experimental work in paper IV was that the varnish used was not a good sealant, which caused unreliable D values. For this reason the development of the displacement measurement method in paper III was initiated. This method was not dependent on an image of the end surface, as was the DSP method. The displacement calculations were based on the movement of the boundaries of the studied object in CT images, which introduced errors. Local displacement differences in the interior of an object, caused, by for example, different moisture content levels, cannot be correctly measured based on the movement of the object's boundaries. However, when the problem of finding correct displacements using DSP becomes severely difficult, as in Figure 17, then the other method (paper III) is probably a better alternative. However, it should be stated that the problem in Figure 17 is less pronounced in other measurements done.

Errors in standard deviations for moisture content measurements were small in the method presented in paper III and applied in paper V. For estimation of diffusion coefficients using the method in paper V, it was of great importance that the derivatives of u were good, which they also were due to the small error deviations in the moisture content data. It is more difficult to evaluate the mean error of the moisture content measurements of the method in paper III, since it is caused by many factors. These factors were mainly the oven dry calibration in the end of drying, the density errors and the displacement errors.

The measurement method presented in paper III gave detailed three-dimensional information about moisture content in the studied sample, even around local variations in the material, e.g., knots and defects. This made it possible to visualize drying wood in a relatively understandable way.

Differences in computed and measured moisture content in Figure 13 might be caused by the permeable varnish. Although D was unreliable due to the permeable varnish, paper IV showed that the optimization scheme used was a powerful tool to find useful D for the studied data. An interesting development of this method would be to test it using other functional forms of D and to extend it to deal with two- and three-dimensional data.

Derived D values in paper V showed some spread. The spread in D and β increased when the moisture content decreased due to the smaller numerical differences in local moisture content values. Also, D 's dependency on distance from the evaporation surface was interesting; this was further discussed in paper V. β in Figure 15 showed how difficult it can be to describe surface mass transfer. Here a simple mass transfer was assumed (eq. 4) using a constant-equilibrium moisture content in the ambient air. Since it was impossible to correctly measure surface moisture content (u_{surf}) due to the spatial resolution, u_{surf} was estimated as described in Figure 15. Different estimations of u_{surf} lead to quite different β values. Due to the higher spread in β at lower u_{surf} , the use of $u_{surf} = u_{\infty}$ as a boundary condition could be considered in modelling at lower u_{surf} values.

Papers IV and V present different ways to derive D . A suggested procedure is to use the method in paper V to get good qualitative information about which parameters influence D . Since those D values have quite a large spread from a modelling point of view, it is of interest to find a functional form of D that can be implemented in simulation models. In paper V this was done by a manual fit of D to the derived D values. Another

way to do it is to guess a functional form of D based on the derived D in paper V and then fit the parameters in that functional form using the optimization scheme presented in paper IV. A functional form of D could also be fitted to the D values using a multivariate approach. This could be done by correlating D (achieved by the method described in paper V) to other parameters, such as, for example, moisture content, temperature, density, material orientation, mass flux and distance to evaporation surface. In this way strong parameters that influence D could be identified, and these parameters could be used to set up a good guess of the functional form for D to be used in the “paper IV method”. Another approach is to calibrate a multivariate prediction model that gives a functional form of D that can be used straight away in simulation of wood drying. In conclusion, there are many ways to combine these methods, and a combination of them will probably produce a good tool for the determination of model parameters.

The example presented of how the multivariate method PLS could be used to model shrinkage behaviour in radiata pine (paper VI) showed that the method was a good tool for qualitative and quantitative evaluation of the responses being studied. PLS will be an important tool in future evaluation of data collected with the methods that have been developed in this work.

Concerning the experimental equipment, improving the possible climate regions would be desirable. For the continuation of this project it is of great importance to improve the climate control in the equipment used and to improve the range of the equipment to include higher temperatures and possibly also to include a pressurized environment.

The methods presented in this thesis will be of use in developing a better understanding of moisture movement and will provide more information on mechanical behaviour. These are the first two points for future work in the wood drying field mentioned in the introduction to this thesis. This will in the long run lead to improved industrial kiln drying, with high-quality drying at low cost.

5 FUTURE RESEARCH

A desirable objective of future research is to contribute to the fundamental understanding of wood drying as well as to improve industrial drying. In this section, some ideas for future work are presented.

- Set up a computerized tool for determining moisture modelling parameters in three dimensions from moisture data measured using X-ray CT scanning. This tool could be useful for characterizing wood material from a drying point of view. One example of such use is when Valutec AB wants to sell wood drying kilns in a new market with unfamiliar wood species.
- Use the methods developed to study moisture flow above fibre saturation point.
- Study mechanical behaviour and estimate stresses based on measured strains and assumptions of the strain-stress relationship at different moisture, temperature and material conditions.
- Implementation of appropriate model descriptions in industrial dry kiln control systems by Valutec AB. The models may be used for offline simulations as well as online simulations based on measured signals, in combination with adaptive control strategies already in use. This is done today for Norway spruce and Scots pine based on modelling parameters found by other researchers.

6 CONCLUSIONS

A noncontact technique that simultaneously measures the displacements on a wood surface by using DSP and the internal wood density distribution by using X-ray CT scanning has been developed. Another noncontact technique based only on X-ray CT scanning has also been developed. Displacements have then been estimated from boundary movements of an object in CT images.

Methods for calculating strain, shear strain and moisture content based on measured displacement and density have been developed.

Methods to derive moisture diffusion coefficients and mass transfer coefficients from measured data have been presented.

An example showed that PLS could be an effective and easy-to-use tool for untangling relationships between variables and generating information from data.

This work showed how nondestructive measurement could be used to collect extensive wood drying information and how to refine this information into useful modelling parameters. These parameters could be used to predict wood behaviour during drying and thereby be used to improve industrial wood drying processes.

7 REFERENCES

- Andersson, A. 2000. Combined Speckle Interferometry and Speckle Correlation for Non-Destructive Testing. Licentiate thesis. Luleå University of Technology, Division of Experimental Mechanics, Luleå, Sweden. Thesis No. 2000:30. ISSN 1402-1757
- Benckert, L. 1992. Wood-drying studies using white light speckle photography. *Measurement* 10(1): 24:30
- Chiorescu, S. and Gronlund, A. 2000. Validation of a CT-based simulator against a sawmill yield. *Forest Products Journal* 50(6):69–76
- Cormack, A.M. 1963. Representation of a function by its line integrals with some radiological applications. *Journal of Applied Physics* 34:2722
- Danvind, J. 1999. Systems to dynamically measure shape changes in wooden sample sticks to determine shrinkage, twist, crook, bow, MOE and Poisson's ratio. Master Thesis. Luleå University of Technology, Skeria 3, 931 87 Skellefteå, Sweden. Thesis No. 1999:132CIV. ISSN 1402-1617
- Danvind, J. and Morén, T. 2004. Using X-ray CT-scanning for moisture and displacement measurements in knots and their surroundings. In: *Proceedings of EU COST 15 Wood-Drying Conference*. April 22–23, 2004, Athens, Greece
- Ekevad, M. 2004. Method to compute fiber directions in wood from computed tomography images. *Journal of Wood Science* 50(1):41–46
- Eriksson, L, Johansson, E, Kettaneh-Wold, N, Wold, S. 2001. Multi- and Megavariate Data Analysis –Principles and Applications. Text book. Umetrics AB, P. O. Box 7960, SE-90719 Umeå, Sweden. ISBN 91-973730-1-X
- Fromm, J.H., Sautter, I., Matthies, D., Kremer, J., Schumacher, P., and Ganter, C. 2001. Xylem water content and wood density in spruce and oak trees detected by high-resolution computed tomography. *Plant Physiology* 127(2):416–425
- Hanhijärvi, A. 1995. Modelling of creep deformation mechanisms in wood. VTT, Technical Research Centre of Finland, Building Technology, P.O. Box 1806, FIN-02044 VTT, Finland. VTT Publication No. 231. ISBN 951-38-4769-1
- Herman, G.T. 1980. Image reconstruction from projections –the fundamentals of computerized tomography. Academic Press, N.Y., USA
- Hukka, A. 1999. The Effective Diffusion Coefficient and Mass Transfer Coefficient of Nordic Softwoods as Calculated from Direct Drying Experiments. *Holzforschung* 53(5):534–540
- Håkansson, H. 1998. Retarded sorption in wood, Experimental study, analyses and modelling. Doctoral thesis. Lund University, Department of Building Science, P.O. Box 118, SE-221 00 Lund, Sweden. Report TABK-98/1012. ISSN 1103-4467
- Jernkvist, L-O. and Thuvander, F. 2001. Experimental Determination of Stiffness Variation Across Growth Rings in *Picea Abies*. *Holzforschung* 55(3):309–317
- Johansson, J. 2001. Property Predictions of Wood Using Microwaves. Licentiate thesis. Luleå University of Technology, Division of Wood Physics, Skeria 3, SE-931 87 Skellefteå, Sweden. Thesis No. 2001:35. ISSN 1402-1757
- Johnson, P. 1998. Dual-beam Digital Speckle Photography –Strain Field Measurements in Aerospace Applications. Licentiate thesis. Luleå University of Technology, Division of Experimental Mechanics, Luleå, Sweden. Thesis No. 1998:02. ISSN 1402-1757

- Kamke, F.A. and Vanek, M. 1994. Comparison of Wood-drying Models. In: Proceedings of 4th International IUFRO Wood-drying Conference, August 9-13, 1994, Rotorua, New Zealand. pp 1-17
- Keey, R., Langrish, T. and Walker, J. 2000. Kiln-Drying of lumber. Springer, Berlin.
- Larsson, R. and Morén, T. 2003. Implementation of Adaptive Control Systems in Industrial Dry Kilns. In: Proceedings of the 8th International IUFRO Wood Drying Conference, 24-29 August, 2003, Brasov, Romania. pp 397-400
- Larsson, R. and Morén, T. 2004. Expert System for Adaptive Control of the Wood Drying Process. In: Proceedings of EU COST 15 Wood-Drying Conference. April 22-23, 2004, Athens, Greece.
- Lindgren, O. 1992. Medical CT-Scanners for Non-Destructive Wood Density and Moisture Content Measurements. Doctoral thesis. Luleå University of Technology, Division of Wood Technology, Skeria 3, SE-931 87 Skellefteå, Sweden. Thesis No. 1992:111D. ISSN 0348-8373
- Lindgren, L.O., Grundberg, S. and Davis, J.R. 1992. Applying digital image processing on CAT-scan images of wood for non-destructive moisture content measurements. Paper VI in: Lindgren, O. 1992. Medical CT-Scanners for Non-Destructive Wood Density and Moisture Content Measurements. Doctoral thesis. Luleå University of Technology, Division of Wood Technology, Skeria 3, SE-931 87 Skellefteå, Sweden. Thesis No. 1992:111D. ISSN 0348-8373
- Lindgren, O. and Lundqvist, S-O. 2000. Geometric Transformation (Warping) of CT- Images An Aid for Non-Destructive Wood Density and Moisture Content Measurements. In: Proceedings of 4th International Wood Scanning Seminar, Aug 21-23, Mountain Lake Resort, Virginia, USA
- Mathworks. 2005. Homepage: <http://www.mathworks.com>
- Morén, T. 2001. Adaptive Kiln Control Systems Based on CT-scanning and Industrial Practise. In: Proceedings of 7th International IUFRO Wood-drying Conference, July 9-13, 2001, Tsukuba, Japan. pp 48-53
- Nordmark, U. and Oja, J. 2004. Prediction of Board Values in Pinus sylvestris Sawlogs Using X-ray Scanning and Optical Three-dimensional Scanning of Stems. Scandinavian Journal of Forest Research 19(5):473-480
- Nyström, J. and Hagman, O. 1999. Real-time spectral classification of compression wood in Picea abies. Journal of Wood Science 45(1):30-37
- Oja, J. 1999. X-ray Measurements of Properties of Saw Logs. Doctoral thesis. Luleå University of Technology, Division of Wood Technology, Skeria 3, SE-931 87 Skellefteå, Sweden. Thesis No. 1999:14. ISSN 1402-1544
- Ormarsson, S. 1999. Numerical analysis of moisture-induced distortions in sawn timber. Doctoral thesis. Chalmers University of Technology, Gothenburg, Sweden. Publication 99:7. ISBN 91-7197-834-8
- Ormarsson, S., Petersson, H., Eriksson, J. and Dahlblom, O. 2001. Improved Shape Stability of Timber Products Obtained by Use of a Numerical Simulation Technique. . In: Proceedings of 7th International IUFRO Wood-drying Conference, July 9-13, 2001, Tsukuba, Japan. pp 312-317
- Rosenkilde, A. and Arfvidsson, J. 1997. Measurement and Evaluation of Moisture Transport Coefficients During Drying of Wood. Holzforschung 51:372-380
- Rosenkilde, A. and Glover, P. 2002. High Resolution Measurement of the Surface Layer Moisture Content during Drying of Wood Using a Novel Magnetic Resonance Imaging Technique. Holzforschung 56:312-317

- Rosenkilde, A., Gorce, J.-P. and Barry, A. 2004. Measurement of Moisture Content profiles during Drying of Scots pine using Magnetic Resonance Imaging. *Holzforschung* 58(2):138–142
- Salin, J.-G. 2002. Theoretical analysis of mass transfer from wooden surfaces. In: Proceedings of 13th International Drying Symposium, Aug. 27–30, Beijing, China.
- Sepúlveda, P., Oja, J. and Grönlund, A. 2002. Predicting spiral grain by computed tomography of Norway spruce. *Journal of Wood Science* 48(6):479–483
- Simpson, W.T. and Liu, J.Y. 1997. An optimization technique to determine red oak surface and internal moisture transfer coefficients during drying. *Wood and Fiber Science* 29(4):312–318
- Sjödahl, M. 1995. Electronic Speckle Photography applied to In-Plane Deformation and Strain Field Measurements. Doctoral thesis. Luleå University of Technology. Division of Experimental Mechanics, Luleå, Sweden. Thesis No. 1995:1710. ISSN 0348-8373
- Svensson, S. 1997. Internal Stress in Wood Caused by Climate Variations. Doctoral thesis. Lund University, Department of Structural Engineering, P.O. Box 118, SE-221 00 Lund, Sweden. Report TVBK-1013. ISSN 0349-4969
- Söderström, O. 1996. The Development of Quality Wood-drying from Skellefteå 1987 to Quebec 1996 and an example of its Effect on a National Research Program. Proceedings from 5th International IUFRO Wood-drying Conference. August 13–17, 1996, Quebec, Canada. pp 3–8.
- Valutec AB. 2005. Address: Valutec AB, P.O. Box 709, SE-931 27 Skellefteå, Sweden. Tel: +46 910 879 50. Homepage: www.valutec.se
- Wiberg, P. 1996. CT-scanning During Drying. Moisture Distribution in *Pinus Silvestris*. 5th IUFRO International Wood Drying Conference. Québec, Canada, August 13–17. pp 231–235
- Wiberg, P. and Morén, T. 1999. Moisture flux determination in wood during drying above fibre saturation point using CT-scanning and digital image processing. *Holz als Roh- und Werkstoff* 57:137–144
- Wiberg, P., Sehlstedt-Persson, S.M.B. and Morén, T.J. 2000. Heat and Mass Transfer During Sapwood Drying Above the Fibre Saturation Point. *Drying Technology* 18(8):1647–1664
- Wiberg, P. 2001. X-ray CT-scanning of Wood During Drying. Doctoral thesis. Luleå University of Technology, Division of Wood Physics, Skeria 3, SE-931 87 Skellefteå, Sweden. Thesis No. 2001:10. ISSN 1402-1544

Paper I

Method for measuring the Shrinkage Behaviour of Drying wood using Digital Speckle Photography and X-ray Computerised Tomography

J. Danvind* *Valutec AB, P.O. Box 709, SE-931 27 Skellefteå, Sweden. E-mail: jonas.danvind@bigfoot.com*

P. Synnergren *Division of Experimental Mechanics, Luleå University of Technology, SE-971 87 Luleå, Sweden*

*) Ph. D. student, Division of Wood Physics, Luleå University of Technology

ABSTRACT

In the present study, we developed a system for simultaneous measurements of surface deformations and density changes in order to improve the understanding of the shrinkage behaviour of drying wood. Our system is a combination of two well-known, non-contact techniques called Digital Speckle Photography (DSP) and X-ray Computerised Tomography (CT). The samples used were 18 mm thick cross-sections of wooden boards from a *Pinus silvestris* tree. During the measurements the end coated samples were dried at 90°C in a climate-controlled chamber. To be able to measure the in plane deformations of the longitudinal end, a white light speckle pattern was created by spraying the varnish with random black dots on a white background. The movement of this pattern was measured using DSP. The lowest noise level obtainable in a typical DSP measurement is about 1/100 pixels. This means that the accuracy depends both on the magnification and the CCD-detector used. In this study we expect the minimum noise in the displacement estimations to be about 2 µm. CT images are captured in a SIEMENS SOMATOM AR.T. scanner on a slice of the material. Recorded CT images have an in-plane spatial resolution of approximately 3 pixels width. Density is displayed in the CT-images and in a similar scanner the density resolution could be estimated to ± 2 kg/m³ for dry wood and ± 6 kg/m³ for wet wood in a 2x2x1.5 mm³ volume.

INTRODUCTION

The use of X-ray Computerised Tomography (CT) for non destructive testing of wood has become a well-known technique for research purposes. Oja (1999) used CT for measuring inner saw log properties, for example knot parameters, resin pockets and log shape. Also the wood density, the moisture content and the spiral grain are possible to measure with CT (Lindgren 1992, Sepulveda 2000). Wiberg (2001) studied the moisture characteristics of drying wood using CT-scanning and has collected experimental data that supports a partially new description of capillary moisture flow. At present much of the moisture behaviour of drying wood using air convective drying below 100°C can be theoretically described. However, the mechanical properties, which are closely related to moisture behaviour, are less understood. Measurements have been carried out on

wood samples in order to achieve stress and strain responses during different loading and drying conditions, for example the measurements done by Svensson (1997) and Hanhijärvi (1997). In their measurements the moisture contents were determined using small continuously weighed control samples. From the weight readings the average moisture contents were calculated, i.e. the moisture contents were not measured on the tested samples. They measured strains by mounting two strain gauges onto the sample. This methodology is sufficient when measuring on thin samples, with fast responses to surrounding climate variations. Though, when measuring on larger samples with interior moisture gradients it is important to know the local moisture behaviour and relate it to the local strain. Local strains in wood can be measured accurately by non contact optical methods, such as a method referred to as Digital Speckle Photography, DSP

(Jernkvist and Thuvander, Choi et al. 1991). Instead of measuring on larger samples it is possible to simulate the moisture and mechanical behaviour based on models fitted to small sample experimental data. A three dimensional model which considers the local variations is presented by Ormarsson (1999). However, there is still use for measurement techniques for local moisture and mechanical determination in larger samples in order to provide useful data for validating and improving existing material models.

This paper presents a technique that simultaneously measures local densities and displacements in a cross section of a drying board. The method is based on the combination of DSP and X-ray CT, which both are non-contact methods. Most effort is put into describing the method and the experimental results are therefore briefly presented here.

MATERIAL

Three 90x40 mm² cross-sections with a thickness of 18 mm were used. All samples were taken from the same cross section of a Scots pine tree (*Pinus sylvestris*). To simulate the drying of a board cross section the end surfaces were coated in order to stop drying through the ends. The coating consisted of three thin layers of Polyurethane Alkyd (PUR) varnish ("Celco Golvlack" (no. 10133) from Nordsjö) and a thin coat of white high-temperature resistant spray paint. The latter served as a background for black randomised spots (speckles) that were applied using an ordinary spray can. Backman (2000) used this varnish and shows that the varnish has good adhesion to wood. Thin samples was chosen in order to have approximately the same moisture distribution in the cross section of the samples, so that the measured displacements corresponded to the measured density distribution. A Ø6 mm hole was drilled 6 mm from the pith side edge in the middle of the samples, refer to Figure 5. During measuring the samples were fastened on a 6 mm Poly Amide screw which was securely tightened to a stable foundation of steel, which was placed in the measuring environment in sufficient time before measuring started. The reason why Poly Amide was used was due to the severe scattering effects that steel screws caused in CT images.

METHOD

Digital Speckle Photography (DSP)

DSP is an advanced image processing technique utilised for surface deformation measurements. In essence, a random pattern is produced on the surface of the specimen and the motion of this pattern deforming with the motion of the specimen is photographed. By comparing 'before' and 'after' images of the random

pattern, accurate surface deformation maps can be deduced. The calculation is performed by cross-correlating small sub-images from each of the two images. Since the images are of a random nature, an image of some small region of the pattern will correlate well only with another image of the same region, even if this region is slightly distorted. By looking for the location of a maximum of the correlation function as one sub-image is moved around over the other image, the local 2-D in-plane displacement field can be deduced. For a more comprehensive description of the algorithm see Sjö Dahl (1997).

The performance of DSP is dependent on the imaged random pattern. Parameters that are of interest are speckle density, contrast and mean speckle size. To be able to perform the measurements we need to have a certain amount of speckles in each subimage. In our experiments we use 30 pixels by 30 pixels large subimages and the speckle density needed for a successful measurement is 5-10 speckles in each subimage. A high contrast speckle pattern is advantageous because it gives a high signal to noise ratio, which facilitates higher correlation between the images. The random error in the measurements (noise) is directly linked to the correlation value and the mean speckle size in the subimages. According to Sjö Dahl (1997) a speckle size of 2 pixels in diameter is ideal to minimise the errors in the measurements. If high correlation values are obtained, random errors as low as 0.01 pixels on the CCD-detector is obtainable.

X-ray Computerised Tomography (CT)

A SIEMENS SOMATOM AR.T medical X-ray CT-scanner was used to measure densities in the samples. The scanner stores data in 2-dimensional images of 512x512 pixels, where the lightness in a pixel shows the density in the corresponding voxel, i.e. volume element. Scans with a slice thickness of 2, 5 or 10 mm could be used, which means that a pixel can correspond to different volumes. In this study 5 mm was used. The spatial resolution was here approximately 0.6 mm, which is in the order of three pixel widths according to a rule of thumb stated by Lindgren (1992). Another factor that is important for the accuracy in CT-scanning is the contrast resolution. The contrast resolution is the ability to separate differences in CT-numbers, corresponding to densities, between neighbouring regions. The contrast resolution is dependent on the measuring volume in such a way that the larger the volume the better is the resolution. On the other hand, increasing the measuring volume decreases the spatial resolution. Therefore it is a trade-off in order to get the best combination of spatial and contrast resolution for the specific measurements. Due to the resolution of this type of medical CT-scanner it should not be used for measuring wood density separately in earlywood and latewood (Lindgren, 1992). It is more suitable for measuring more uniform regions

or a sufficient mix of the different types of wood. No study on the best combination of spatial and contrast resolution for these measurements has been done. However, if the wood density is evaluated with corresponding spatial resolution as in the DSP-calculations (the subimage size is here 30 pixels by 30 pixels, which corresponds to an area of 4.5 mm by 4.5 mm on the specimen surface) then the measuring volume becomes $4.5 \times 4.5 \times 5 \text{ mm}^3$. Lindgren (1992) found from studies in a similar medical CT-scanner that the accuracy is $\pm 2 \text{ kg/m}^3$ for dry wood and $\pm 6 \text{ kg/m}^3$ for wet wood with moisture contents ranging from 6-100%. This accuracy was estimated for a $2 \times 2 \times 1.5 \text{ mm}^3$ volume at a significance level of 0.05. The measuring volume used here was larger and therefore we expect that the accuracy was slightly better than stated above.

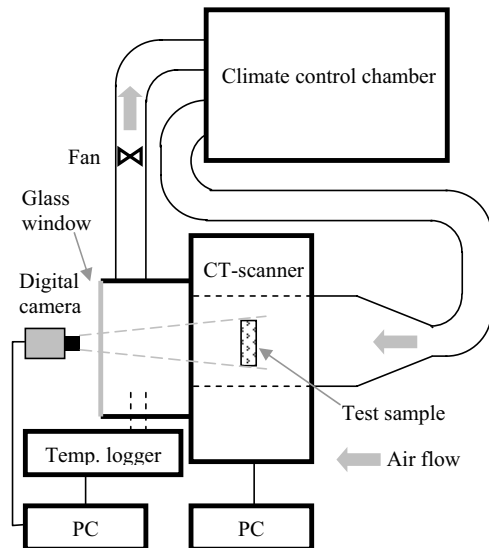


FIGURE 1. Experimental equipment.

Experimental equipment

The experimental equipment used by Wiberg (2001) for simultaneous drying and CT-scanning of wood was slightly modified in order to incorporate a digital camera and a box with glass windows, Figure 1. Glass windows were needed for capturing images of the wood samples using an external digital camera. Drying air was circulated through a plastic tube in the gantry of the CT-scanner. Air velocity was controlled by a fan and humidity and temperature was controlled by a climate chamber. The plastic tube was mounted on the box and the rest of the parts were connected via flexible tubes. Temperature could be controlled between -5°C to 115°C and humidity could be controlled between 15 %RH and 98 %RH in the temperature range between

25°C to 80°C (Wiberg, 2001). In this study the climate was constant at approximately 90°C temperature and 0 %RH. The climate was continuously measured using a PC-logger. The CT-scanner and the digital camera were connected to computers, see Figure 1. The capturing of DSP and CT images was controlled manually to guarantee that both images were captured simultaneously.

Software

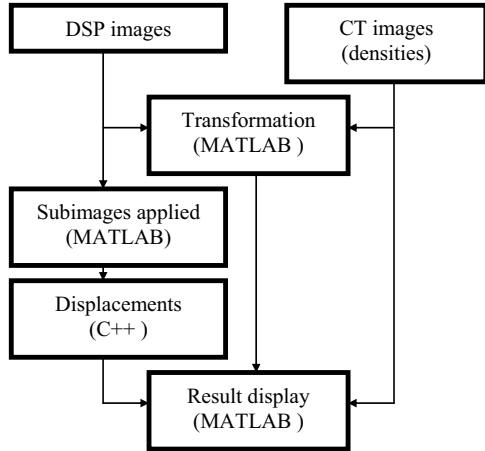
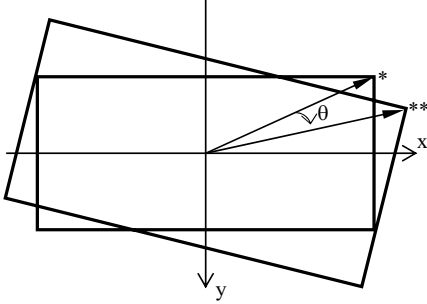


FIGURE 2. Flow for treatment of collected image data.

After the images were captured, the DSP images were divided into subimages using a custom made MATLAB routine. This routine let the user mark a region of interest (ROI), in which the DSP-calculation should be performed. The wanted size of the subimages was given as input to the routine, which calculated the positions of the subimages within the ROI. To calculate the displacements, the information from the preceding MATLAB routine was fed into the DSP-program that was executed. In order to display the displacements, calculated from the DSP images, on top of the CT images a transformation from DSP to CT images was performed using another custom MATLAB routine described below. Since the DSP images and the CT images have different spatial resolution and they may also have been rotated in relation to each other, a transformation was needed to match them. The transformation was based on the assumptions that there had been a rotation around the centre of the screw and that elongation or contraction of the image had taken place in the x- and y-direction. The elongation or contraction was assumed to be equal in both x- and y-direction. Based on the assumptions the origo of local image co-ordinates in the DSP image was moved to the centre of the screw by subtraction of the co-ordinates for the centre of the screw, called $x_{c,DSP}$ and $y_{c,DSP}$. The same procedure was done on the CT image, where the

co-ordinates for the centre of the screw were called $x_{c,CT}$ and $y_{c,CT}$. Rotation around the centre of the screw is denoted θ , Figure 3.



$$* = (x_{DSP} - x_{c,DSP}, y_{DSP} - y_{c,DSP})$$

$$** = (x_{CT} - x_{c,CT}, y_{CT} - y_{c,CT})$$

FIGURE 3. Transformation from DSP to CT image.

The following transformation equation (1) was used:

$$\begin{bmatrix} x_{CT} - x_{c,CT} \\ y_{CT} - y_{c,CT} \end{bmatrix} = \begin{bmatrix} k_x \cos \theta & -k_y \sin \theta \\ k_x \sin \theta & k_y \cos \theta \end{bmatrix} \begin{bmatrix} x_{DSP} - x_{c,DSP} \\ y_{DSP} - y_{c,DSP} \end{bmatrix}$$

where k_x is the elongation or contraction in the x-direction and k_y is the corresponding in the y-direction. By using a custom made MATLAB routine the centre of the screw in the DSP and CT images were manually marked and the co-ordinates $x_{c,DSP}$, $y_{c,DSP}$, $x_{c,CT}$ and $y_{c,CT}$ were determined. Thereafter the four corners of the cross section were marked and each corner in combination with the centre of the screw gave a solution of the equation system (1), for which k_x and k_y could be calculated at the rotation θ . According to the assumptions stated above there should be one solution for θ and the elongation and contraction, k_x or k_y , should be equal and only give one solution, called k . Since the equation system is over determined using four points, giving four solutions for each of θ , k_x and k_y , the solutions was found by a least-square fit of a straight line, where the k was a function of θ , Figure 4. The solution for θ was determined as the mean value of the four solutions for θ . Then the solution for θ was put into the equation of the fitted line and thereby a solution for k was determined.

RESULTS

A considerable amount of data was generated with this measuring technique. For three samples with 90 subimages, of the size 30x30 pixels, and a measuring

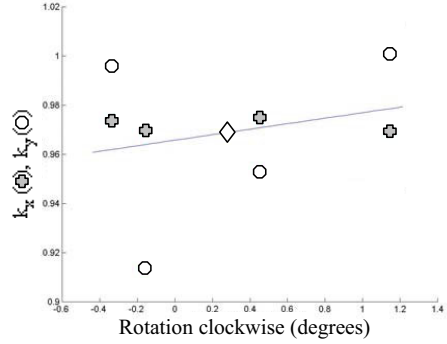


FIGURE 4. Least square fit of straight line for finding transformation constants k and θ . The diamond shape point was taken as a solution, which gave $k=0.97$ and $\theta=0.28$.

sequence of approximately 25 images, 6480 displacement vectors were generated. Therefore it is necessary to use methods for data analysis in order to have use of this data. Since this paper describes the method, only examples of collected data is presented.

Table 1 shows the displacements of the subimages in the x- and y-direction, u and v , the obtained correlation value in the cross-correlation, $corr$, and the size and position of the subimages. An estimated random error for the calculated displacement, err , is also given. The random error is estimated using a method presented by Sjö Dahl (1997). He showed that the error in the displacement estimation can be calculated by

$$e = 0.03 \cdot \sigma^{1.67} \sqrt{(1-\delta)/\delta} \quad (2)$$

where σ is the mean speckle size and δ is the correlation value. In Table 1 we estimate the mean speckle size to two pixels.

Figure 5 shows a visual representation of the displacements in Table 1. The transformation described earlier was used in order to visualise displacements in the CT image. Note that the displacement arrows were autoscaled, which means that the true displacements are less than in Figure 5.

Table 1. The in- and output of the DSP program for a selection of subimages. These results were the displacements after 34 hours of drying for the sample containing both sapwood and heartwood.

Subimage	u (mm)	v (mm)	err (mm)	corr	x-centre (pixels)	y-centre (pixels)	x-size (pixels)	y-size (pixels)
1	2.347	1.562	0.007	0.791	59	301	30	30
2	2.022	1.295	0.010	0.680	89	301	30	30
3	1.725	1.127	0.007	0.701	119	301	30	30
4	1.360	0.923	0.010	0.652	149	301	30	30
...								
89	-1.410	0.027	0.008	0.780	449	451	30	30
90	-1.645	0.158	0.007	0.824	479	451	30	30

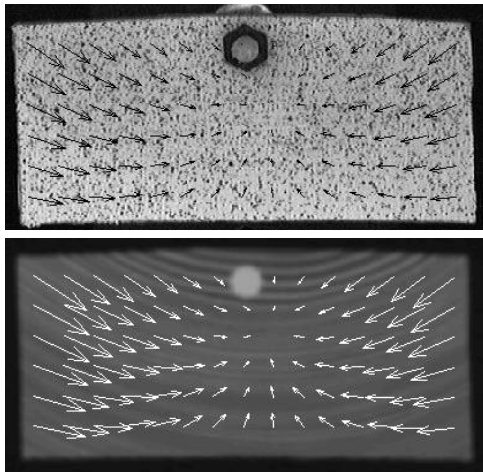


FIGURE 5. Displacement field after 34 hours drying for the sample containing both sapwood and heartwood. Each arrow corresponds to the movement of a subimage area and the subimages are numbered from left to right starting at the left upper corner. Upper: Displacement field in DSP image. Lower: Displacement field overlapped on CT image.

DISCUSSION

The measured shrinkage and density changes seemed to be correct, for example, expected differences in tangential and radial movements could be detected.

The PUR varnish may have influenced the behaviour of the wood during the measurements done here. Backman (2000) found that the glass transition temperature of the PUR varnish applied to wood is well below the testing temperature of 90°C, which was used in this study. At this temperature the dynamic modulus of elasticity for the PUR varnish, measured by Dynamic Mechanical Temperature Analysis (DMTA), was less than 1/10 of the tangential modulus of wood with a moisture content of 7 % (Backman, 2000). The applied

PUR varnish also has good adhesion to the wood, which can be seen in microscopic images and from DMTA measurements (Backman, 2000). These findings strengthens the theory that the PUR varnish did not influence the wood behaviour to a larger extent and also that the measured displacements on the speckled surface corresponded to the movements of the underlying wood. Another factor of the PUR varnish that might have affected the measurements is the increased diffusion of water molecules through the varnish above the glass transition temperature. This might have influenced the moisture profile (which can be derived from the density profile) within the samples, but since the density profile continuously was measured the collected data still describes the true behaviour of the samples. Hence, there might be a difference in behaviour between the tested samples and the cross-sections in a full-length board, which we intended to simulate. We expect that the diffusion through the PUR varnish is very low in comparison to the evaporation from the wooden surfaces, if so the effect of moisture diffusion through the paint can be neglected.

The large surface deformation of the specimen results in a distortion of the speckle pattern. The distortion lowers the correlation and thus increases the noise in the DSP measurements. Speckles were applied using an ordinary spray can, therefore, it might be local variations in speckle density and speckle size which results in local variations in the measurement accuracy as well. However, judging from the obtained results the method is robust enough to collect reliable data.

Out-of-plane movements may be present in these measurements. This method can not compensate for such movements, but probably they are very small in comparison to the in-plane movements. If it becomes a problem, the third dimension of displacement can be calculated by using stereoscopic digital speckle photography (Synnergren, 1999). The air temperature is changing during the measurement cycle, which means that the refraction index of the air that surrounds the specimen is changing as well. This might influence the DSP measurements in such a way that false displacements are introduced. However, due to the

rather low change in temperature the refraction index is only changing very little and as long as the temperature is approximately constant, this effect could be neglected. Another disturbance is vibrations that might move the whole equipment and introduce false rigid-body movements in the DSP-measurements. In most applications, however, it is the displacement derivatives (e.g. the strain field) that are of most interest due to their connection to the stress and strain state in the measured object. Luckily the rigid-body movements do not influence the displacement derivatives.

The transformation for matching DSP and CT images introduces an error when coupling density and displacement data. On the other hand this error might be relatively small in comparison to the size of the measuring regions and may therefore not influence the collected data to a larger extent. Since this type of error is systematic it gives the same error for all images in a measuring series, thereby the same area with a small positioning error is found in all the images and is therefore valid for comparing studies, despite the error.

Mounting the samples using a screw through the wood probably influenced the material behaviour, but the screw was put on the pith side of the sample, which is less susceptible to drying checks.

A problem that is likely to appear later is when a more humid drying environment is used and water might condense on the glass window and influence the DSP measurements. This can be dealt with by using a heating device controlled by a PC that heats the glass prior to image capturing in order to evaporate the water. Measuring of displacements by applying the DSP technique directly in the CT images were not possible here, due to lack of correlation. But for other types of scanners and for measuring deformations in regions with small moisture content changes it could be possible.

FUTURE DEVELOPMENTS

Next step in the development of the measuring technique will be to include the calculations of strains and moisture contents and to set up a computerised control of the image capturing.

CONCLUSIONS

We have presented a technique that simultaneously measures the displacements of a wood surface by using DSP and the internal wood density distribution by using X-ray CT-scanning. We are convinced that the presented method will be of use to improve the understanding of the behaviour of drying wood. The combination of DSP and CT are useful in many other applications where the measured quantities are of interest.

ACKNOWLEDGEMENTS

This research was supported by Valutec AB, The Foundation for Technology Transfer and the Swedish Foundation for Strategic Research through the Woodtechnology research program

REFERENCES

- Backman, A.C.; Lindberg, K.A.H. 2000. Interaction between wood and polyurethane-alkyd lacquer resulting in a decrease in the glass transition temperature. Paper II in Backman's licentiate thesis "Interaction and Adhesion at the Interface Between Wood and Paint, Glue, Lacquer Measured with DMTA and SEM". Lulea University of Technology, Sweden.
- Choi, D.; Thorpe, J.L. and Hanna, R.B. 1991: Image-analysis to measure strain in wood and paper. *Wood Science and Technology* 25 (4): 251-262.
- Hanhijärvi, A. 1997: Perpendicular-to-grain creep of Finnish softwoods in high temperature drying conditions. Technical Research Centre of Finland. Espoo.
- Jernkvist, L-O.; Thuvander, F. :Experimental determination of stiffness variation across growth rings in *Picea abies*. Accepted for publication in *Holzforschung*.
- Oja, J. 1999: X-ray measurements of properities of saw logs. Doctoral thesis. Lulea University of Technology, Sweden.
- Ormarsson, S. 1999: Numerical analysis of moisture-induced distortions in sawn timber. Doctoral thesis. Chalmers University of Technology, Göteborg, Sweden.
- Lindgren, O. 1992: Medical CT-scanners for non-destructive wood density and moisture content measurements. Doctoral thesis. Lulea University of Technology, Sweden.
- Sepulveda, P. 2000: Non-destructive measurement of spiral grain with Computed Tomography. Licentiate thesis. Lulea University of Technology, Sweden.
- Sjödahl, M. 1997: Accuracy in electronic digital speckle photography. *Applied Optics* 36: 2875-2885.
- Svensson, S. 1997: Internal stress in wood caused by climate variations. Lund Institute of Technology, Sweden.
- Synnergren, P.; Sjödahl, M. 1999: A stereoscopic digital speckle photography system for 3-D displacement field measurements. *Optics and Lasers in Engineering* 31: 425-443.
- Wiberg, P. 2001: X-ray CT-scanning of wood during drying. Doctoral thesis. Lulea University of Technology, Sweden.

Paper II

Measuring strain and moisture content in a cross section of drying wood using Digital Speckle Photography and X-ray Computerised Tomography

J. DANVIND*

Valutec AB, Box 709, SE-931 27 Skellefteå, Sweden

**)Ph. D. student at Luleå University of Technology, Division of Wood Physics, Skellefteå Campus, SE-931 87 Skellefteå, Sweden*

E-mail: jonas.danvind@bigfoot.com

ABSTRACT

In an earlier study, a method for measuring shrinkage behaviour of wood during drying using Digital Speckle Photography (DSP) and X-ray Computerised Tomography (CT) was presented. These two noncontact techniques were used for two-dimensional simultaneous measurement of surface deformation and interior density. The samples studied were cross sections of Scots pine boards with a size of approximately 90x40x18 mm³. In this study, a method has been developed to calculate strain, shear and moisture content from the measured displacement field and density distribution. To obtain the in-plane strain fields, a numerical differentiation of the deformations was performed using a first-order Savitzky-Golay filter. An experimental test resulted in a maximum strain error of 1.1 mstrain. Accuracy in density measurements was expected to be less than ± 6 kg/m³ for wood with moisture content ranging from 6-100% and less than ± 2 kg/m³ in dry wood, at a significance level of 0.05. By combining the uncertainties in strains and densities, the error in calculated moisture content could be estimated to $\pm 1.8\%$ at a significance level of 0.05 by using Monte Carlo simulations. Data collected with the technique presented here will improve understanding of the behaviour of drying wood.

1. INTRODUCTION

Danvind and Synnergren (2001) present a method for measuring displacement and density distribution throughout the cross section of a drying wooden board. Their method is based on using Digital Speckle Photography (DSP) to measure displacements on the end surface and an X-ray Computerised Tomography scanner (X-ray CT scanner) which collects images of the interior density distribution. By combining these two noncontact measuring techniques, the local density and displacement can be determined. For further information, refer to Danvind and Synnergren (2001).

The objective of this study is to present a method for the calculation of local strain, shear and moisture content based on data from the previous method (Danvind and Synnergren 2001).

Response data that is acquired with the method presented in this study is useful for improving understanding of drying wood. For example, the data can be used to improve and/or justify two-dimensional simulation models of drying wooden boards. Another

example is to use multivariate statistics on response data to create descriptive models of drying wood characteristics (see Danvind 2002).

2. MATERIAL

Wood samples studied with this method are prepared in the same way as described by Danvind and Synnergren (2001). In this study, only one sample of Scots pine, *Pinus sylvestris*, was used. The sample size was approximately $150 \times 50 \times 18 \text{ mm}^3$. To simulate the drying of a board cross section, the end surfaces were coated in order to stop drying through the ends. The coating consisted of three thin layers of Polyurethane Alkyd (PUR) varnish ("Celco Golvlack" no. 10133 from Nordsjö) and a thin coat of white high-temperature resistant spray paint. The latter served as a background for black randomised spots (speckles) that were applied using an ordinary spray can. Backman (2000) used this varnish and showed that the varnish has good adhesion to wood.

3. METHOD

This study presents a development of the method presented by Danvind and Synnergren (2001) which measures two-dimensional surface displacements and interior density distribution. The development consists mostly of new software for calculation of strain, shear and moisture content.

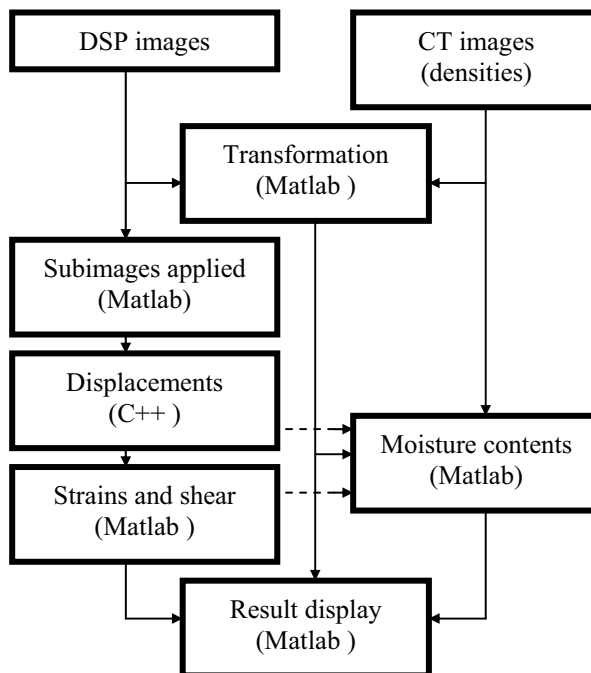


Figure 1. Flow chart for calculating strain, shear and moisture content distribution from image data.

The experimental setup is identical, and the DSP and X-ray CT methods remain the same. For further information on these subjects, refer to Danvind and Synnergren (2001). Figure 1 shows the basic principles of how the strain, shear and moisture content were calculated. The Matlab routines developed in this work are represented by the boxes named “Strains and shear” and “Moisture contents” in Figure 1. The “Result display” box in Figure 1 was developed as a way of presenting the new results.

Here follows a short description of Figure 1. First, DSP images of the end surfaces covered with randomised speckles were captured simultaneously with CT images of the interior. Through a transformation, the positions of points in a DSP image could be found in the corresponding CT image. The DSP image was divided into subimage regions using a custom made Matlab application. A DSP algorithm in C++ calculated the displacements of each subimage region. Then the new functionalities presented in this paper were used to derive strain, shear and moisture content.

3.1. Strain and shear

When wood dries, it shrinks, and the shrinkage is uneven over the cross section due to different shrinkage properties in radial, tangential and longitudinal directions of the tree. Moisture gradients also contribute to uneven shrinkage. In this study, the two-dimensional shrinkage strain field was derived from the previously calculated displacements. To obtain the in-plane strain fields, numerical differentiations of the measured displacements were performed using a Savitzky-Golay filter of the first order (Press et al. 1994). This means that a plane was fitted by the least-square method, having displacement in x - or y -direction, u or v , on the z -axis and original x - and y -positions of the subimage regions on the other axes (Figure 2). The number of neighbouring subimage regions that should be used when fitting the plane was defined by the user. This was typically set to 3×3 subimages, which is equivalent to “`filtsize = 3`” in the Matlab routine. When the plane was fitted, a new “filtered” value for the displacements, u and v , was determined by getting the value of the plane at that point. The equation for a plane is of the form $ax+by+c=0$, and a and b are the gradients of the plane in the x - and y -directions. For the planes fitted to u or v this means that the gradients du/dx , du/dy , dv/dx and dv/dy are acquired and these gradients are the same as the strain and shear in the two dimensions x and y . These planes can be fitted several times, each time reducing noise, but this can also reduce information. Here, the number of times that the planes were fitted was called “smoothings”, and it was typically set to 2.

Information on the co-ordinates of the corners of deformed subimages was needed in order to calculate the moisture content of the subimage regions. To calculate these co-ordinates, the obtained strains and shear were used in equations (4) to (7) in Choi et al. (1991). See also Figure 3.

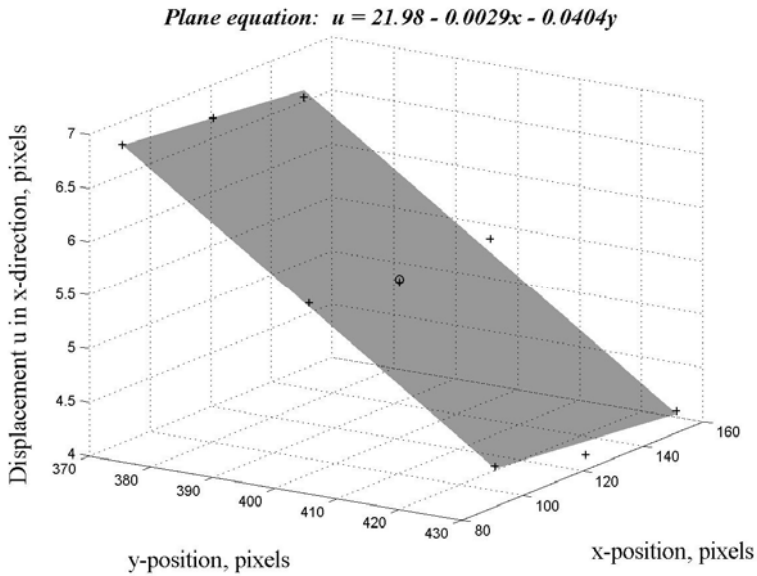


Figure 2. Least-square fit of plane to displacements, first order Savitzky-Golay. Here, a filtered value for the displacement u was calculated for 3×3 neighbouring subimage regions (see the point marked “O”). The strain components $du/dx=0.0029$ and $du/dy=0.0404$ were also acquired. The points marked “+” were the unfiltered displacements of the subimage regions.

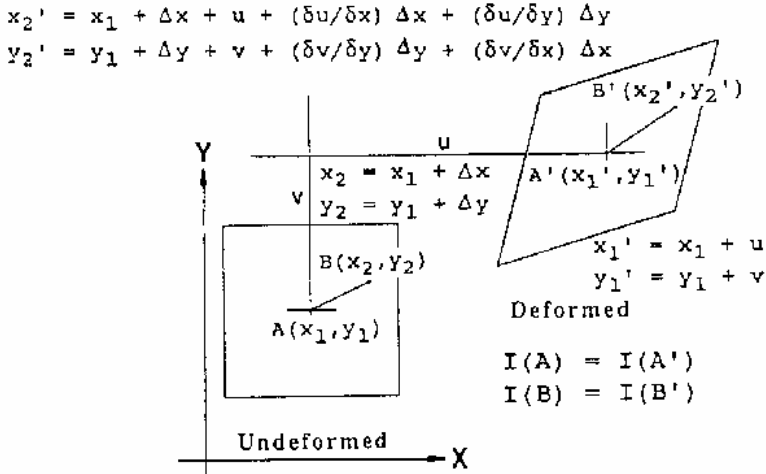


Figure 3. Geometry relationship between deformed and undeformed subimage regions, presented in Choi et. al. (1991).

3.2. Moisture content

As mentioned earlier, moisture gradients contribute to the shrinkage behaviour of wood; therefore, it is interesting to know the local moisture content. Moisture content is defined as the mass of water divided by the mass of absolutely dry wood.

The local combined density of wood and water in each subimage region was found in CT images. In order to calculate the mass, M_t , of the subimage from the density, the local volume for each “pixel region” had to be determined by calculating the area, $A_{i,t}$, (see Figure 4). By “pixel region” is meant the part of a pixel that is inside the subimage region. For most pixels, the whole pixel is within the subimage region, and for these $A_{i,t}=1$. Calculation of $A_{i,t}$ can be quite complicated when the “pixel region” is crossed by one or two of the sidelines of the subimage region, but this is described later on in this paper. Here follow the calculations of area, mass, density and moisture content for a subimage region.

$$A_t = \sum A_{i,t} \quad (1)$$

$$M_{i,t} = \rho_{i,t} \cdot A_{i,t} \cdot d \quad (2)$$

$$M_t = \sum M_{i,t} = \sum \rho_{i,t} \cdot A_{i,t} \cdot d \quad (3)$$

$$M_{t_{dry}} = \sum \rho_{i,t_{dry}} \cdot A_{i,t_{dry}} \cdot d \quad (4)$$

$$\rho_t = \frac{\sum \rho_i \cdot A_i}{\sum A_i} \quad (5)$$

$$MC_t = \frac{M_t - M_{t_{dry}}}{M_{t_{dry}}} = \frac{\sum \rho_{i,t} \cdot A_{i,t} - \sum \rho_{i,t_{dry}} \cdot A_{i,t_{dry}}}{\sum \rho_{i,t_{dry}} \cdot A_{i,t_{dry}}} \quad (6)$$

In equations 1-6, index t is time, index i denotes the current “pixel region”, M is mass, A is area, ρ is density, d is depth of measuring volume and MC is moisture content. All sums are made over the number of “pixel regions” in the subimage region of interest. t_{dry} denotes the time when the sample has 0% moisture content. In case the sample is not dried to 0%, the software can use a manually set reference equilibrium moisture content, which is used to calculate the dry density from the density in the last captured CT image. However, the drawback of doing this is that the reference moisture content is assumed to be equal throughout the cross section; since this is not true, it will introduce an error. Therefore, it is recommended to dry the sample to 0% in the end of the drying session.

The area of a “pixel region”, $A_{i,t}$, was determined by first determining which of the studied pixel’s corner points were within the subimage region and then by checking if the “sidelines of the pixel” were intersected by the limits of the current subimage region (Figure 5). A final check was done in order to determine whether a corner of the subimage region was to be found within $A_{i,t}$. This gave a set of corner points for the “pixel region”, and by using this set, $A_{i,t}$ was obtained.

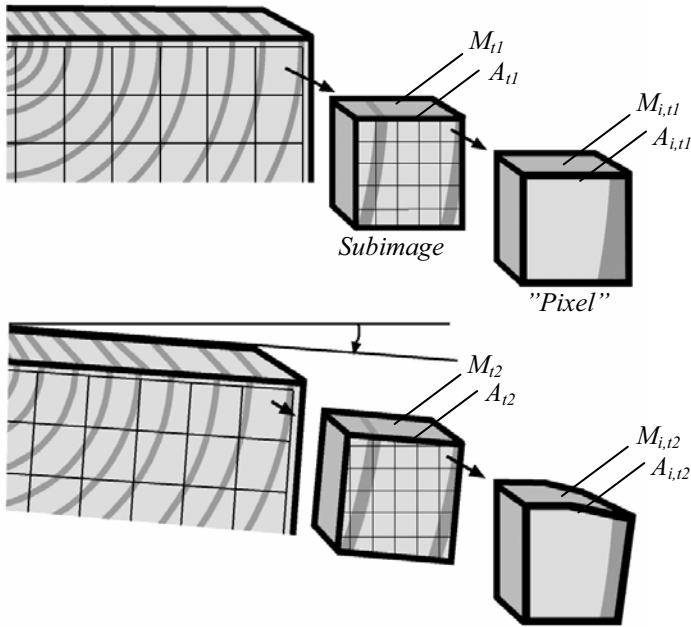


Figure 4. Mass, area and density determination in subimages at time t_1 and t_2 . See text for interpretation of notations.

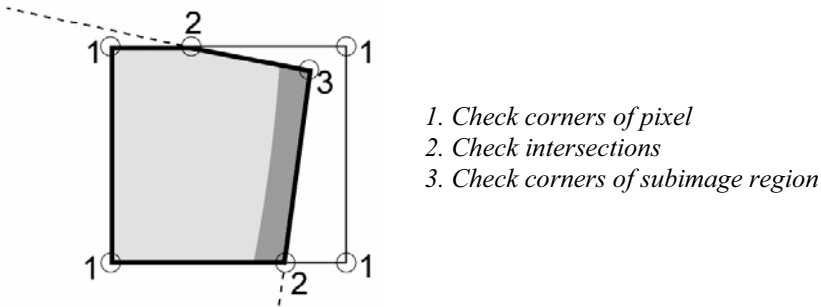


Figure 5. Principles for finding area of a “pixel region”, $A_{i,t}$, within a subimage.

It is not only in the image plane that the measuring volume changes, but also perpendicular to the plane, i.e. in the longitudinal direction. This is due to the longitudinal shrinkage of the sample. However, the measured volume is still limited by the depth of the CT scan, which was set to five millimetres. By assuming a longitudinal swelling coefficient, α_l , and linear shrinkage from an assumed fibre saturation moisture content, u_{fsp} , to zero moisture content, u_0 , the measured moisture content can be compensated according to the following equation:

$$u = u_{final} + \frac{u_{meas} - u_{final}}{1 - \frac{\alpha_l}{u_{fsp}} \cdot (u_{meas} - u_{final} + 1)} \quad (7)$$

where u_{meas} is the measured moisture content, u is the compensated moisture content and u_{final} is the moisture content in the last captured image. u_{final} is the same as the reference moisture content that was mentioned earlier. If $\alpha_l=0.00417$, $u_{fsp}=0.30$, $u_{meas}=0.29$ and $u_{final}=0$, then the compensated moisture content becomes $u=0.2953$. For lower moisture content, the difference between u_{meas} and u is smaller until it reaches zero at $u_{meas}=u_{final}$.

3.3. Moisture content gradients

Once moisture contents in the subimages have been determined, other moisture properties can be calculated, such as moisture gradients in space and time. Moisture gradients in x - and y -direction, dMC/dx and dMC/dy , can be calculated in the same way as the calculation of strains from displacements, as described earlier. The difference here was that the parameters a and b of the fitted plane were the moisture gradients in spatial dimension. Also, the x - and y -values were set as the deformed co-ordinates. An estimation of the time derivative of the moisture content, i.e. the moisture flow dMC/dt , in a subimage was found by subtracting the moisture content of the same subimage in the previous measurement in time and dividing by the length of the time step.

3.4. Local co-ordinates, annual ring orientation

When studying wood behaviour it is more interesting to know the responses in the radial and tangential directions of the wood itself, rather than in the x - and y -directions of the images. This was achieved by transforming the x - and y -results by using the following equation:

$$response_{\theta} = response_x \cdot \cos \theta - response_y \cdot \sin \theta \quad (8)$$

where $response$ is the studied response in the different directions x , y and θ . See Figure 6 for definition of angle θ .

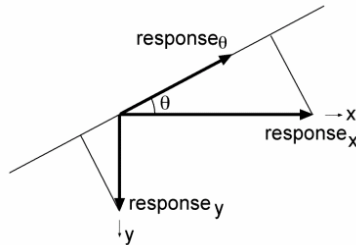


Figure 6. Response in an angle θ from the x -axis.

When calculating strain and shear in radial, r , and tangential, t , directions, the displacements were first transformed to local r - and t -directions of the current subimage. This was done since strains cannot be transformed according to equation (8) due to the influence of shear strains. Also, the x and y co-ordinates of the surrounding subimages used in the Savitzky-Golay filtering were transformed to r and t co-ordinates of the current subimage. Then the radial and tangential strain and shear could be calculated in the same way as in the x - and y -directions.

Local radial and tangential directions were set by defining a position of the pith in relation to a known point in the first digital image. Then the software calculated r - and t -directions in each subimage. The pith position was assumed to be fixed, which was not the case in true behaviour, therefore this introduced an error. Another source of errors was the assumption that the directions of the r and t co-ordinates of the current subimage were unchanged during deformation.

3.5. Additional filtering of erroneous values

Sometimes it is difficult for the DSP algorithm to calculate the correct displacement of a subimage region due, for instance, to low correlation. In order to exclude erroneous displacement values, a threshold was used which was set according to the error value calculated by the DSP algorithm. The error value for a subimage region was output as “0” if the correlation was above 50%. Otherwise, the displacement was considered erroneous and the error was output as “1”. Also filtering based on conditions in relation to nearby displacements was used. As for example; displacement values that differed by more than $\pm 45^\circ$ angle from 60% of neighbouring displacement values were deleted.

3.6. Software user interface

All functions developed for this research were connected to a Graphical User Interface, GUI, in Matlab. This makes it more easily handled by users unfamiliar to the Matlab environment.

4. RESULTS

4.1. Accuracy in measurements

This study focused on the development of a measuring method, therefore the results presented here deal with the accuracy of the measurements.

4.1.1. Displacements

The main parameters influencing the accuracy in DSP measurements are speckle density, contrast and mean speckle size. If high correlation values are obtained, random errors as low as 0.01 pixels on the CCD detector are achievable. According to Sjö Dahl (1997), the random displacement error in the DSP measurements of a 32 by 32 pixel subimage can be estimated by

$$e = 0.03 \cdot \sigma^{1.67} \sqrt{(1 - \delta) / \delta} \quad (9)$$

where σ is the mean speckle size, and δ is the correlation value achieved from the DSP algorithm. The random error is the error corresponding to one standard deviation. The main uncertainty involved in using the error estimation above in this application is the true mean speckle size. However, a good estimation of mean speckle size will result in a good estimation of the displacement error.

4.1.2. Strain and Shear

An experimental evaluation of strain measurement accuracy was done by subjecting a test sample to a rigid body translation in the x -direction, which was approximately 18 pixels or 3.5 millimetres. A translation should give zero measured strain if there are no errors. This means that the measured strains were a measure of the true strain errors for the setup used. The region studied was divided into 4×4 subimage regions each sized 32×32 pixels, approximately $6 \times 6 \text{ mm}^2$ on the sample surface (Figure 7). Strains were calculated using first order Savitzky-Golay filtering (Press et al. 1994) with a 3×3 subimage-region neighbourhood and two smoothing operations. In Table 1, the measured translations, the correlation values, estimated errors and the measured strains are shown. It was found that the largest measured strain error in the x -direction was 1.11 mstrain, which is 0.0011. This can be compared with the maximum magnitude of shrinkage from green to dry which is approximately 40 mstrain and 80 mstrain respectively in the radial and tangential directions of Scots pine and Norway spruce.

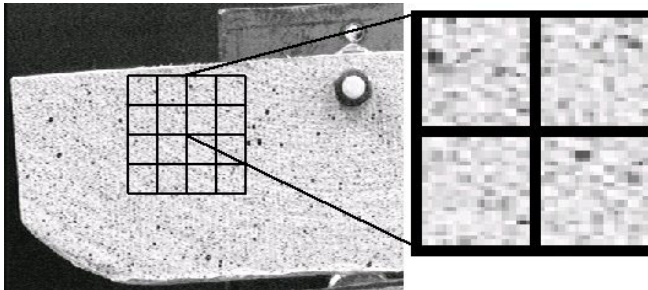


Figure 7. Surface region and 32×32 pixel subimage regions used in experimental evaluation of strains. The whole sample is approximately $150 \times 50 \times 18 \text{ mm}^3$ in size.

An important phenomenon that is not handled by the algorithm for calculation of strains is rotation. No estimation of the influence of rotation of the object on measurement accuracy has been done in this study. This can influence accuracy, especially far away from the rotation centre, which is often the case for the corners of the cross section studied.

4.1.3. Density

The accuracy of density measurements was expected to be better than $\pm 6 \text{ kg/m}^3$ for wet wood with moisture contents ranging from 6-100%, and better than $\pm 2 \text{ kg/m}^3$ in dry wood at a significance level of 0.05. This accuracy was estimated in a $2 \times 2 \times 1.5 \text{ mm}^3$ measuring volume by Lindgren (1992), who performed validations in a similar CT scanner.

Further information on the accuracy of DSP and X-ray CT scanning is given by Danvind and Synnergren (2001).

Table 1. Results from an experimental evaluation of strains. The trial was done by a rigid-body translation of the sample. The translation was approximately 18 pixels in the x -direction and should ideally result in zero strains. *Error* is the calculated estimation of random error (equals one standard deviation) in the measured displacements u and v , according to equation (9). $dudx$ and $dvdv$ are the strains measured in x - and y -direction. For the error estimations, the mean speckle size is set to two pixels in this evaluation. The resolution here was 0.19 mm/pixel.

Subimage	u (mm)	v (mm)	Correlation	Error (mm)	$dudx$ (mstrain)	$dvdv$ (mstrain)
1	3.49	-0.05	0.95	0.0040	1.11	-0.19
2	3.50	-0.05	0.97	0.0033	1.05	-0.10
3	3.50	-0.06	0.96	0.0037	0.89	0.04
...
14	3.51	-0.06	0.95	0.0042	0.90	-0.84
15	3.51	-0.06	0.93	0.0052	0.77	-0.86
16	3.52	-0.07	0.93	0.0052	0.75	-0.84
Mean	3.51	-0.06	0.95	0.0042	0.91	-0.46
Min	3.49	-0.07	0.93	0.0033	0.74	-0.86
Max	3.52	-0.05	0.97	0.0052	1.11	0.15
St.dev.	0.01	0.01	0.01	0.0005	0.13	0.35

4.1.4. Moisture content

The determination of moisture content is influenced by many error sources, such as longitudinal shrinkage, measured density, calculated strain and calculated shear. Longitudinal shrinkage error was corrected by equation (7). Density, strain and shear errors all influence the moisture content calculation, as can be seen in equations (1) to (6), where the subimage region area is dependent on correct strain and shear values. Monte Carlo simulations (Press et al. 1994) of moisture content error on a subimage level were performed based on equation (6). Errors in density and strain were randomised in each simulation, based on a standard deviation of 3.6 kg/m^3 for wet wood (6-100% moisture content), 1.2 kg/m^3 for dry wood and a mean of 1 mstrain and a standard deviation of 0.3 mstrain for the strains in the x - and y -direction. Normal distribution was assumed. The mean error of strain was set as positive +1 mstrain for the strain both at time= t and at time= t_{dry} . Shear was not taken into consideration. The “true” moisture content was subtracted for each moisture content value derived from the randomised values with errors. Fibre saturation point was assumed to be at 0.3, dry density was set to 400 kg/m^3 , maximum shrinkage in the x -direction was assumed to be 4%, and maximum shrinkage in the y -direction 8%. The area, A_t , at time= t was set to $6 \times 6 \text{ mm}^2$. For every 10 kg/m^3 density interval between 400 and 1000 kg/m^3 , 1000 simulations of the error in moisture content was made. In each interval, the mean value of the error and the limits for 0.05 significance level were calculated. The results can be seen in Figure 8, where the mean values are around zero and the upper and lower limits for the 0.05 significance interval for the reference value are approximately $\pm 1.8\%$. Reference value was calculated from the settings stated above. It could be seen that the level of accuracy was most sensitive to errors in the density measurements. Setting the wet density standard deviation to 1.8

kg/m³ and dry density standard deviation to 0.6 kg/m³ reduced the size of moisture content errors by approximately half (values labelled “0.5xStd Density” in Figure 8).

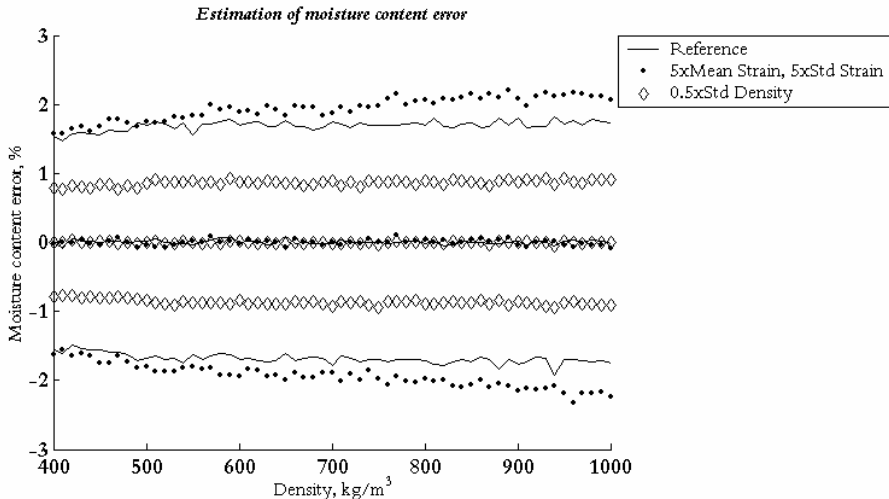


Figure 8. Monte Carlo simulations of estimated errors in moisture content determination caused by density and strain errors. Mean value of estimated errors and confidence interval at 0.05 significance level.

Increasing the mean strain errors and standard deviations fivefold did not influence moisture content to any great extent (values labelled “5xMean Strain, 5xStd Strain” in Figure 8).

It should be remembered that the accuracy of estimated moisture content calculated here has not taken into consideration errors in strain and shear caused by a possible rotation.

5. DISCUSSION

Due to the filtering, “smoothing”, of strains in the neighbourhood of each subimage, strong local differences in strain will not be detected very well. If local strain gradients are important, for example, strain differences in latewood and earlywood, the optical magnification of the digital camera must be increased. This can be achieved by using a microscope, but then the spatial resolution of the CT scanner used here is too low. Instead, high resolution Nuclear Magnetic Resonance (NMR) equipment (Callaghan 1995) or micro tomography equipment (Lindbäck 1999) could be used in combination with the DSP method.

The filtering of strains was very sensitive to erroneous displacement values; hence, the setting of the threshold limit for excluding values was important. If the threshold was low, many erroneous readings were included, and the opposite was true if the threshold was too high. Finding a good trade-off for the threshold is very important in order to achieve as good measuring results as possible.

An interesting result was that the simulations that were used to estimate the accuracy of moisture content measurements (Figure 8) showed that the error in density was the main cause of low accuracy in moisture content determination. However, it should be remembered that the experimental strain error from a rigid body translation was used, and errors caused by rotation were not taken into account. In addition, errors in shear have not been taken into consideration.

Rotation of the measured surface allows strain and shear to be calculated for the subimage regions, although they might not be strained or sheared at all, but only displaced and rotated. Due to the annual ring structure of wood, the subimage regions far away from the polyamide screw will be exposed to a rotation around the screw at the same time as the region might be sheared, strained and translated. The rotation will produce an error that will influence the calculated appearance of the subimage region and thereby also the calculation of moisture content.

A computational test was done in order to compensate for rotation by using polar coordinates with their origin in an estimated pith position outside the sample cross section. The test showed that the method did not work well, since the pith position is not fixed due to the shrinkage of the sample. A reasonable movement of the pith by approximately 4% of the radii towards the sample resulted in an absolute error up to 40 mstrain, which is of the same magnitude as the true movement. Consequently, other ways to compensate for rotation have to be used in this measuring application. Sjødahl (1994) describes three methods based on displacements measured on focused speckles, as used in this study. The first is a differentiating method, which is similar to the one used here. Sjødahl shows that significant errors are introduced by rigid body rotation, which also was the case in this study. In the second method, Sjødahl assumes that the strain of the studied surface is constant, and thereby the strains can be calculated without large influence from rotation. That methodology cannot be used here, since the strains cannot be assumed to be constant. The third method Sjødahl presents uses the compatibility equation of elastic theory, where the following should be satisfied in the xy -plane (the explanations of the variables are excluded here):

$$\frac{d^2 \varepsilon_{xx}}{d^2 y} + \frac{d^2 \varepsilon_{yy}}{d^2 x} = 2 \cdot \frac{d^2 \varepsilon_{xy}}{dxdy} \quad (10)$$

Sjødahl's trials show that this approach also introduces large errors in strain due to rigid body rotation.

As can be understood from this discussion there are some uncertainties considering the performance of this method. However, preliminary full cycle drying tests (not presented here) are quite promising, since strains and moisture contents seem to be at expected levels. Hence, future use of this measuring method will probably contribute to further understanding of error sensitivity in measured properties.

6. FUTURE DEVELOPMENTS

The author proposes that a modified differentiating method that rotates the local coordinate system should be tested in future work. Then the strains can be calculated on a local level. In the proposed method, the rotation, θ , is estimated by an average of the

rotation of the neighbours, mean of θ_A , θ_B , θ_C and so on. Thereafter, the local co-ordinate system is rotated to x' and y' . The positions for the undeformed points are set to the same value in the rotated co-ordinate system (refer to A_{rot} , B_{rot} and C_{rot} in Figure 9). Positions for deformed points are calculated using the DSP algorithm and denoted A' , B' , C' and so on. Now the relative displacements, u' and v' , of the neighbours are calculated in $x'y'$ co-ordinates. Then strain and shear can be calculated by using a first order Savitzky-Golay filtering of the local relative displacements, u' and v' , in the $x'y'$ plane. This method is also useful to determine radial, r , and tangential, t , values, since the rt directions follow the rotation of the xy plane. However, the rt co-ordinates are inclined to the $x'y'$ co-ordinates, and that angle can be determined for the first undeformed image where the pith position is known. Points A to I in Figure 9 are the centre points for subimage regions, and for these points, the displacements are known through calculations using the DSP algorithm.

Calculation of moisture contents based on the area, A , with its corners in the centre points of the subimage regions should be implemented. Faster calculations in software can be achieved by using more intelligent algorithms. By combining this method with measurement of interior pressure, interior temperature and surface temperature, it would be possible to collect even more useful data from drying wood.

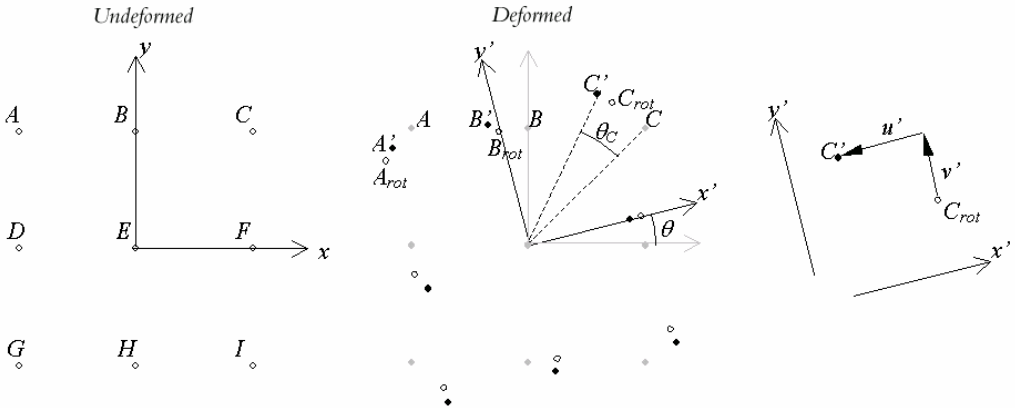


Figure 9. Proposed methodology to handle local rotation of subimage regions by rotating the local co-ordinate axis. Points A to I are the centre points for subimage regions, and for these points, the true displacements are known. Refer to the text for further explanations.

7. CONCLUSIONS

Methods for calculating two-dimensional strain, shear and moisture data of wood have been presented. Suggestions for improvements to the methods were also proposed. The calculations were based on wood-displacement and density data acquired by the presented method earlier (Danvind and Synnergren 2001). Custom made Matlab applications have been developed to perform the calculations and display the results. Data collected with this technique will be of use to improve understanding of the behaviour of drying wood.

8. ACKNOWLEDGEMENTS

This research was supported by Valutec AB, The Foundation for Technology Transfer and the Swedish Foundation for Strategic Research through the Wood Technology research program. Thanks to Per Synnergren and Mikael Sjö Dahl at the Division of Experimental Mechanics, Luleå University of Technology, who made the DSP algorithm and functions for Savitzky-Golay filtering available for use in this application. Thanks to Margot Sehlstedt-Persson for the drawings in Figures 4–6.

9. REFERENCES

- Backman, A.C.; Lindberg, K.A.H. 2000. Interaction between wood and polyurethane-alkyd lacquer resulting in a decrease in the glass transition temperature. Paper II in Backman's Licentiate thesis "Interaction and Adhesion at the Interface Between Wood and Paint, Glue, Lacquer Measured with DMTA and SEM". Luleå University of Technology, Sweden. Thesis No. 2000:51. ISSN 1402-1757
- Callaghan, P.T. 1995. Principles of Nuclear Magnetic Resonance Microscopy. Oxford University Press, Walton Street, Oxford OX2 6DP
- Choi, D.; Thorpe, J.L.; Hanna, R.B. 1991: Image-analysis to measure strain in wood and paper. *Wood Science and Technology* 25 (4): 251-262
- Danvind, J. 2002. PLS prediction as a tool for modeling wood properties. *Holz als Roh- und Werkstoff* 60: 130-140
- Danvind, J.; Synnergren, P. 2001. Method for measuring Shrinkage Behaviour of Drying wood using Digital Speckle Photography and X-ray Computerised Tomography. In: Proceedings of 7th International IUFRO Wood Drying Conference. July 9-13, 2001, Tsukuba, Japan. Pp 276-281
- Lindbäck, S. 1999. Use of Microtomography to measure Resin Penetration and Strains in Wood/FRP Bonds. Master Thesis. Luleå University of Technology, Skeria 3, 931 87 Skellefteå, Sweden. Thesis No. 1999:280 CIV. ISSN 1402-1617
- Lindgren, O. 1992. Medical CT-scanners for non-destructive wood density and moisture content measurements. Doctoral thesis. Luleå University of Technology, Sweden. Thesis No. 1992:111D. ISSN 0348-8373
- Press, W.; Teukolsky, W.; Vetterling, W.; Flannery, B. 1994. Numerical recipes in C, second edition. Textbook. Published by the Press Syndicate of the University of Cambridge. The Pitt Building, Trumpington Street, Cambridge CB2 1RP.
- Sjö Dahl, M. 1994. Strain field measurements using electronic speckle photography: A comparison. In: Recent Advances in Experimental Mechanics, Silva Gomes et. al., ed. A. A. Balkema, Rotterdam, Netherlands, 1994. Pp 325-330
- Sjö Dahl, M. 1997. Accuracy in electronic digital speckle photography. *Applied Optics* 36: 2875-2885

Paper III

USING X-RAY CT-SCANNING FOR MOISTURE AND DISPLACEMENT MEASUREMENTS IN KNOTS AND THEIR SURROUNDINGS

Jonas Danvind ^{1,2}, Tom Morén ²

1: Valutec AB, Box 709, SE-931 27 Skellefteå Sweden, e-mail: jonas.danvind@bigfoot.com

web: <http://www.valutec.se>

2: Luleå University of Technology, Division of Wood Physics, Skellefteå Campus, SE-931 87 Skellefteå Sweden, e-mail: tom.moren@tt.ltu.se

ABSTRACT

Wooden boards that are to be manufactured into planed products are sensitive to checks in knots, since these knots cause problems when planed and surface treated. Knot checks develop mostly during drying, therefore knowledge of moisture movement, strain and stresses in wood during drying is of importance. In this study, a method for non-destructive and non-contact determination of three-dimensional moisture content (MC) distribution was developed. Density scans of a 54x59x200 mm³ piece of Pine wood (*Pinus sylvestris*) have been captured every third millimetre using X-ray Computerised Tomography (CT) technique in a medical Siemens Somatom AR.T. scanner. A method for estimating the two-dimensional pixel displacements, during drying, in these scans (CT images) has been developed. This method is based on the observed pixel's position in relation to the total number of pixels in the object prior to and after deformation caused by drying, which is further explained in the paper. Displacements were used to calculate strains, which are the spatial derivative of the displacements. Displacements and strains were then used to track movements and deformation of local regions in CT images. Final MC distribution for the test piece was estimated using the oven-dry method. When knowing two-dimensional displacements, strains, densities and final MC in the CT images, three-dimensional MC distribution, throughout the drying, was derived. Finally, the MC gradients in three dimensions could be used to estimate directions of moisture flows, based on the assumption that moisture gradient was the driving force.

1. INTRODUCTION

Branches in living trees are vital, since they transport water to the needles or leaves where the photosynthesis take place. This transport of water in branches and their surroundings are probably of importance also when the tree has been felled and cut into sawn timber. Due to the sizes of knots and the strong differences in material orientation near knots it is difficult to study moisture transport phenomenon in these regions. In this paper a method for estimating local three-dimensional (3D) moisture content (MC) distribution using X-ray Computerised Tomography (CT) is presented.

Moisture changes in combination with deviating material orientation around knots cause shape deformation of sawn timber, which can be of practical importance in industry. Foley (2001) presents an approach called the fibre paradigm that describes how material orientation in and around knots can be modelled. The fibre paradigm approach could be used in combination with data collected in this study to derive moisture transport characteristics, such as diffusion coefficients, in different directions of the material.

An important part of this work is the way of estimating displacements in CT images. Lindgren (1992) uses a combined linear, bilinear and nonlinear movement interpolated between the corner points of the cross section in order to calculate the displacements of points between a non-deformed and a deformed CT image. Their method could probably be used in this work

with good results, but the method has the draw back of a tedious work on marking all the reference points.

Digital Speckle Photography (DSP) (Sjödahl, 1995) and other Digital Image Correlation Techniques (Choi et al, 1991) are efficient methods for measuring local displacements in images. It would have been useful to apply such methods directly on CT images, but in the wood drying application the density and thereby the greyscale in CT images are changed a lot. Thereby these methods have poor correlation in the algorithms used, which means they have difficulties finding where the local regions have been displaced.

Danvind and Synnergren (2001) use Digital Speckle Photography (DSP) for high resolution displacement measurements on the surface of a drying wood cross-section using a digital CCD camera. The displacement information is combined with interior density data captured in X-ray CT images which can be used to derive moisture content (Danvind, 2003). In this study the sample was scanned several times along its length and hence it was not sufficient to measure the displacements only on one end surface.

The aim of this work is to present a method for estimating 3D moisture content data in a sample of drying wood based on X-ray CT-images. However, an important limitation in this work is that no evaluation of the estimation error of the method has been done.

2. MATERIAL & METHOD

In this section the material used and the general principles for deriving three-dimensional (3D) moisture content (MC) from CT images are presented.

2.1 X-ray Computerised Tomography, test material and drying

Density scans during drying of a 54x59x200 mm³ piece, Figure 4, of Pine wood (*Pinus sylvestris*) have been captured every third millimetre using X-ray Computerised Tomography (CT) technique in a medical Siemens Somatom AR.T. scanner. This equipment was also used by Wiberg (2001), but for these trials the sample was mounted so that it could be moved in longitudinal direction without taking it out from the drying environment. In this way 3D density data during drying was collected four times, at 0 h, 15.5 h, 24 h and 40 h. The drying air had a dry and wet bulb temperature of approximately 50°C and 30°C, the air speed was approximately 4 m/s. Lindgren (1992) found from studies in a similar medical CT-scanner that the accuracy is ± 6 kg/m³ for wet wood with moisture contents ranging from 6-100%. This accuracy was estimated for a 2x2x1.5 mm³ volume at a significance level of 0.05. In this study the slice thickness for each CT scan was set to 2 mm and sub-image regions were 10x10 pixels, which corresponded to a measuring volume of 2.7x2.7x2 mm³. The larger the measuring volume is the better is the contrast/density resolution, hence the spatial resolution was slightly worse in this study but the contrast resolution was expected to be slightly better than stated above.

2.2 Filtering of object edges

The CT reconstructing algorithm of the image has difficulties near strong gradients in density, i.e. the edges of the studied object. This causes some two-three rows of blurry pixel density values in CT images near the edges of the object. Here the spatial resolution was 0.27 mm per pixel, hence three pixels correspond to approximately 1 mm. As a consequence an edge filtering was introduced. First the CT images in all stacks were processed using a density threshold value of 150 kg/m³, for setting all density values outside the object to zero and all within were set to one. After the threshold operation there remained images that still had blurry edges, with low values near the edge. In order to reduce this noise a new threshold was found for each stack by eroding five pixels from all edges, i.e. the object was shrunk and

values near edges were set to zero, and finding the minimum density values within the eroded object in each stack. These values subtracted by 1 kg/m^3 were used as new thresholds for the stacks, which seemed to give a good filtering of object edges.

2.3 Matching stacks

When scanning the wooden sample there was an uncertainty if the position of the sample was the same each time a stack of CT images was captured. There were probably movements of the object, since it was not fixed in the plastic tube where it was placed. Due to this, a manual matching of the first image in each stack was done. This procedure introduced a positioning error and an estimate is that the error is approximately $\pm 1 \text{ mm}$, considering the scanning interval of 3 mm , the CT slice thickness of 2 mm and the sizes of recognition patterns in the scans used for matching manually. After each scan the sample was automatically translated 3 mm , this movement was assumed to be exact.

2.4 Pixel displacement

A method for estimating two-dimensional displacements of an object in CT images was developed. The method is based on finding a pixel position within the object prior to and after deformation. PM_{ij} is the so called pixel mass in a pixel, with co-ordinates (i,j) , and it has the value 1 if the pixel is within the studied object, otherwise it is 0. These pixel masses were summed and weighted by the total sum for the original image O , equation (1), and the deformed image O' , equation (2). The summation was started from four different directions, namely the four corners of the images, to get more solution lines, which will be explained later. The four summation directions were achieved by flipping the images prior to summation.

$$\frac{\sum_{i=1}^m \sum_{j=1}^n PM_{ij}}{\sum_{i=1}^M \sum_{j=1}^N PM_{ij}} \quad (1)$$

$$\frac{\sum_{i'=1}^{m'} \sum_{j'=1}^{n'} PM_{i'j'}}{\sum_{i'=1}^{M'} \sum_{j'=1}^{N'} PM_{i'j'}} \quad (2)$$

In equations (1) and (2) the pixel mass sum of a pixel, co-ordinates (m,n) in O and (m',n') in O' , weighted by the total sum of pixel masses are given. (M,N) and (M',N') are the image size of O and O' . The apostrophe notation, ', denotes the deformed state. In Figure 1 a graphical presentation of equations (1) and (2) is shown.

The pixel mass sum of a pixel of interest, with the co-ordinates (m,n) , weighted by the total sum in the O image was subtracted from all pixels' mass sums in the deformed image, O' . In equation (3) this is shown for the case when $(m,n)=(131,131)$.

$$\frac{\sum_{i'=1}^{m'} \sum_{j'=1}^{n'} PM_{i'j'} - \sum_{i=1}^{m=131} \sum_{j=1}^{n=131} PM_{ij}}{\sum_{i'=1}^{M'} \sum_{j'=1}^{N'} PM_{i'j'} - \sum_{i=1}^M \sum_{j=1}^N PM_{ij}} \quad (3)$$

Where these new sums are 0, i.e. crosses the xy -plane, there are possible solutions of where the pixel has moved in the deformed state. By repeating this procedure for three more summation directions, four 2nd degree polynomial lines of solutions were achieved and where these intersected it was assumed that the most likely true solutions were, Figure 1. For pixels near the diagonals of the image there were almost parallel solution lines for those lines

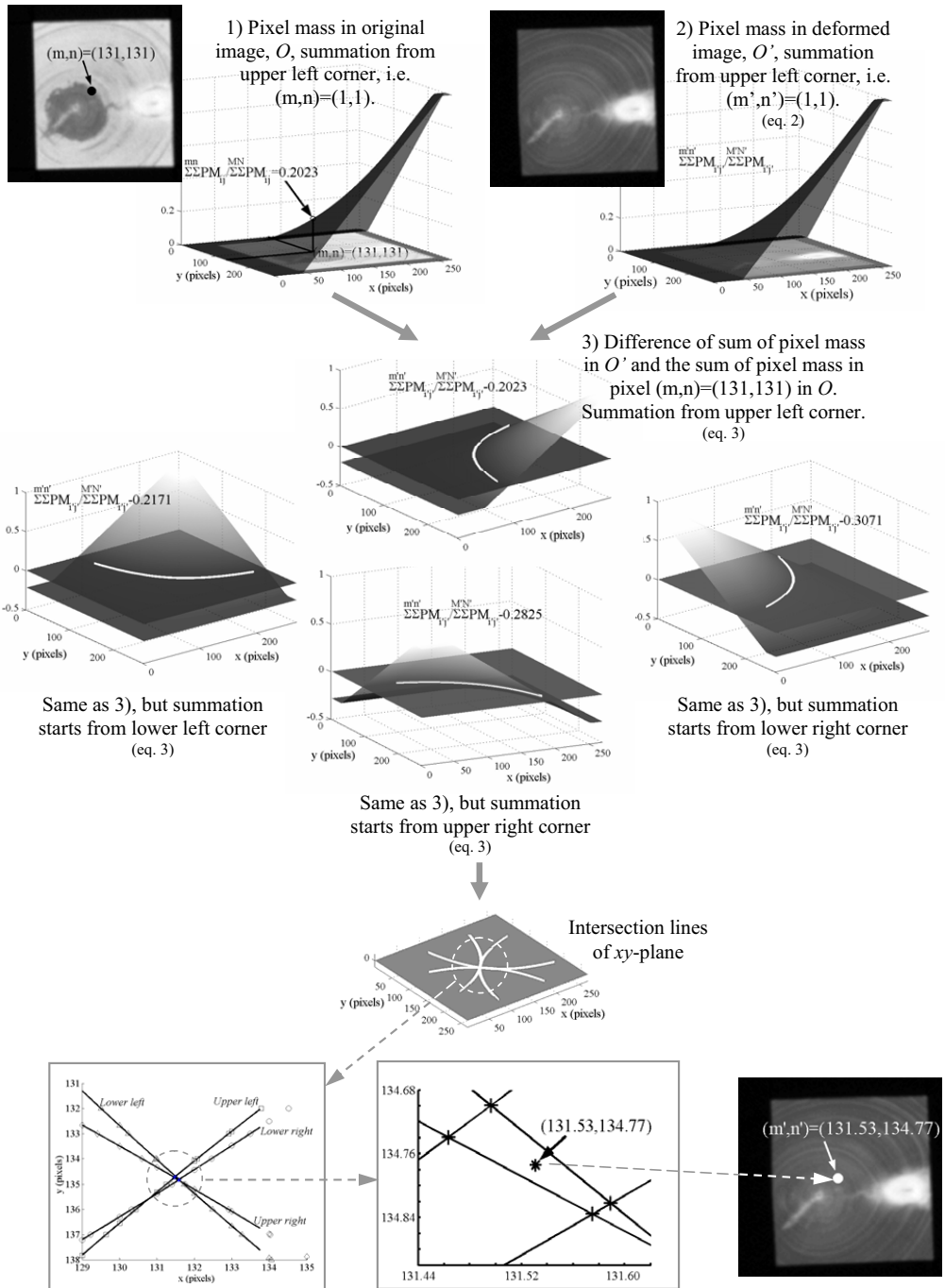


Figure 1. Procedure for estimating the displacement of pixel $(m,n)=(131,131)$ in the original image, O . Through the steps shown above it was estimated that the pixel had moved to $(m',n')=(131.53,134.77)$ in the deformed image, O' .

derived from opposite summation directions, i.e. opposite corners of the image. Therefore the intersections of these almost parallel solution lines were not used for estimating the displacement. In Figure 1 it is shown how the centre of these four intersection solutions was set as the new position for that pixel.

The displacement estimation has difficulties when deriving displacements near edges of the object. This is caused by almost parallel solution lines, as in the case for pixels near the image diagonal as mentioned earlier, and it could have been compensated for by choosing appropriate intersections of solution lines. However, this has not been done here, since a classification of each pixel's position in relation to the image diagonal and the object's edges should have been needed to choose the appropriate intersections of solution lines. Instead, a sub-image displacement on the edge of the object were estimated by fitting a plane equation ($z=a+bx+cy$), using least-squares, to the nearby sub-image displacements off the edges. By inserting the co-ordinates of the sub-image on the edge into the equation, the estimated displacement was returned.

2.5 Increasing computational speed

Displacements of the centres of square sub-image regions were estimated using the developed method. If the displacement for each pixel was to be calculated with this method, the computational time would be long using an ordinary PC. In order to increase computational speed a Matlab built-in linear interpolation function was used when estimating the displacements on pixel level in between the centres of the sub-images. For a pixel outside all centres of sub-image regions, but still within the studied object, the displacement was estimated by fitting a plane equation to the nearby interpolated pixel displacement values. The co-ordinates of the pixel of interest was put into the equation and the estimated pixel displacement was returned.

2.6 Strain and shear

Strain and shear are the spatial derivatives of the displacements, i.e. the gradients of displacements. In this work the 2D displacements in each CT image were calculated and thereby 2D strain field could be estimated. To obtain these in-plane strain fields, numerical differentiations of the measured displacements were performed using a Savitzky-Golay filter of the first order (Press et al. 1994). This means that a plane equation was fitted by the least-square method, having displacement in x - or y -direction, u or v , on the z -axis and original x - and y -positions of the sub-image regions on the other axes. The number of neighbouring sub-image regions was 3×3 sub-images. The equation of a plane is on the form $ax+by+c=z$, and a and b are the gradients of the plane in the x - and y -directions. For the planes fitted to z equal u or v this means that the gradients $\partial u/\partial x$, $\partial u/\partial y$, $\partial v/\partial x$ and $\partial v/\partial y$ are acquired and these gradients are the same as the strain and shear in the two dimensions x and y .

2.7 Moisture content calibration

In the end of drying the wooden test sample was cut into 8-9 mm thick cross sections perpendicular to the sample's longitudinal direction. The MCs of these cross sections were determined using the oven dry method. Also MC gradient measurements were done by cutting each of three clear wood cross sections into 16 smaller samples and oven dry those. In order to set the final MC at pixel level a custom Matlab application was set up. This application matched MC determined by the oven dry tests with corresponding position in the final stack of CT images. It was assumed that the surface MC was equal to the equilibrium MC (EMC) in the ambient air. This assumption is likely if the test sample has been kept in constant climate during long time. By combining the oven dry measured MCs and the surface MC, the MC

distribution in CT images, in the end of drying, could be approximated through 3D interpolation.

2.8 Moisture content during drying

In order to estimate MC in local regions their displacements, sizes, shape changes, densities and densities at 0 % MC had to be known. The displacements were estimated using the method described earlier and the shape changes were achieved through the strain values. The depth size, d , in the z -direction perpendicular to the CT images of each local region, was assumed to be constant. The z -direction is nearly parallel to the longitudinal direction of clear wood in the test sample.

When knowing how the local regions, pixels or sub-image regions, were displaced and deformed throughout the drying process it was possible to also track the density changes in them from the CT images.

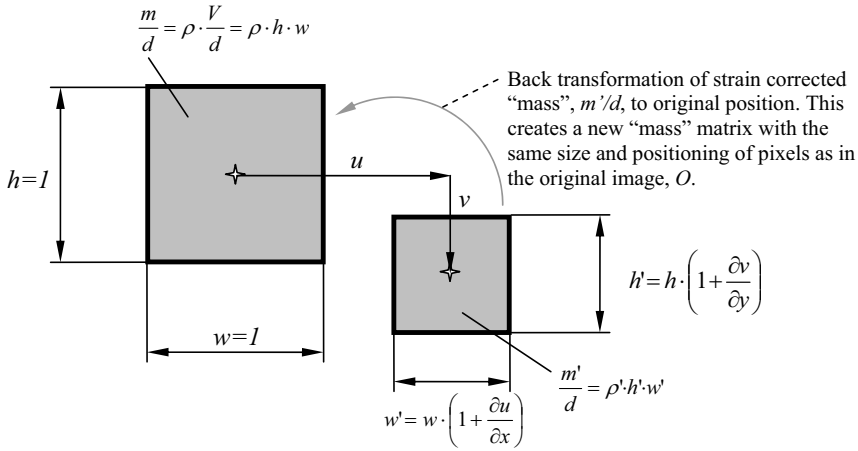


Figure 2. Displacement and shape change of a pixel region. m is mass, u is x -displacement, v is y -displacement, V is volume, ρ is density, h is height, w is width and d is depth. d was assumed to be constant. Apostrophe index denotes deformed state.

Based on the information of density and volume of each region at all scanning points in time, the local region masses could be estimated throughout the drying. From the final calibration MC, MC_{cal} , and final mass, $\rho_{cal} \cdot V_{cal}$, the mass at 0 % MC, m_0 , in each region could be derived (equation 4). By using the masses at 0 % MC, m_0 , and the masses at all points in time, m_t , the MC distribution throughout the drying was found (equation 6). Index t denotes a point in time, h is height of the element and w is width of the element, also see Figure 2.

$$m_0 = \rho_0 \cdot V_0 = \frac{\rho_{cal} \cdot V_{cal}}{1 + MC_{cal}} \quad (4)$$

$$\frac{m_0}{d} = \rho_0 \cdot h_0 \cdot w_0 = \frac{\rho_{cal} \cdot h_{cal} \cdot w_{cal}}{1 + MC_{cal}} \quad (5)$$

$$MC_t = \frac{m_t}{m_0} - 1 = \frac{\rho_t \cdot h_t \cdot w_t \cdot d_t}{\rho_0 \cdot h_0 \cdot w_0 \cdot d_0} - 1 = \{d_t = d_0 = d\} = \frac{\rho_t \cdot h_t \cdot w_t}{\rho_0 \cdot h_0 \cdot w_0} - 1 = \frac{m_t/d}{m_0/d} - 1 \quad (6)$$

It can be seen in equation 6 that the calculation of MC at time t is independent of the depth, d , of the volume elements, since d was assumed constant. Therefore d was not used in the calculations in Matlab, however, it was added here to clarify the explanation of the procedure. For simpler matrix calculations it is convenient to work with matrices of the same size. Hence, matrices with the same sizes as the original images, O , were set up, one for each point in time, where the “mass”, m_t/d , for each pixel was set at the pixels’ original positions (Figure 2). Also matrices for the oven dry “mass”, m_0/d , were set up. Then the MCs in each pixel at all scanning points in time were calculated using equation 6.

Note that only strain was used for estimating shape changes and not the shear values. This approach was chosen since the local regions used were of pixel size and therefore it would not improve the MC accuracy much to shear the displaced local region, pixel, when retrieving its density, since the spatial resolution is no better than one pixel. The displaced pixel’s co-ordinates were not coinciding with the deformed image’s, O' , pixel co-ordinates, hence the density value for the displaced pixel was interpolated from surrounding pixels.

2.9 Moisture gradients and moisture flow

Moisture content spatial gradients were determined on the sub image level by numerical differentiation using the built-in “gradient” function in Matlab. When estimating the most likely flow direction below fibre saturation point the negative gradients of MC in three directions were used, i.e. assuming diffusion controlled flow. Moisture was assumed to be transported in negative moisture gradient direction.

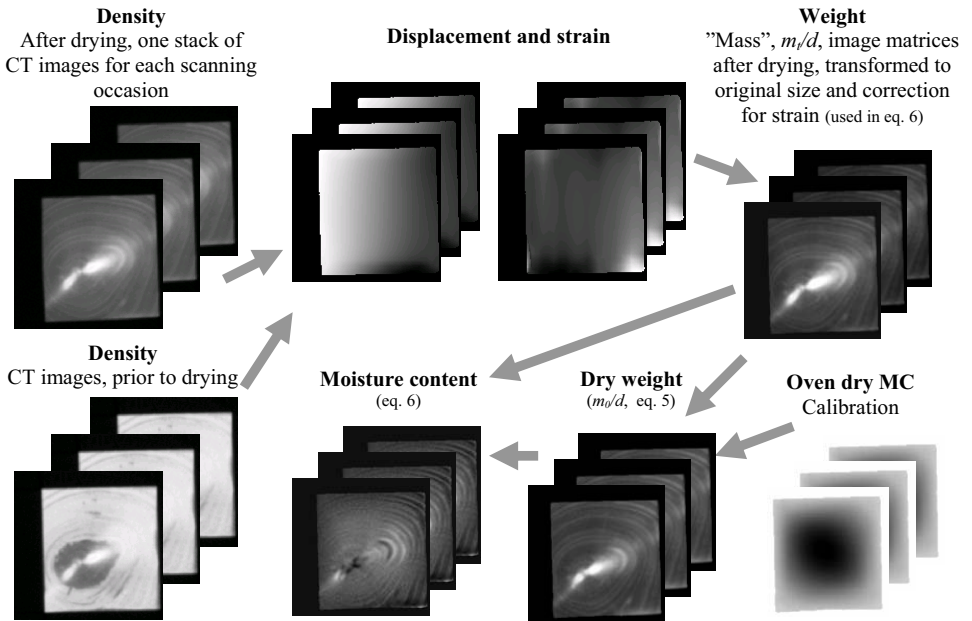


Figure 3. MC estimation procedure.

3. RESULTS

By using the developed methods estimations of 3D density and MC distribution data were achieved. Also 2D in-plane displacements and strains were derived. Considering the large amount of data, graphical presentation of data is a convenient way to get a view of the results.

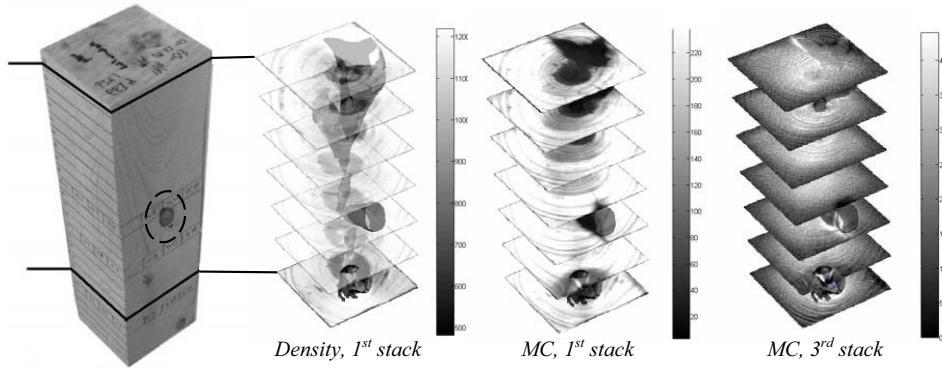


Figure 4. Examples of 3D density and MC distribution. So called iso-surfaces at the constant dry density of 700 kg/m^3 are shown in all images, showing density changes between low and high density regions, for example the knot boundaries.

As expected the MC was lower in knots than in clear wood, and MC in heartwood was lower than for sapwood initially. An interesting result was that MC seemed to be higher under a knot, i.e. on the root side, than above, Figure 5. This could be caused by an orientation of the transport ways of moisture along the fibre direction in the living tree, to transport water from the root via branches to the needles (or leaves). It could also be that a higher density in those regions may result in less moisture movement, which keeps the moisture at a high level when its surroundings dry faster. However, there was not a significant difference in density above and under the knot in this data.

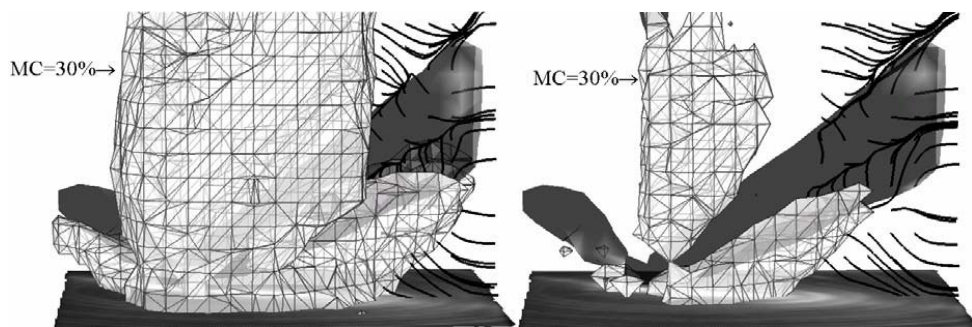


Figure 5. MC iso-surfaces at 30 % MC near two knots, *left: 2nd stack, right: 3rd stack*. Black lines starting from points within and near the right-hand knot are so called stream-lines orientated along negative MC gradient direction. The knot marked by a circle in the left-most image in Figure 4 is the right-hand knot here.

In Figure 5 the main directions of the moisture flow, estimated by MC gradients, are tracked using stream-lines. Stream-lines on the upper side of the knot seem to follow the boundary of

the knot, rather than going into the knot. On the lower side, stream-lines near the knot boundary go into the knot, but stream-lines further down flow away from the boundary. If this is correct, this knot itself can be considered to transport some of the water that comes from its surrounding and some is transported adjacent to the knot boundary. The wood near the knot has a fibre orientation following the knot and has a potential of being a good moisture transport path. It should be noted that if following the annual ring of this lower density wood in the vicinity of the knot, it can turn out that it becomes a part of the knot as it approaches the bark, due to the fibres' orientations follow the knot. However, any conclusions drawn from the stream-lines results near the knot boundaries should be critically reviewed, as discussed in the discussion section.

4. DISCUSSION

It is not recommended to draw any general conclusions on the drying behaviour of knots and their surroundings, considering the limited material studied here.

An important factor influencing the results is the assumption that MC gradient was the driving force for moisture flow. This is most likely in the diffusion regime, i.e. below fibre saturation, and should not be applied in other phases of the drying. Studying the stream-line results in Figure 5 raises the question whether there is a moisture transport from the wood near a high density knot, approximately 1000 kg/m^3 , into to the knot and out to the surface. This can be an artefact of the assumption that the moisture flow is driven by MC gradient. It seems more likely that moisture from the wet region below the knot is not transported into the knot. In order to clarify these questions more sophisticated methods should be used in order to derive directions of flow and also their magnitudes.

There were many steps in the deriving of MC, hence there were many error sources. As errors in density, positioning, displacement, strain and oven dry calibration. An error estimation study, similar to a study by Danvind (2003), should be performed in order to evaluate the influence of accuracy in these factors on MC determination.

Considering all the errors stated above one could question whether this data could be believed in at all. The answer depends on the purpose of the study. When studying relative differences between different local regions within the studied sample the data is believed to be useful. As in this case when studying MC differences in knots and their surroundings.

Based on the information from an evaluation of the displacement errors, as proposed above, the error sensitivity near edges can be studied. Thereby information for testing better ways of choosing the appropriate "solution lines", as described in the section Pixel displacement, for displacements near edges can be tested. If it is shown that different "solution lines" should be used for pixels near edges and pixels near the image diagonal, then an automatic strategy for this can be implemented in the displacement estimation. It is also of interest to evaluate the filtering of object edges in order to increase measuring accuracy near edges to study the development of a "dry shell" (Wiberg, 2001, and Rosenkilde, 2002).

Initial moisture contents above 200 % were estimated for large regions of the sapwood in this trial. This is not impossible if the porosity is high enough, but it can be questioned. No initial MC test was performed that could confirm if the estimated MC levels were reasonable or not.

If there are checks in the deformed images these are often set as a part of the object, depending on the spatial resolution of the tomography algorithm and on the threshold level set for edge filtering. This is difficult to compensate for and therefore moisture content readings near checks should not be trusted.

The displacement method can be used for accurate measurements of larger deformation measurements in CT-images, if there is no drying and the total density is therefore constant (as in the study by Blomberg, 2004). This is done by using the pixel density values in the calculation of displacements and not setting pixel values within the studied object to 1.

5. FUTURE WORK

As emphasized in the discussion it is of importance to perform an error estimation study on the developed method for estimating 3D MC distribution. It is also of interest to estimate the magnitude of moisture flow.

6. CONCLUSIONS

A method for estimating 3D moisture distribution has been presented. The method will be of use to increase the fundamental understanding of drying wood. Results from this study show that knots influence the moisture transport in wood.

7. REFERENCES

Blomberg, J., 2004: Compression mechanisms and strength properties of semi-isostatically densified wood. Licentiate thesis. Luleå University of Technology, Division of Wood Technology, Skeria 3, SE-931 87 Skellefteå, Sweden. Thesis No. 2004:07. ISSN 1402-1757

Choi, D.; Thorpe, J.L.; Hanna, R.B., 1991: Image-analysis to measure strain in wood and paper. *Wood Science and Technology* 25 (4): 251-262

Danvind, J.; Synnergren, P., 2001: Method for measuring Shrinkage Behaviour of Drying wood using Digital Speckle Photography and X-ray Computerised Tomography. In: *Proceedings of 7th International IUFRO Wood Drying Conference*. July 9-13, 2001, Tsukuba, Japan. Pp 276-281

Danvind, J., 2003: Measuring strain and moisture content in a cross section of drying wood using Digital Speckle Photography and X-ray Computerised Tomography. In: *Proceedings of 13th International Symposium on Nondestructive Testing of Wood*, 19-21 August, 2002, University of California, Berkeley Campus, California, USA.

Foley, C., 2001: A three-dimensional paradigm of fiber orientation in timber. *Wood Science and Technology* 35(5): 453-465

Lindgren, O., 1992: Medical CT-Scanners for Non-Destructive Wood Density and Moisture Content Measurements. Doctoral thesis. Luleå University of Technology, Division of Wood Technology, Skeria 3, SE-931 87 Skellefteå, Sweden. Thesis No. 1992:111D

Press, W.; Teukolsky, W.; Vetterling, W.; Flannery, B., 1994: *Numerical recipes in C*, second edition. Textbook. Published by the Press Syndicate of the University of Cambridge. The Pitt Building, Trumpington Street, Cambridge CB2 1RP.

Rosenkilde, A., 2002: High resolution measurement of the surface layer moisture content during drying of wood using a novel magnetic resonance imaging technique. *Holzforschung* 56: 312-317

Sjödahl, M., 1995: Electronic Speckle Photography applied to In-Plane Deformation and Strain Field Measurements. Doctoral thesis. Luleå University of Technology. Division of Experimental Mechanics, Luleå, Sweden. Thesis No. 1995:1710. ISSN 0348-8373

Wiberg, P., 2001: X-ray CT-scanning of Wood During Drying. Doctoral thesis. Luleå University of Technology, Division of Wood Physics, Skeria 3, SE-931 87 Skellefteå, Sweden. Thesis No. 2001:10. ISSN 1402-1544

Paper IV

CALIBRATION OF A CONSTITUTIVE MODEL FOR DIFFUSIVE MOISTURE TRANSPORT IN WOOD USING DATA FROM X-RAY CT-SCANNING AND DIGITAL SPECKLE PHOTOGRAPHY

Jonas Danvind¹, John Eriksson², Håkan Johansson²

¹ Valutec AB, Box 709, SE-93127 Skellefteå, Sweden
e-mail: jonas.danvind@bigfoot.com, web: <http://www.valutec.se>

² Chalmers University of Technology,
Dept of Structural Engineering and Mechanics, SE-41296 Göteborg, Sweden
e-mail: johne@sm.chalmers.se

1 ABSTRACT

An unsteady-state diffusion model is applied for studying wood drying below the fibre saturation point. The moisture diffusion coefficient in Fick's law for Norway spruce under isothermal drying conditions are determined. Using X-ray CT-scanning and Digital Speckle Photography, the wood density and moisture content are obtained in the radial direction of the wood samples. An optimization scheme is used to minimize the difference between observed and computed moisture content in order to calibrate the values of a set of parameters describing the diffusion coefficient. The general idea discussed is not limited to a specific model, but can be used for a wide class of parameter identification problems. In this study, however, the values of the parameters for a parameterization of Arrhenius' type are determined. The results show a good agreement between observed and computed moisture content and the conclusion is that the numerical realization of the optimization scheme works well. Nevertheless, the value of the diffusion coefficient is somewhat higher than expected. This is likely the consequence of a permeable coating of the samples.

2 INTRODUCTION

Models based on diffusion, empiricism and transport mechanics have been developed for analyzing drying of timber (Eriksson, 2004), (Keey et al., 2000). When studying drying that occurs under isothermal conditions below the fibre saturation point, unsteady-state diffusion models have frequently been applied. Such a simplified approach can work quite well if good material data is available. Different experimental techniques such as the cup method combined with analytical or numerical solutions have been applied to determine the material properties. To overcome the shortcomings connected with these techniques, (Olek et al., 2001) points out that a so-called inverse method appears to be a valuable tool for determining the diffusion coefficient. In particular, such a method does not put restraints on the boundary condition or moisture distribution in the sample. In fact, the general idea discussed

is not limited to the diffusion model, but can be used for a wide class of parameter identification problems. For instance, the inverse identification method is useful to take into account surface resistance (Koc et al., 2002) or to determine material parameters in a heat and mass transfer model (Dantas et al., 2003). The aim of this paper is to describe the general idea and to derive a specific scheme for the inverse problem in the context of diffusion. Here, the moisture diffusion coefficient in Fick’s law for a sample of Norway spruce under isothermal drying conditions is determined.

By means of X-ray CT-scanning and Digital Speckle Photography, it is possible to determine the moisture content and wood density in the radial direction of the wood samples. Based on these experimental data and computed results from finite element simulations, an optimization scheme is used to minimize the difference between observed and computed moisture content. In the literature, several parameterizations describing the diffusion coefficient dependencies are proposed and each involves a set of parameter values, c.f. (Koponen, 1984), (Hukka, 1999) and (Keey et al., 2000). In this study the parameter values in an Arrhenius’ type parameterization (c.f. Eq. (24)) are determined. It is noted, however, that in the general setting, the parameters may vary within the sample under consideration and that the implementation of any other parameterization is straightforward.

3 THEORETICAL BACKGROUND

The moisture transport in wood below the fibre saturation point may be described with a diffusion-type partial differential equation in space-time, whereby $x \in \Omega$ and $t \in I = (0, T)$ denote space and time coordinates, respectively. The diffusion coefficient is denoted $D(p, \omega)$, indicating its dependence of the moisture content $\omega(x, t)$ [kg/m³], and a set of parameter values denoted by p . The governing state equation (in the strong form) is then:

$$\dot{\omega} - \frac{\partial}{\partial x} \left(D(p, \omega) \frac{\partial \omega}{\partial x} \right) = 0 \quad x \in \Omega \quad (1)$$

$$\omega = \omega_D, \quad x \in \partial\Omega_D, \quad \text{and} \quad q_n = q_N, \quad x \in \partial\Omega_N$$

with the initial condition $\omega(x, 0) = \omega_0$. The aim of finding the values of the material parameters p to obtain the optimal fit between predicted and measured values of the moisture content may then be formulated as a constrained optimization problem: Find $p \in \mathbb{P}^1$ such that the objective function

$$\mathcal{F} \stackrel{\text{def}}{=} \frac{1}{2} \sum_{i=1}^{N^{\text{obs}}} c_i [\omega(\bar{x}_i, \bar{t}_i) - \omega_i^{\text{obs}}]^2 \quad (2)$$

is minimized for measured values ω_i^{obs} at times $t = \bar{t}_i$ and coordinates $x = \bar{x}_i$ with weight factor c_i (chosen as $c_i = 1/N^{\text{obs}}$). It is noted that, in order to evaluate \mathcal{F} for given values of p , the solution of the state equation (1) is needed to obtain ω .

¹ \mathbb{P} being a space containing all allowable values of p .

There are numerous approaches for minimizing (2). Commonly, these methods are divided into gradient-based and non-gradient methods, where the latter do not need analytical derivatives of the objective function. In general, non-gradient methods are more likely of finding the global minimum among many local ones; however, they also tend to need a greater number of evaluations of the objective function, which in this case is a drawback, since each evaluation of \mathcal{F} involves the solution of a finite element problem and is therefore computationally expensive. Thus, a gradient-based method is preferred. There are methods of combining gradient-based and non-gradient methods to obtain the good features of both types of algorithms, however, this is beyond the scope of this text. For a comprehensive discussion of parameter identification, see (Mahnken, 1998) and references therein.

In order to obtain the derivative of \mathcal{F} with respect to p , a Lagrangian formulation will be utilized. For a detailed description of the methodology, c.f. (Johansson et al., 2003). First, the general idea will be described in an abstract format followed by the interpretation of the general idea in the context of wood drying.

In the abstract setting, the weak variational form of the state equation (1) is represented by (with v as a test function in a suitable test space \mathbb{V})

$$a(p, \omega, v) = l(p, v) \quad \forall v \in \mathbb{V} \quad (3)$$

where $a(p, \omega, v)$ and $l(p, v)$ are semilinear forms, linear only in v . The Lagrangian corresponding to minimizing \mathcal{F} under the constraint (3) is

$$\mathcal{L}(p, \omega, \lambda) = \mathcal{F}(p, \omega) + a(p, \omega, \lambda) - l(p, \lambda) \quad (4)$$

which allows p, ω, λ to be treated as *independent*; in particular, ω is not a function of p . The non-fulfillment of the state equation is embedded in the *costate*, λ , which plays the role of a Lagrangian multiplier.

Then, it can be shown that the minimum of \mathcal{F} corresponds to a stationary Lagrangian \mathcal{L} , i.e., the derivatives of \mathcal{L} with respect to p, ω, λ are all zero

$$\mathcal{L}'_p(p, \omega, \lambda; \delta p) = \mathcal{F}'_p(p, \omega; \delta p) + a'_p(p, \omega, \lambda; \delta p) - l'_p(p, \lambda; \delta p) \quad \forall \delta p \in \mathbb{P} \quad (5)$$

$$\mathcal{L}'_\omega(p, \omega, \lambda; \delta \omega) = \mathcal{F}'_\omega(p, \omega; \delta \omega) + a'_\omega(p, \omega, \lambda; \delta \omega) \quad \forall \delta \omega \in \mathbb{V} \quad (6)$$

$$\mathcal{L}'_\lambda(p, \omega, \lambda; \delta \lambda) = a(p, \omega, \delta \lambda) - l(p, \delta \lambda) \quad \forall \delta \lambda \in \mathbb{V} \quad (7)$$

In (7), it was used that $a(p, \omega, \lambda)$ and $l(p, \lambda)$ are linear in λ . By use of an even shorter notation, $z \stackrel{\text{def}}{=} (p, \omega, \lambda)$, (5)-(7) may be written as

$$\mathcal{L}'_z(z; \delta z) = 0 \quad \forall \delta z \in \mathbb{P} \times \mathbb{V} \times \mathbb{V} \quad (8)$$

Thus, the task of finding p such that \mathcal{F} is minimized under the constraint that the equation of state (3) is satisfied is the equivalent of finding z that solves (8).

In order to solve (8) numerically, the FE-format (subsequently, subscript h denotes the discrete counterpart of a continuous quantity) of (8) is introduced: Find $z_h = (p_h, \omega_h, \lambda_h) \in \mathbb{P}_h \times \mathbb{V}_h \times \mathbb{V}_h$ such that

$$\mathcal{L}'_z(z_h; \delta z_h) = 0 \quad \forall \delta z_h \in \mathbb{P}_h \times \mathbb{V}_h \times \mathbb{V}_h \quad (9)$$

with the particular choice \mathbb{V}_h such that it corresponds to a cG(1)dG(0)-discretization, i.e. piecewise linear and continuous in space and piecewise constant (discontinuous) in time. With a time discretization with N intervals $I_n = (t_{n-1}, t_n)$ of length $k_n = t_n - t_{n-1}$, the discrete format of ω becomes $\omega_h = \sum_{i,n} {}^n W_i {}^n N_i$ where the basis function ${}^n N_i(x_i, t) = 1$, $t \in I_n$ and the nodal values collected in a vector \underline{W} . Analogously, $\lambda_h = \sum_{i,n} {}^n \Lambda_i {}^n N_i$. The simplest assumption of letting p be constant in time and space is made, and $\underline{P} = [p_1, p_2, \dots]$ denotes the values of p in the finite element setting. The Lagrangian may then be considered as a sum of contributions from each time interval n as

$$\mathcal{L}(p, \omega, \lambda) = \sum_{n=1}^N \mathcal{L}_{[n]}(p, \omega, \lambda) \quad (10)$$

where

$$\mathcal{L}_{[n]}(p, \omega, \lambda) = \mathcal{F}_{[n]}(p, \omega) + a_{[n]}(p, \omega, \lambda) - l_{[n]}(p, \lambda) \quad (11)$$

with

$$a_{[n]}(p, \omega, \lambda) = \int_{\Omega} \left[\int_{I_n} \left[\frac{\partial \omega}{\partial t} \lambda + D(p, \omega) \frac{\partial \omega}{\partial x} \frac{\partial \lambda}{\partial x} \right] dt + \llbracket \omega \rrbracket (t_{n-1}) \lambda(t_{n-1}^+) \right] d\Omega \quad (12)$$

where $\llbracket \omega \rrbracket (t_{n-1})$ denotes the "jump" in ω at t_{n-1} , i.e. $\omega(t_{n-1}^+) - \omega(t_{n-1}^-)$.

By the introduction of the residual as $\underline{r} \stackrel{\text{def}}{=} -\mathcal{L}'_z(z_h; \delta z_h)$, the FE-version of (5)-(7) are written as,

$$\underline{r}_p = - \sum_{i=1}^N k_n \int_{\Omega} D'_p(\underline{P}, \omega_h) \frac{\partial \omega_h}{\partial x} \frac{\partial \lambda_h}{\partial x} d\Omega \quad (13)$$

$$\begin{aligned} \underline{r}_{\omega} = & - \sum_{i=1}^{N^{\text{obs}}} c_i [\omega_h(x_i, t_i) - \omega_i^{\text{obs}}] {}^n \underline{N}(x_i, t_i) - \dots \\ & - \int_{\Omega} \left[k_n \left[D'_\omega(p, \omega) \frac{\partial \omega_h}{\partial x} \frac{\partial \lambda_h}{\partial x} {}^n \underline{N} + \dots \right. \right. \\ & \left. \left. + D(p, \omega) \frac{\partial {}^n \underline{N}}{\partial x} \frac{\partial \lambda}{\partial x} \right] - \llbracket \lambda_h \rrbracket (t_n) {}^n \underline{N} \right] d\Omega \quad (14) \end{aligned}$$

$$\underline{r}_{\lambda} = - \int_{\Omega} k_n D(p, \omega) \frac{\partial \omega_h}{\partial x} \frac{\partial {}^n \underline{N}}{\partial x} + \llbracket \omega_h \rrbracket (t_{n-1}) {}^n \underline{N} d\Omega \quad (15)$$

By viewing $\underline{r} = \underline{0}$, $\underline{r} = [\underline{r}_p, \underline{r}_{\omega}, \underline{r}_{\lambda}]^T$, as a set of nonlinear equations in z_h , it is convenient to solve them by means of a Newton method, i.e. for a given iterate $\underline{Z}^{(k)}$, containing the nodal values of z_h as $\underline{Z} = [\underline{P}, \underline{W}, \underline{\Lambda}]^T$, find an update $d\underline{Z}$ by solving

$$\underline{K}^{(k)} d\underline{Z} = \underline{r}^{(k)} \quad (16)$$

involving \underline{K} as the derivative of $-\underline{r}$ with respect to \underline{Z} , i.e. $\underline{K} = \mathcal{L}''_{zz}(z_h; \delta z_h, \delta z_h)$, and obtain the new iterate as $\underline{Z}^{(k+1)} = d\underline{Z} + \underline{Z}^{(k)}$. The procedure is repeated until some optimality criterion is met, usually that some norm of \underline{r} becomes

smaller than a predefined tolerance. On component form, (16) becomes

$$\begin{bmatrix} \underline{K}_{pp} & \underline{K}_{p\omega} & \underline{K}_{p\lambda} \\ \underline{K}_{p\omega}^T & \underline{K}_{\omega\omega} & \underline{K}_{\omega\lambda} \\ \underline{K}_{p\lambda}^T & \underline{K}_{\omega\lambda}^T & \underline{0} \end{bmatrix}^{(k)} \begin{bmatrix} dP \\ dW \\ d\Lambda \end{bmatrix} = \begin{bmatrix} r_p \\ r_\omega \\ r_\lambda \end{bmatrix}^{(k)} \quad (17)$$

where the components are

$$\underline{K}_{pp} = \sum_{n=1}^N \int_{\Omega} k_n D''_{pp}(\underline{P}, \omega_h) \frac{\partial \omega_h}{\partial x} \frac{\partial \lambda_h}{\partial x} d\Omega \quad (18)$$

$$\begin{aligned} \underline{K}_{p\omega[n]} = \int_{\Omega} k_n \left[D''_{p\omega}(\underline{P}, \omega_h) \frac{\partial \omega_h}{\partial x} \frac{\partial \lambda_h}{\partial x} {}^n \underline{N}^T + \dots \right. \\ \left. + D'_p(\underline{P}, \omega_h) \frac{\partial {}^n \underline{N}^T}{\partial x} \frac{\partial \lambda_h}{\partial x} \right] d\Omega \quad (19) \end{aligned}$$

$$\underline{K}_{p\lambda[n]} = \int_{\Omega} k_n D'_p(\underline{P}, \omega_h) \frac{\partial \omega_h}{\partial x} \frac{\partial {}^n \underline{N}^T}{\partial x} d\Omega \quad (20)$$

$$\begin{aligned} \underline{K}_{\omega\omega[n]} = \sum_{i_i \in I_n} c_i {}^n \underline{N}(x_i) {}^n \underline{N}^T(x_i) + \dots \\ + \int_{\Omega} k_n \left[D''_{\omega\omega}(\underline{P}, \omega_h) \frac{\partial \omega_h}{\partial x} \frac{\partial \lambda_h}{\partial x} {}^n \underline{N} {}^n \underline{N}^T + \dots \right. \\ \left. + D'_\omega(\underline{P}, \omega_h) \frac{\partial {}^n \underline{N}^T}{\partial x} \frac{\partial \lambda_h}{\partial x} {}^n \underline{N} + \dots \right. \\ \left. + D'_\omega(\underline{P}, \omega_h) \frac{\partial {}^n \underline{N}}{\partial x} \frac{\partial \lambda_h}{\partial x} {}^n \underline{N}^T \right] d\Omega \quad (21) \end{aligned}$$

$$\begin{aligned} \underline{K}_{\omega\lambda[n,n]} = \int_{\Omega} k_n \left[\left[D'_\omega(\underline{P}, \omega_h) \frac{\partial \omega_h}{\partial x} {}^n \underline{N} + \dots \right. \right. \\ \left. \left. + D(\underline{P}, \omega_h) \frac{\partial {}^n \underline{N}}{\partial x} \right] \frac{\partial {}^n \underline{N}^T}{\partial x} + {}^n \underline{N} {}^n \underline{N}^T \right] d\Omega \quad (22) \end{aligned}$$

$$\underline{K}_{\omega\lambda[n,n+1]} = - \int_{\Omega} {}^n \underline{N} {}^n \underline{N}^T d\Omega \quad (23)$$

For a particular choice of diffusion coefficient parameterization, the Arrhenius' relationship can be written as

$$D(p, \omega) = p_1 e^{p_2 \omega} \quad (24)$$

Thus there are only two parameter values to be determined, denoted by $\underline{P} = [p_1, p_2]$. The derivatives of $D(p, \omega)$ are now obtained in a straightforward fashion as

$$\underline{D}'_p(p, \omega) = \begin{bmatrix} e^{p_2 \omega} \\ p_1 \omega e^{p_2 \omega} \end{bmatrix} \quad (25)$$

and

$$D'_\omega(p, \omega) = p_1 p_2 e^{p_2 \omega} \quad (26)$$

Further, second derivatives are given as

$$\underline{D}''_{pp}(p, \omega) = \begin{bmatrix} 0 & \omega e^{p_2 \omega} \\ \text{sym.} & p_1 \omega^2 e^{p_2 \omega} \end{bmatrix} \quad (27)$$

$$D''_{p\omega}(p, \omega) = \begin{bmatrix} p_2 e^{p_2 \omega} \\ (1 + p_2 \omega) p_1 e^{p_2 \omega} \end{bmatrix} \quad (28)$$

$$D''_{\omega\omega}(p, \omega) = p_1 p_2^2 e^{p_2 \omega} \quad (29)$$

4 MATERIALS AND METHODS

Five green samples were cut from cross sections of Norway spruce, Scots pine and Downy birch, see Figure 1. However, only results from the second sample from the top in Figure 1 are presented below. The sample size was approximately $130 \times 20 \times 20 \text{ mm}^3$ and the softwood samples contained both sapwood and heartwood. All sample surfaces, except the tangential surfaces, were coated using three thin layers of Polyurethane Alkyd (PUR) varnish ("Celco Golvlack" no. 10133 from Nordsjö). A thin coat of white high-temperature resistant spray paint was applied on the front surfaces, Figure 1. The spray served as a background for black randomized spots (speckles) that were applied using an ordinary spray can. In addition to the varnish, a silicone sealing was applied between the samples and on the back surfaces of samples in order to fix them during drying.

Samples were dried at 60°C dry bulb temperature and a varying wet bulb

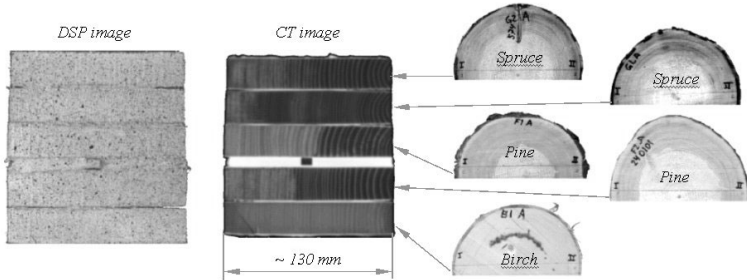


Figure 1: Left: Digital Speckle Photography (DSP) image and X-ray Computerised Tomography (CT) image of samples. Right: Cross sections from where the samples were cut.

between 33 and 46°C , see Figure 2. The speed of the circulation air was approximately 4 m/s .

During drying the moisture content (MC) gradient was estimated every 10th minute using a combination of X-ray Computerized Tomography (CT) and Digital Speckle Photography (DSP). These two techniques measured wood density and drying displacements. Hence, by combining them, MC could be derived (Danvind et al., 2001) and (Danvind, 2003). In Figure 1, a digital CCD image and an X-ray CT image are shown. MC was estimated in 11 equidistant positions in the radial direction of each sample.

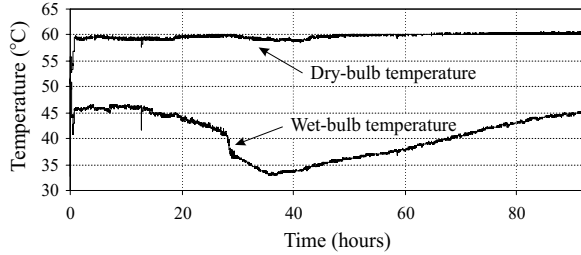


Figure 2: Drying conditions.

5 RESULTS

For a sample of Norway spruce, it was found that the parameter values $\underline{P}=[7.76\text{e-}9,7.63\text{e-}3]$ corresponded to a local minimum with objective function value $\mathcal{F}=5.32$. In Figure 3, the convergence history is shown for starting point $\underline{P}=[5.00\text{e-}9,0]$ using 30 space and 300 time elements. Several combinations of different starting points and space/time discretizations converged to the same optimum. It is thus concluded that the optimization scheme has found the global minimum.

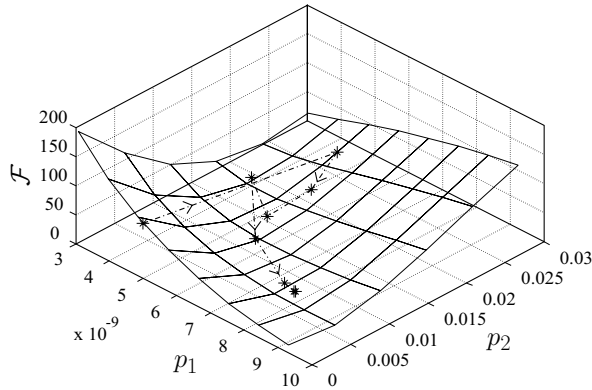


Figure 3: Objective function surface for \mathcal{F} and sequence of \underline{P} used during the optimization procedure.

The fit between the experimental data and the computed moisture content is presented in Figure 4. There, the time zero is set when all moisture measurement points are below the fibre saturation point. It can be concluded from Figure 4 that the agreement is relatively good. Further, the strong dependence of the diffusion coefficient on the moisture content is also captured. Comparison with the results obtained by (Hukka, 1999) shows, however, an unexpectedly high value of the diffusion coefficient.

For other samples (one Norway spruce, two Scots pine and one Downy birch)

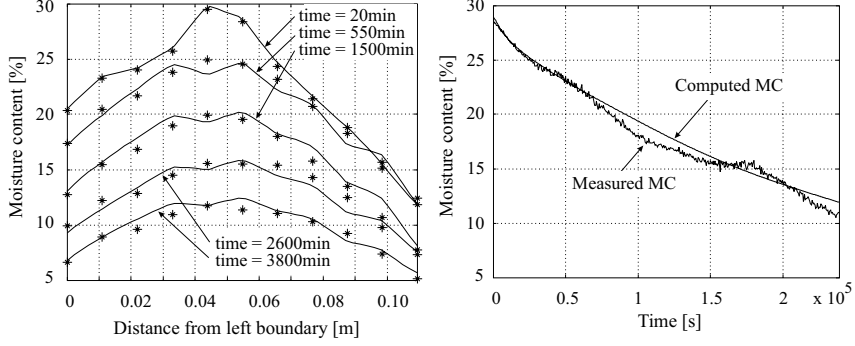


Figure 4: Measured (*) and computed (-) moisture content distribution (left) in space at certain times (right) at $\bar{x} = 0.0547\text{m}$ during drying.

even higher diffusion parameter values ($p_1 \approx 2\text{e-}8$) were found, however, with relatively distinct minima of the objective function.

6 CONCLUSIONS AND DISCUSSION

A reference trial was done in order to investigate if there was any moisture diffusion through the PUR varnish and not only through the tangential surfaces. A new green sample was coated with three layers of varnish and placed in a drying environment of 65°C dry and 51°C wet bulb temperature during 53 hours. The sample was cut from the same cross-section and had similar size as the 2nd sample from the top in Figure 1. It turned out that the varnish was not sufficient to prevent drying, the sample's weight decreased from 22.08 g to 17.34 g. Hence, there was a significant drying by diffusion through the varnish coating or through openings in the coating. The surface coating of the reference sample was studied using a light microscope, but it did not seem to be any visual openings in it. It should be noted that the samples used for diffusion coefficient determination were studied from 30% moisture content and below, and the reference sample was measured from green. The studied samples also had a silicone sealing and a white spray paint on some surfaces, c.f. Section 4. It was believed that the permeable surface coating does question the magnitudes of diffusion coefficients, but not the calibration scheme for deriving them. A further investigation into the characteristics of the varnish is strongly recommended.

On comparing experimentally obtained MC with the predicted ones from the simulation, it is obvious that the diffusion model is able to predict the drying quite well using the calibrated diffusion coefficient. The good fit, despite the permeable coating of the specimens, may be explained by the fact that moisture loss through the coating was compensated in the model by a higher diffusion coefficient. It can, finally, be concluded that the optimization scheme based on FE analysis provides a valuable tool, not only for determin-

ing diffusion coefficients, but may also readily be extended to include surface resistance coefficients. The process can be used for further study of the influence on drying of distance to pith, specie, surrounding climate, wood type etc. in a highly accurate manner.

7 REFERENCES

- Dantas, L. B., Orlando, H. R. B., and Cotte, R. M. (2003). An inverse problem of parameter estimation for heat and mass transfer in capillary porous media. *International Journal of Heat and Mass Transfer*, 46:1587–1598.
- Danvind, J. (2003). Measuring strain and moisture content in a cross section of drying wood using digital speckle photography and x-ray computerised tomography. *Proceedings of 13th International Symposium on Nondestructive Testing of Wood, August 19-21, 2002 University of California, Berkeley Campus, California, USA*. Proceedings available from <http://www.forestprod.org/>.
- Danvind, J. and Synnergren, P. (2001). Method for measuring shrinkage behaviour of drying wood using digital speckle photography and x-ray computerised tomography. *Proceedings of 7th International IUFRO Wood Drying Conference, July 9-18, 2001, Japan*, pages 276–281.
- Eriksson, J. (2004). *Study of moisture flow and moisture-induced distortions in sawn boards and laminated timber products*. Lic. thesis, Chalmers University of Technology.
- Hukka, A. (1999). Diffusion and mass transfer coefficients of nordic softwoods. *Holzforschung*, 53:534–540.
- Johansson, H. and Runesson, K. (2003). Parameter identification in constitutive models via optimization with a posteriori error control. Submitted for publication.
- Keey, R., Langrish, T., and Walker, J. (2000). *Kiln-Drying of lumber*. Springer, Berlin.
- Koc, P. and Houška, M. (2002). Characterization of the sorptive properties of spruce wood by the inverse identification method. *Holz als Roh- und Werkstoff*, 60:265–270.
- Koponen, H. (1984). Dependencies of moisture diffusion coefficients of wood and wooden panels on moisture contents and wood properties. *Paperi ja Puu*, 12:740–745.
- Mahnken, R. (1998). Theoretische und numerische aspekte zur parameteridentifikation und modellierung bei metallischen werkstoffen. Report nr. f 98/2, Institut fuer Mechanik und Numerische Mechanik, University of Hannover.

Olek, W. and Weres, J. (2001). The inverse method for diffusion coefficient identification during water sorption in wood. *Proceedings of the 3rd European COST E15 workshop on wood drying, June 11-13, 2001, Helsinki, Finland.*

Paper V

Local water vapour diffusion coefficient when drying Norway spruce sapwood

Jonas Danvind^{1,2} and Mats Ekevad¹ (corresponding author)

1) Division of Wood Technology, Skellefteå Campus, Luleå University of Technology,
Skeria 3, SE-931 87 Skellefteå, Sweden
Tel. +46 910 585300; Fax +46 910 585399

2) Valutec AB
Box 709, SE-931 27 Skellefteå, Sweden

e-mail: jonas.danvind@valutec.se, mats.ekevad@ltu.se

Key words

Wood, FEM, Drying, Diffusion coefficient, Computed Tomography

Abstract

In this paper a one-dimensional and a two-dimensional approach to the evaluation of local diffusion coefficients for Norway spruce sapwood from measured moisture content (MC) values are presented. A studied wood sample was dried from the initial green condition to about 15% mean MC, but here only the diffusive part of the drying process between approximately 25% and 15% mean MC was treated. Measured local MC values were based on nondestructive x-ray computed tomography data. Finite element calculations were performed with two alternative diffusion coefficients to test the appropriateness of the diffusion coefficients which were evaluated from the measured MC values.

The evaluated diffusion coefficients show interesting dependence on MC and distance from evaporation surface. The advantage of using the methods presented is that the diffusion coefficient is calculated on a local level without having to define a function for the diffusion coefficient's dependency on other parameters.

Introduction

When physically describing the drying behaviour of wood, the drying process can be divided into the capillary part and the diffusion part. In the capillary part the MC (moisture content as mass of water/mass of dry wood) is high and there is free water present in the voids of the wood fibres. When the MC is lower and there is moisture only bound in the cell walls of the fibres, then the moisture flux is driven by diffusion. Internal stresses are induced in the diffusion part of the drying process due to anisotropic shrinkage which may cause checking and drying distortions that reduce the quality of the timber. Large MC gradients during the diffusive part give a fast drying process but cause large stresses. It is of importance to understand the drying behaviour of wood in order to avoid quality degrade due to drying. One way to do this is through simulation.

Simulations of the wood drying process using three-dimensional (3D) finite element method (FEM) can provide detailed and realistic information about the local MC, local stress and global deformation history. 3D FEM calculations require, among other material data, diffusion coefficients that are valid locally throughout the material. The objective of this work is to determine local diffusion coefficients using non-destructive measurements and numerical methods.

Alternative approaches to the evaluation of local diffusion coefficients for Norway spruce sapwood are presented based on experiment. A clearwood sample (Fig. 1) was dried from the initial green condition to about 15% mean MC (mean value for the wood sample in question), but here only the diffusive part of the drying process between approximately 25% and 15% mean MC was treated. The measured local MC values were based on nondestructive x-ray computed tomography (CT) data.

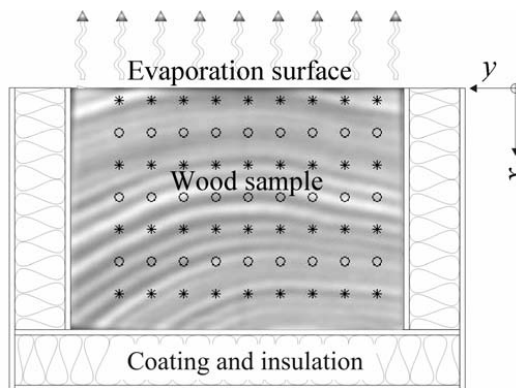


Fig. 1. Wood sample. * and ° denote centre points of cells.

Several authors (Hukka,¹ Hukka and Oksanen,² Liu and Simpson,³ Rosenkilde and Arfvidsson⁴) find that the diffusion coefficient for a certain wood sample is not constant, but dependent on MC in addition to the dependence on temperature. The diffusion coefficients obtained are global mean values for a wood sample of a certain size.

The CT method used here to measure local interior two-dimensional (2D) densities and MCs of the wood sample is described by Lindgren,⁵ Danvind and Moren⁶ and Wiberg⁷. The advantage of using the methods presented in this paper is that the diffusion coefficient is calculated on a local level without having to define a function for the diffusion coefficient's dependencies on other parameters such as MC. The possibility of using CT data to determine other local properties in wood than moisture properties, such as spiral grain angles, is demonstrated by Ekevad⁸ and Sepulveda, Oja and Grönlund⁹.

Theory

Isothermal conditions are considered, and a Cartesian coordinate system and a referential (Lagrangian) viewpoint are adopted in order to deal with the shrinkage of the material. Thus the coordinates x , y and z denote the coordinates of a material point in the green condition, and all lengths, areas and volumes are values in this green state and remain constant during the drying process. In the first approach to determining the diffusion coefficient D , the moisture flux is assumed to be one dimensional (1D) in the radial direction (x) and a modified Fick's first law is stated as

$$g = -D \frac{du}{dx} \quad (1)$$

$g = g(x,t)$ is the mass flux in the positive x direction per area unit, at position x at time t , $u = u(x,t)$ is the MC at x and t . u is used as the driving potential in the modified Fick's first law (Eq.1) instead of using the moisture concentration

$w = u \rho_0$, where $\rho_0 = \rho_0(x)$ is the basic density of wood (dry mass of wood per green volume). It was found experimentally that u is a better way to express the amount of moisture in our case where ρ_0 varied in space (Fig. 2). This was confirmed in our experiments, since it was found that a gradient $dw/dx \neq 0$ could exist without creating a mass flux, due to local variations of ρ_0 . In that case, $dw/dx \neq 0$ due to a gradient $d\rho_0/dx \neq 0$ but $du/dx = 0$. Physically it can be reasoned that u is a better measure of MC than w when it comes to bound water diffusion since water molecules are attracted to wood molecules and not to a specific volume.

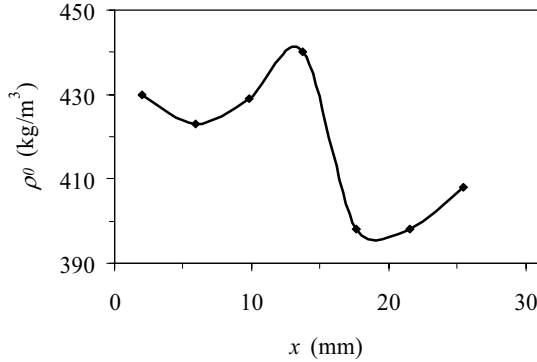


Fig. 2. Measured basic density $\rho_0(x)$.

Mass conservation and Eq. 1 gives

$$\dot{u} = \frac{1}{\rho_0} \frac{d}{dx} \left(D \frac{du}{dx} \right) \quad (2)$$

which is a modified Fick's second law. The general boundary conditions to be used with Eq. 1 and 2 are specified values of u (essential conditions) or g (natural conditions) or

$$g = \beta(u - u_\infty) \quad (3)$$

(convective conditions or mixed conditions) on all or parts of the boundaries. Here the convective condition is used for the evaporation surface and the natural condition $g = 0$ for all the other surfaces. The initial condition is $u = u_0(x, t_0)$ at the starting time t_0 . β is the mass transfer coefficient

for the moisture vaporization into the surrounding air on the boundary surface, and u_∞ is the equilibrium MC for wood under the ambient air conditions.

The equations for 2D mass flux in the x and y directions are a modified Fick's first law for an orthotropic material,

$$\mathbf{g} = (g_x, g_y)^T = -\mathbf{D} \text{grad}(u) = -\mathbf{D} \left(\frac{\partial u}{\partial x}, \frac{\partial u}{\partial y} \right)^T \quad (4)$$

where

$$\mathbf{D} = \begin{bmatrix} D_{xx} & D_{xy} \\ D_{yx} & D_{yy} \end{bmatrix} \quad (5)$$

is the symmetric diffusion coefficient matrix. Here it is assumed that radial and tangential directions coincide with x and y directions, respectively (Fig. 1). Mass conservation and Eq. 4 gives

$$\dot{u} = \frac{1}{\rho_0} \text{div}(\mathbf{D} \text{grad}(u)) \quad (6)$$

or written out

$$\rho_0 \frac{\partial u}{\partial t} = \frac{\partial}{\partial x} \left(D_{xx} \frac{\partial u}{\partial x} + D_{xy} \frac{\partial u}{\partial y} \right) + \frac{\partial}{\partial y} \left(D_{yx} \frac{\partial u}{\partial x} + D_{yy} \frac{\partial u}{\partial y} \right) \quad (7)$$

which is a modified Fick's second law. The boundary conditions are specified values of u or \mathbf{g} or convective conditions (Eq. 3). The initial condition is $u = u_0(x, y, t_0)$.

Materials and methods

A wood sample made of clear sapwood of Norway spruce (*Picea abies*) with the green dimensions 31 mm, 42 mm and 205 mm in the x (radial), y (tangential) and z (longitudinal) directions, respectively, was dried in this study. Five surfaces of the sample were coated using polyurethane glue (Cascol 1809 from Casco) and aluminium foil (Fig. 1). The coated surfaces were also thermally insulated using Styrofoam. Three temperature sensors were placed within the sample at 1 mm, 11 mm and 21 mm depth from the surface, but in different positions in the longitudinal direction. One additional sensor was placed on the surface. During drying, the humidity, temperature and speed of the circulating air was approximately constant at 43% relative humidity, 50°C and 4 m/s, respectively. A Siemens Somatom AR.T. X-ray CT scanner was used to capture a density image in the tangential-radial plane of the interior at a constant longitudinal position every 10 minutes during drying.

Evaluation of D from the CT data, 1D method

$u(x, t)$ values for small volumes (0.14 x 0.14 x 5 mm³) in 3D space (voxel values) were measured with CT (see Danvind and Morén⁶ for a description of the method). In order to reduce spread and increase accuracy, mean MCs $u(x_i, t_j)$ for seven discrete volumes along the x axis with centre positions at $x_i = 2.0, 5.9, 9.8, 13.7, 17.6, 21.6$ and 25.5 mm for $i = 1$ to 7 were evaluated. A value of u at $x_8 = 29.2$ mm was set equal to the value of u at $x = x_7$. $x_0 = 0$ was the surface position, and $x_9 = 31.0$ mm denoted the inner, insulated boundary. u values were measured at discrete time points, t_k ,

between $t_0 = 0$ h and $t_{200} = 100$ h with a time step of 0.5 h, except between $t = 83$ h and $t = 95$ h and between $t = 42.5$ h and $t = 44$ h due to malfunction of the equipment. Denoting d/dx with a prime, using mass conservation and a central difference scheme we get the mass flux gradient,

$$g_i^{\prime k} = -\rho_{0i} \dot{u}_i^k = -\rho_{0i} \frac{(u_i^{k+1} - u_i^{k-1})}{(t_{k+1} - t_{k-1})} \quad (8)$$

where the subindex i denotes the position $x_i = 2.0, 5.9 \dots 29.2$ mm for $i = 1$ to 8 and superindex k denotes the time step $t_k = 0, 0.5, 1.0 \dots$ h for $k = 1$ to 199. An integration of Eq. 8 gives the surface mass flux

$$g_{surf}^k = g(0, t_k) = -\int_0^l g' dx = -\sum_{i=1}^8 g_i^{\prime k} \Delta x_i \quad (9)$$

where $\Delta x_i = x_{i+1} - x_i$ is the length in the x direction of the volume associated with each value u_i . The mass flux at position i is

$$g_i^k = g(x_i, t_k) = g_{surf}^k + \int_0^{x_i} g^{\prime k} dx = g_{surf}^k + \sum_{l=1}^i g_l^{\prime k} \Delta x_l \quad (10)$$

where Δx_l is the length in the x direction of each of the volumes that has x coordinates lower than x_i . Now Eq. 1 with a central difference scheme gives

$$D_i^k = -\frac{g_i^k}{u_i^{\prime k}} = -\frac{g_i^k (x_{i+1} - x_{i-1})}{(u_{i+1}^k - u_{i-1}^k)} \quad (11)$$

The mass transfer coefficient β is evaluated from Eq. 3 as

$$\beta^k = \frac{g_{surf}^k}{(u_{surf}^k - u_\infty)} \quad (12)$$

where u_{surf}^k is evaluated by a parabolic extrapolation to the surface using the three u_i values which are closest to the evaporation surface.

Evaluation of D from the CT data, 2D method

Mean $u(x, y, t)$ values for cells, $4.1 \times 4.1 \times 5 \text{ mm}^3$, in 3D space are evaluated from the CT data. The total mass flux, g_{surf}^k , transferred from the sample at time $t = t^k$ is calculated by using the total mass decrease, the time step $\Delta t^k = t^{k+1} - t^{k-1}$ and the area of the convective surface, A_{surf} . The mass flux is

$$g_{surf}^k = \frac{\sum_{i=1}^M \sum_{j=1}^N (m_{i,j}^{k+1} - m_{i,j}^{k-1})}{\Delta t^k \cdot A_{surf}} \quad (13)$$

where subindices i and j denote the positions in the x and y directions, respectively. $M = 7$ and $N = 9$ are the number of cells in the x and y directions, respectively (Fig. 1), and m is mass.

The mass transfer coefficient, β^k , at time $t = t^k$ is calculated as

$$\beta^k = \frac{g_{surf}^k A_{surf}}{\sum_{j=1}^N (u_{\infty} - u_{surf,j}^k) A_{surf,j}} \quad (14)$$

where $u_{surf,j}^k$ is the MC at time $t = t^k$ for the surface of a cell adjacent to the evaporation surface with $y = y_j$. $u_{surf,j}^k$ is linearly extrapolated from the MCs of the two cells next to the surface. $A_{surf,j}$ is the evaporation surface area of the cell at $y = y_j$. The modified Fick's first law of diffusion (Eq. 4) is used for the mass flux of the interior cell's boundary surfaces. In the first iteration of an iterative scheme, the coupling term, D_{xy} in Eq. 5, is set equal to zero. For a cell on the evaporation surface at position $(i,j) = (surf,j)$, surface mass transfer is assumed to govern the mass flux, which is calculated using β^k from Eq. 14. The modified Fick's second law (Eq. 7) is used for mass balances in cells, and the spatial derivatives of D are assumed to be zero in a cell. Based on these assumptions, Eq. 7 can be stated in numerical form as:

$$\begin{aligned} \rho_0 \frac{u_{ij}^{k+1} - u_{ij}^{k-1}}{t^{k+1} - t^{k-1}} &= \frac{1}{\Delta x} \left[D_{x,i-0.5,j}^k \cdot \frac{u_{i-1,j}^k - u_{i,j}^k}{x_{i-1,j} - x_{i,j}} - D_{x,i+0.5,j}^k \cdot \frac{u_{i,j}^k - u_{i+1,j}^k}{x_{i,j} - x_{i+1,j}} \right] + \\ \frac{1}{\Delta y} \left[D_{y,i,j-0.5}^k \cdot \frac{u_{i,j-1}^k - u_{i,j}^k}{y_{i,j-1} - y_{i,j}} - D_{y,i,j+0.5}^k \cdot \frac{u_{i,j}^k - u_{i,j+1}^k}{y_{i,j} - y_{i,j+1}} \right] &= \left. \begin{aligned} \left. \begin{aligned} x_{i-1,j} - x_{i,j} &= x_{i,j} - x_{i+1,j} = \Delta x; \\ y_{i,j-1} - y_{i,j} &= y_{i,j} - y_{i,j+1} = \Delta y; \\ D_{x,i-0.5,j}^k &= D_{x,i+0.5,j}^k = D_{x,i,j}^k; \\ D_{y,i,j-0.5}^k &= D_{y,i,j+0.5}^k = D_{y,i,j}^k \end{aligned} \right\} \end{aligned} \right\} = \quad (15) \\ &= D_{x,i,j}^k \cdot \frac{1}{\Delta x^2} \cdot [u_{i-1,j}^k - 2u_{i,j}^k + u_{i+1,j}^k] + D_{y,i,j}^k \cdot \frac{1}{\Delta y^2} \cdot [u_{i,j-1}^k - 2u_{i,j}^k + u_{i,j+1}^k] \end{aligned}$$

In the equation above it is assumed that all elements have the same size, Δx and Δy . From the CT experiments, all parameters except $D_{x,i,j}$ and $D_{y,i,j}$ can be achieved for each cell of 30 x 30 voxels in the CT image. Hence, there is one equation (Eq. 15) and two unknowns for each cell; thus the equation system for all elements is underdetermined. By setting $D_{x,i,j}$ and $D_{y,i,j}$ equal in adjacent cells, in this case 2 x 6 cells (8.1 x 24.3 mm), the number of unknowns for the equation system is reduced, and thereby an overestimated system is achieved which is solved in a least-squares sense using standard Matlab¹⁰ routines. By moving the position of the 2 x 6 cells and repeating the calculation procedure 12 times, once for each movement of the cells, 12 sets of $D_{x,i,j}$ and $D_{y,i,j}$ are achieved in each cell. The median values of the 12 solution sets are then taken as estimated solutions of $D_{x,i,j}$ and $D_{y,i,j}$ in each cell.

In a second iteration using u_{ij} , $D_{x,i,j}$ and $D_{y,i,j}$, the mass fluxes, $g_{x,i,j}$ and $g_{y,i,j}$, are calculated using a numerical form of Eq. 4. $g_{x,i,j}$ and $g_{y,i,j}$ are used to recalculate the diffusion coefficients, including the coupling term, D_{xy} . This procedure gives two equations and three unknowns, D_{xx} , D_{yy} and D_{xy} , per cell; i.e., when setting up a matrix system of equations for all cells, an underdetermined system is obtained. This time the number of unknowns is reduced by setting D_{xx} , D_{yy} and D_{xy} constant in 2 x 2 cells and by solving the overdetermined system in a least-squares sense. As before, by moving the position of the 2 x 2 cells and by solving the system 4 times, 4 sets of diffusion coefficients per cell are achieved in each cell, and the median values are chosen as solutions. Using the coupled diffusion coefficients, local mass fluxes can be derived, and the procedure of deriving diffusion coefficients can be iterated until values stabilized. Here, only the first and second iterations have

been done. In this study, the diffusion in the radial direction (x) was to be studied. Therefore diffusion coefficients in the horizontal direction (y) of the CT image are not presented.

FEM calculation

ABAQUS¹¹ was used with a 3D isothermal and isotropic diffusion model as a solver of the diffusion equation (Eq. 6). As boundary conditions, we had zero mass flux on 5 surfaces and convection on the evaporation surface (Fig. 1). The initial condition $u(x, t_0)$ at $t_0 = 30.1$ h was taken from the measured data. Based on experimental findings shown below, two alternatives for D were used. As the first alternative $D = D(u)$ was adapted, and as a second alternative $D = D(u, x)$ was used. The measured values of $\beta(u)$ were used during the FEM calculations.

Results

All results shown in this paper relate to the diffusion part of the total drying process and hence use a time scale which starts at time 30.1 h. The temperature differences between three internal positions in the test sample and in the air were $< 0.8^\circ\text{C}$ during the test. $\rho_0(x)$ is shown in Fig. 2, $u(t)$ for different x values is shown in Fig. 3 and $u(x)$ for different times in Fig. 4. $D(u)$ for the 1D method is shown in Fig. 5a-b for $x \leq 13.7$ mm and $\beta(u)$ is shown in Fig. 6. For the 2D method, $D(u)$ is shown in Fig. 7 and $\beta(u)$ in Fig. 6. The objective in the FEM calculations was to find D values which gave $u(x)$ good correlation to the experimental result at the final time $t = 99$ h. The agreement between experiment and calculation was then checked at an intermediate time $t = 65$ h. The FEM simulation using the first alternative $D = D(u)$ according to Fig. 8a gives an agreement with the CT measurements according to Fig. 4a. The second alternative $D = D(u, x)$ according to Fig. 8b has an agreement according to Fig. 4b. The initial conditions u_0 at $t_0 = 30.1$ h for the FEM simulations are the same for both alternatives.

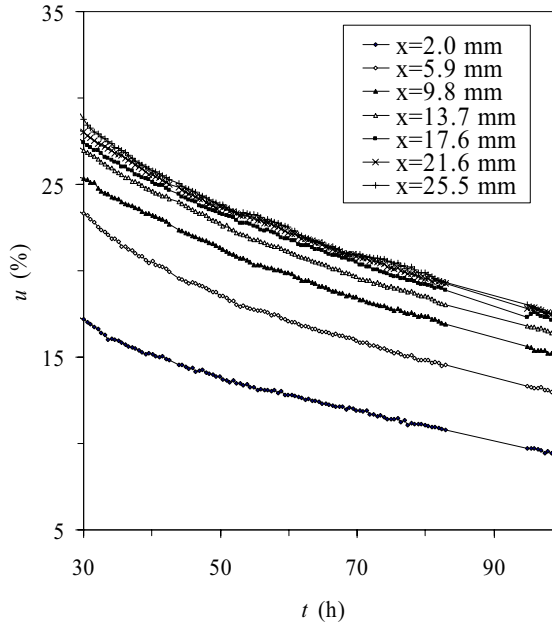


Fig. 3. Measured moisture content $u(t)$ for different x values in consecutive order from the lowest curve with the lowest x value.

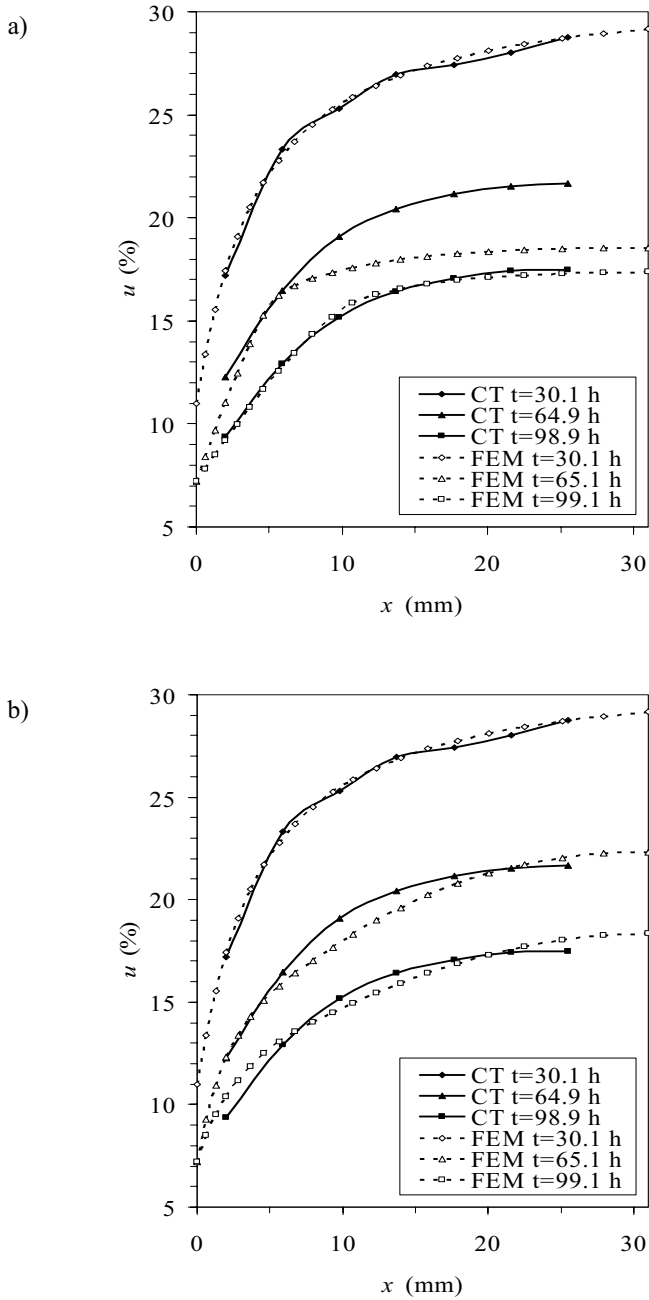


Fig. 4. Moisture content $u(x)$ at different times t measured with CT and calculated with FEM. a: FEM approach $D = D(u)$. b: FEM approach $D = D(u, x)$.

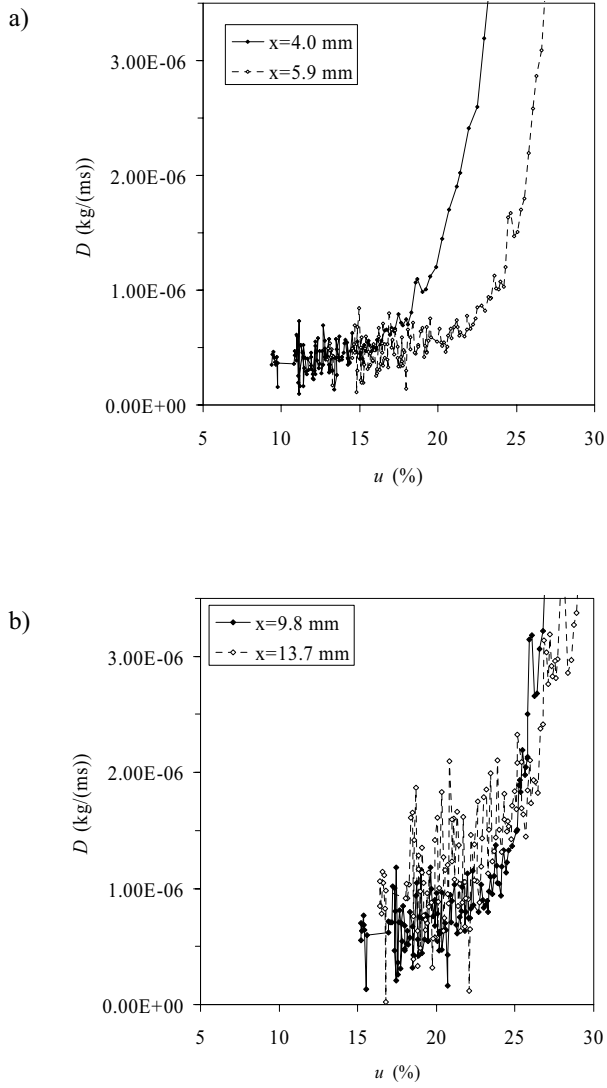


Fig. 5. $D(u)$ evaluated with the 1D method for different x values. a: $x = 4.0$ and 5.9 mm. b: $x = 9.8$ and 13.7 mm.

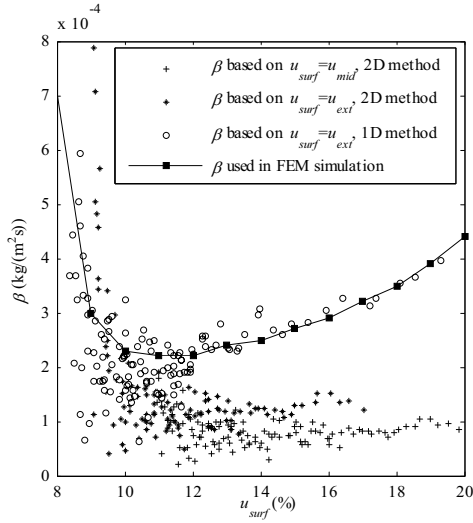


Fig. 6. $\beta(u)$ evaluated with the 1D and the 2D method with alternative surface MCs; u_{ext} – linear extrapolation from two adjacent u values or parabolic extrapolation from three adjacent u values, u_{mid} – mean value of the surface cell; i.e., $u_{mid} = u(x_i = 1, t^k)$.

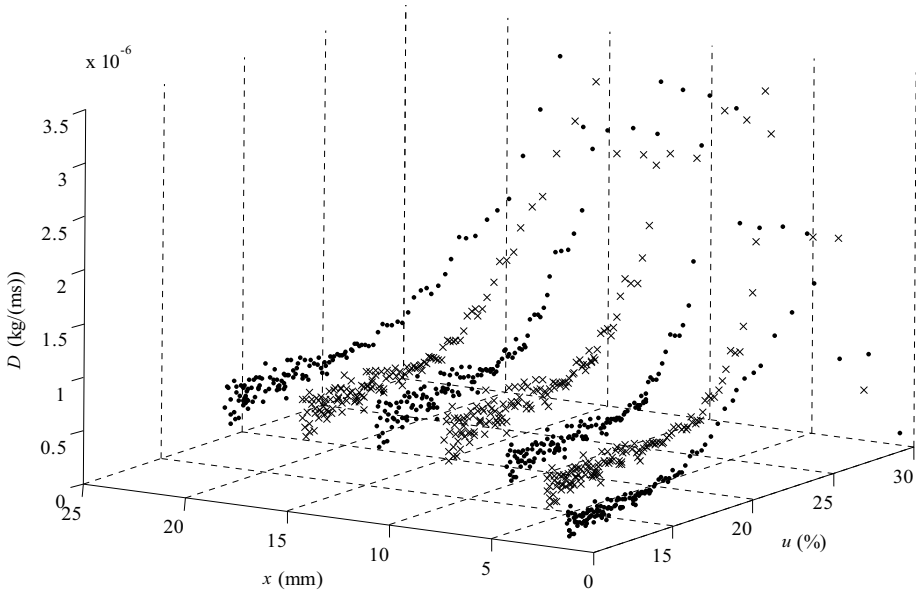


Fig. 7. Diffusion coefficient $D(u,x)$ evaluated with the 2D method. $x = 2.0, 5.9, 9.8, 13.7, 17.6, 21.6, 25.5$ mm.

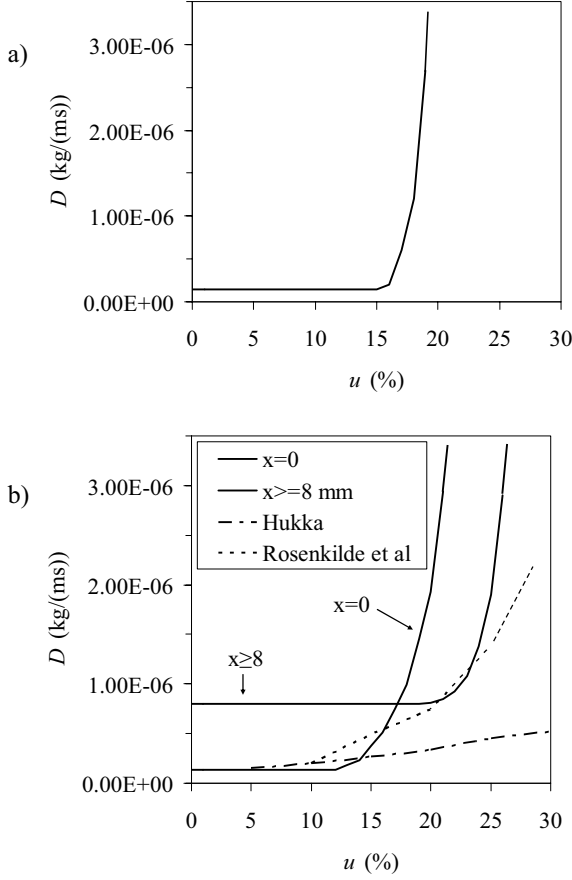


Fig.8. a: $D(u)$ used in the first approach of FEM calculations.
 b: $D(u,x)$ used in the second approach of FEM calculations. Linear interpolation of D for $0 < x < 8$ mm using the curves for $x = 0$ and $x = 8$ mm. Comparison with Hukkas¹ values for Norway spruce heartwood and Rosenkilde and Arfvidssons⁴ values for Scots pine sapwood.

Discussion

For the 1D method, D shows a rather clear dependence on u and x as is seen from Fig. 5a-b. The curves for $x = 5.9, 9.8$ and 13.7 mm agrees well (Fig. 5) but the curve for $x = 4.0$ mm is translated to the left and downwards compared to the other curves. The curve for $x = 17.6$ mm (not shown) agrees quite well with the curves for $x = 5.9, 9.8$ and 13.7 mm, but shows more spread. The curves for $x = 21.6$ and 25.5 mm (not shown) show even more spread, but they seem to agree with the curves for $x = 5.9, 9.8, 13.7$ and 17.6 mm. Thus there is a unique curve for $x = 4.0$ mm, and all of the rest of the curves at the other x values seem to agree reasonably well. The reason for the large spread of D for large x values is probably the decreasing MC gradient and the decreasing mass flux with depth (x), which make the numerical errors large (Eq. 11). The overall conclusion is that the diffusion coefficient is a function of MC and depth, $D = D(u,x)$. The dependence on u is especially large in the interval where $16 < u < 30\%$, while for $u < 16\%$, D seems rather constant. The dependence on the distance from surface x is only significant when $x < 5$ mm, i.e., near the surface. β shows more spread at lower mean MC due to smaller $u_{surf} - u_{\infty}$ than at higher mean MC (Fig. 6).

For the 2D method, only D_x values are presented. This is due to large spread in D_y , probably caused by the one-directional drying resulting in almost constant values of u in the y direction, which strongly influenced the derivation of D_y . D_x values (Fig. 7) are similar to the results from the 1D method, but the results have less spread. A reason for the lower spread is probably the calculation method in which the median values of several solution sets are taken as D . β values for the 2D method are lower than for the 1D method (Fig. 6). This is due to the different choices of u_{surf} .

When trying to reproduce the original, measured $u(x)$ -values at $t = 99.1$ h with the FEM calculation, the second alternative with $D = D(u, x)$ is best (Fig. 4b). This shows the validity of the experimentally derived D values and the dependence of D on distance to the evaporation surface. The first alternative with $D = D(u)$ gave good correlation at $t = 99.1$ h but poor correlation at $t = 65.1$ h (Fig. 4a).

In Fig. 8b, evaluations of D from Hukka¹ and Rosenkilde and Arfvidson⁴ are compared to our values used for FEM calculations. Their values and ours agree quite well, at least for $u < 15\%$. The discrepancy in D for $u > 20\%$ between our values and theirs could be due to differences in wood material (Hukka¹ used Norway spruce heartwood and Rosenkilde and Arfvidson⁴ used Scots pine sapwood) and differences in evaluation methods. Hukka¹ has assumed that $D(u)$ is an exponential function and Rosenkilde and Arfvidson⁴ have used another type of curve fitting method. The rate of the mean MC for a wood sample is essentially controlled by β and not D when u is high, and vice versa. However, an appropriate $D(u)$ description is important for realistic local $u(x)$ -values.

The dependence on depth can be a dependence not on depth itself but via some other parameter (not measured here), which itself is a function of depth. Such a parameter is stress, since there are probably large stresses near the surface. Also, \dot{u} is a function of depth since the material near the surface has a faster changing moisture situation than the material far away from the surface does.

Another possible reason for the behaviour of D near the surface could be the position of the evaporation front during drying. Wiberg⁷ and Rosenkilde and Arfvidsson⁴ show how the evaporation front recedes into the material in the capillary regime of drying, creating a dry “shell” near the surface. This dry shell probably exists also in the beginning of the diffusion regime. The dry shell may have caused $u_{i = 1, j}$ to have lower values than they would have had if the dry shell had not existed. Hence, one can propose to include a dry shell formulation in future evaluations of D , as suggested by Salin¹².

The calculations of D are sensitive to measurement errors of ρ_0 , u , t and x values, since derivatives of u in space and time are estimated by numerical schemes (Eq. 8–11 and Eq. 13–15). An error estimate of u based on the spread of the graph of $\dot{u}(t)$ calculated with a central difference approximation (Eq. 8) was made. The assumption was that $u(t)$ is a normally distributed stochastic variable and that t values are exact, which results in an estimated standard deviation of u on the order of 0.04% when u is approximately 20%. This standard deviation of u is considered low in comparison with earlier values (see Danvind¹³). It is believed that this spread in measured u values is the main cause of spread in D . The spread in D increases when u decreases.

Acknowledgements

The authors express their gratitude to Valutec AB, Formas (the Swedish Research Council for Environment, Agricultural Sciences and Spatial Planning), Vinnova (the Swedish Agency for Innovation Systems) through the Skewood programme and to Kempestiftelsen for their support.

References

1. Hukka A (1999) The Effective Diffusion Coefficient and Mass Transfer Coefficient of Nordic Softwoods as Calculated from Direct Drying Experiments. *Holzforschung* 53:534–540
3. Liu J Y, Simpson W T, Verrill S P (2001) An inverse moisture diffusion algorithm for the determination of diffusion coefficient. *Drying Technology* 19(8):1555–1568
4. Rosenkilde A, Arfvidsson J (1997) Measurement and Evaluation of Moisture Transport Coefficients during Drying of Wood. *Holzforschung* 51:372–380.
5. Lindgren O (1992) Medical CT-scanners for Non-Destructive Wood Density and MC Measurements, Doctoral Thesis, Luleå University of Technology, Thesis No.1992:111D
6. Danvind J, Morén T (2004) Using X-ray CT-scanning for moisture and displacement measurements in knots and their surroundings. EU COST 15 Wood Drying Conference Proceedings, April 22–23, Athens, Greece
7. Wiberg P (2001) X-ray CT-scanning of wood during drying, Doctoral Thesis, Luleå University of Technology, Thesis No.2001:10
8. Ekevad M (2004) Method to compute fiber directions in wood from computed tomography images. *J Wood Sci* 50:41–46.
9. Sepulveda P, Oja J, Grönlund A (2002) Predicting spiral grain by computed tomography of Norway Spruce. *J Wood Science* 48:479–483
10. Anon. Matlab Version 6.1.0.450 release 12.1 (2001) The MathWorks Inc., 3 Apple Hill Drive Natick, MA 01760-2098, USA
11. Anon. ABAQUS Users Manual Version 6.4 (2003), ABAQUS Inc. 1080 Main Street, Pawtucket, USA
12. Salin J G (2002) Theoretical analysis of mass transfer from wooden surfaces. 13th international drying symposium, Aug. 27–30, Beijing, China
13. Danvind J (2002) Measuring strain and moisture content in a cross-section of drying wood using Digital Speckle Photography and Computerised X-ray Tomography. 13th International Symposium on Nondestructive Testing of Wood. 19–21 August, Berkley, California, USA

Paper VI

PLS prediction as a tool for modeling wood properties

J. Danvind

130

During an earlier study, material responses of shrinkage and deformation during air-drying were measured on small wood specimens cut from the cross section of a *Pinus radiata* log. In this paper the analysis of the collected data and the modeling of studied responses were done using multivariate methods. A first model with all variables and all 104 observations was created. In this model there were observations that deviated from the rest and some of them were therefore excluded from further modeling. Also, weak variables and undesired variables were excluded from further modeling. After these exclusions, 77 observations of wood responses below fiber saturation point remained. The results showed good modeling of radial, tangential and volumetric shrinkage between 0–22% MC, with explained variance (R^2) and predicted variance (Q^2) at approximately 0.9, and moderate modeling of longitudinal shrinkage, $R^2 = 0.67$ and $Q^2 = 0.65$. It was also shown that longitudinal shrinkage has weak correlation to density-related variables in the studied wood. No model with good predictability of deformation was found. This study showed that PLS prediction modeling of shrinkage and deformation in studied wood samples was found to be an effective and easy-to-use tool for untangling relationships between variables and generating information from data.

PLS-Vorhersage als Werkzeug zum Modellieren von Holzeigenschaften

In früheren Studien wurden Materialänderungen wie Schwinden und Deformationen während des Lufttrocknens gemessen. Die kleinen Proben waren aus einer Kiefernzscheibe (*P. radiata*) geschnitten worden. In dieser Arbeit erfolgt die Analyse der gesammelten Daten und die Modellierung der beobachteten Veränderungen mit Hilfe multivariater Methoden. Ein erstes Modell wurde mit allen Variablen und allen 104 Beobachtungen erstellt. In diesem Modell wichen einige Beobachtungen stark von den übrigen ab und wurden daher von der weiteren Modellierung

ausgeschlossen. Ebenso ausgeschlossen wurden schwache und unerwünschte Variablen. Danach verblieben 77 Beobachtungen von Holzveränderungen unterhalb des FSP. Radiales, tangenciales und Volumenschwinden im Bereich von 0–22% Feuchte konnten gut modelliert werden mit erklärten Varianzen (R^2) und vorhergesagten Varianzen (Q^2) von rund 0,9. Mäßige Modellierung ergab sich für longitudinales Schwinden ($R^2 = 0,67$ und $Q^2 = 0,65$). Longitudinales Schwinden zeigte zudem eine schwache Korrelation mit den Dichte bezogenen Variablen. Für die Holzverformung wurde kein gut vorhergesagendes Modell gefunden. Die Ergebnisse der Schwind- und Verformungsmodellierung zeigen, daß die PLS-Vorhersage eine gute und leicht zu handhabende Methode ist, um verdeckte Beziehungen zwischen Variablen zu ermitteln und Informationen aus Datensätzen zu gewinnen.

1 Introduction

Wood is a material with strong variations in characteristics, and therefore it is difficult to extract significant information from collected data and generate applicable prediction models.

Partial Least Squares (PLS) regression can be used to study many correlated or uncorrelated variables at the same time and create models with good predictive power, avoiding noise and maximising information, if there are relations to be found. The development of multivariate statistics, such as PLS, accelerated in the field of chemometrics when more sophisticated measuring instruments appeared around 1970, since new instruments generated more information than existing chemical data analysis could handle at that stage (Wold 1996). New powerful methods, Principle Component Analysis (PCA) and others, proved to be useful for describing multivariate data and data classification. Later, PLS was developed for the quantitative modeling of data (Wold 1996). There are several tools for applying multivariate statistics to data sets. This study was done in order to show an example of how PCA and PLS, using SIMCA P 7.01 by Umetrics AB (Anon. 1998), can be applied when creating, evaluating and improving models of wood properties, in this case shrinkage and deformation in wood samples.

When modeling, there are often problems with overfitting of data, i.e. modeling of random variations, or underfitting the data, not being able to extract the maximum possible information from the data set. With PCA and PLS a number of orthogonal latent variables, principal components (PCs), based on original variables, are generated.

J. Danvind
Luleå University of Technology,
Division of Wood Physics, Skellefteå Campus,
SE-93187 Skellefteå, Sweden
e-mail: jonas.danvind@bigfoot.com

This work is financed by Valutec AB, Sweden, Granginge Skog & Trä AB, Sweden, and the Swedish Foundation for Strategic Research (SSF), through the research program Wood Technology. Thanks to Louw van Wyk, Forest Research, Rotorua, New Zealand, for his help with measuring methods.

These variables are used to describe information in the data. In the generation of latent variables for PCA no difference is made between the X and the Y data set; they are treated as one data set. PCA can be useful for data description and data classification. PCA models can approximate large amounts of data and can therefore be useful for data reduction (Wold et al. 1987).

PLS is an extended form of PCA which applies to data sets with two or more blocks of variables (Wold et al. 1987), for example, one independent set of variables, the X-block, and one dependent set of variables, the Y-block. The latent variables of PLS are generated with respect to both the X-block and the Y-block, the set of responses, in order to optimise the latent variables' ability to describe the variance in responses and to yield good predictability. Hence PLS is useful for both data classification and prediction of responses, while PCA is limited to data description and classification.

There are also methods developed for validating data and thereby avoiding modeling of noise. Examples of validation methods are cross validation, permutation testing and external validation (Eriksson et al. 1996).

Lindgren (1994) mentions three advantages for PLS in comparison with Multiple Linear Regression (MLR). PLS can handle correlated variables, noise in the X-data and patterns in residuals, while MLR is based on assumptions of independent x-variables, exact x-variables (no-noise or unbiased modeling, see below) and random distribution of residuals.

According to Wold (1996), PLS is a method based on the existence of bias between model and reality, therefore PLS regressions can never yield "true" models. On the other hand, classical methods, for example MLR, are unbiased regression methods, which try to find "exact" parameters and converge towards "true" values if the underlying model is "true". However, new projection methods with bias, such as PLS, give better predictions and less variance than classical methods and are therefore more useful for studying characteristics in many sets of technical data.

The rule for MLR that the number of variables must be smaller than the number of observations does not apply to PCA and PLS (Geladi and Kowalski 1986), due to the use of projection methods with latent variables. That is the reason why PCA and PLS can treat larger numbers of variables than observations.

According to Geladi and Kowalski (1986), PLS regression is more robust than more classical MLR and Principal Component Regression (PCR) methods. For instance, when using a PLS model, parameters are more stable when calibrating models with new samples taken from the studied population.

The above stated characteristics of PLS regression are some of the reasons why the PLS method, and not classical statistics, was used in this study. PLS regression can be a suitable tool for untangling relations within wood, which are complex due to the diversity of wood characteristics and the lack of well founded fundamental theories applicable to solid wood behavior. In this way the responses can be studied and related to an almost limitless number of factors, independent of fundamental assumptions, and

thereafter the agreement with fundamental theories or the search for new theories can be investigated. However, experimental studies using this method of analysis can be designed with fundamental theories as a base for easier verification or falsification. Regression methods like PLS can thereby become a useful tool for further fundamental understanding of solid wood behavior.

A lot of work using multivariate methods has been done. An instructive example is presented by Eriksson et al. (1996), where three different data sets were modeled and the modeling procedure was well described. Some studies related to the study of wood: Nyström and Hagman (1999) detected compression wood in boards using image analysis, Andersson (1997) sorted saw logs using external features and Marklund et al. (1998) predicted strength parameters of softwood kraft pulps.

The main objective of this study was to present an example of how the software SIMCA-P 7.01 by Umetrics AB (Anon 1998) can be used for PLS-modeling of wood properties. In this case the wood properties studied were shrinkage and deformation during drying of small specimens cut from pith to bark in one slab of *Radiata* Pine.

2

Material and methods

During a study in New Zealand (Danvind 1999) parameters for wooden samples from the cross section of one *Pinus radiata* log during air drying were measured, but the results were not analysed.

The original material and methods used for collecting data are briefly presented in this section. However, the objective is to present the multivariate methods used for analysing collected data.

2.1

Material and experimental methods

Data was collected from *Pinus radiata*. 26 samples sized 300 × 20 × 20 mm and 13 samples sized 300 × 10 × 10 mm, where 300 mm was in the vertical direction of the tree. The samples were cut from a slab taken from the cross section of an approximately 25 year old tree (refer to Fig. 1). No strong visible defects, such as compression wood or severe grain disturbances, were found in the samples.

For 13 of the thicker samples, dimension, deformation and weight were recorded eight times for each sample during drying. Density, moisture content, shrinkage, crook and rotation of the cross section were calculated. The first seven measuring occasions were done during air-drying and the eighth measurement of the samples was done after oven-drying. During air-drying the samples were placed in an upright position in order to avoid constraints and allow them to distort freely. The climate was regulated by an air conditioning system to provide a constant temperature of 20 °C and constant humidity. After air-drying the samples were oven-dried at 103 °C, placed on a metal sheet. In this study the recorded observations from the measuring of samples during drying were denoted, for example, "3 E2", where the first number "3" indicates the third measuring occasion in time and "E2" is the second specimen from pith on the east side of the standing tree.

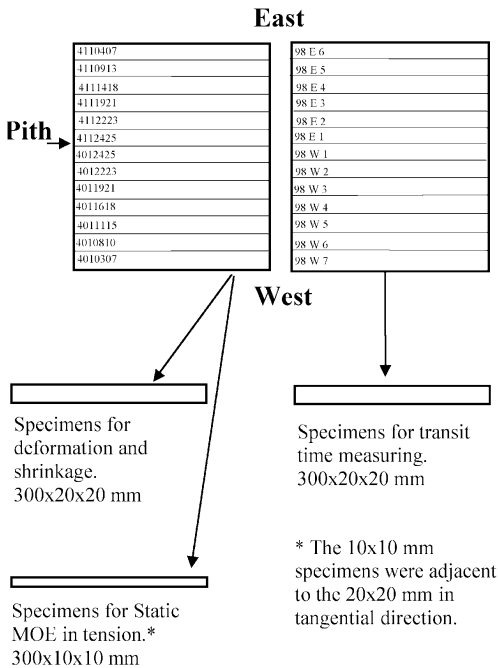


Fig. 1. Specimens cut from the cross section of a *Pinus radiata* slab
Bild 1. Probeneinschnitt aus dem Querschnitt einer Holzscheibe (*P. radiata*)

The $300 \times 10 \times 10$ mm specimens were used for measuring Modulus of Elasticity (MOE) in tension along the longitudinal axis. Transit times for sound waves were measured in the remaining 13 $300 \times 20 \times 20$ mm samples in green state.

Weight, dimensions and deformation were measured with a newly developed measuring system called Stick-Master DD. The system has three Linear Variable Differential Transformers that measure dimensions in three axes and three Laser Displacement Sensors for measurement of deformation. These sensors and a balance were connected to a computer controlling the measuring procedure using software programmed in LabVIEW. MOE was measured with a Zwick Universal Testing Machine and transit times were measured with an ultrasonic emitter and receiver connected to an oscilloscope.

Shrinkage was calculated as the percentile difference in dimension, recorded by the Stickmaster DD, from the first measurement, green, and the actual dimension. Tangential shrinkage, as denoted in this document, was not measured along the tangential direction, but perpendicular to the radial direction. Longitudinal shrinkage was measured along the length of the specimen, not considering spiral grain or other grain deviations.

Deformation was stated in terms of crook and rotation of the cross section.

Density was calculated as dry weight over green volume.

Moisture-content values were generated by recording the weight on each measuring occasion, not considering

whether there were moisture gradients present or not. This was used in combination with the oven dry weight to calculate the moisture content.

For further information on the material, the collected data set and the experimental methods refer to Danvind (1999).

2.2 Theory

In this section a short description of PCA, PLS and validation theory applied in this study is presented.

PCA is a very useful tool used to study the data set and to find hidden patterns, outliers and relations, i.e. data description and data classification (Marklund et al. 1998), in order to get an overview of the data (Wold et al. 1987). However, PCA is not useful for prediction modeling. PCA decreases the number of variables in order to explain as much of the information in the data set as possible with as few components as possible, Principal Components (PC). PCs are created by projecting observations with the use of least square fit. The projected observations on a PC are called scores and the created PCs are orthogonal to each other.

The PCA results are often presented in score plots, where the axes correspond to the direction of the PCs. In score plots outliers and groupings of observations can be identified. By naming the observations in a convenient way one can identify outliers' relations within groups of observations. The axes of the score plots correspond to the PCs. Relations between the different variables can be found in loading plots, in which the axes also correspond to the PCs. The further a variable is from the origin of coordinates of the loading plot, the more important the variable for explaining relations in the data set. However, the distance along the first PC component is more important than the distance along the second and so on, since the first PC explains more of the information in the data set than the second one does. Variables with similar influence on the explanation of the information form groups in loading plots.

PLS is a bilinear regression method for creating prediction models of one or several responses, Y , from a set of factors, X . This method considers both the X -space and the Y -space when finding the optimal principal components. The PCs are found in a similar way as for the PCA, in order to find most of the information in the data set. The PLS algorithm for calculating the PCs is described by Lindgren (1994). Conditions are set to obtain a number of PCs that are significant for modeling and predicting the studied responses and not the additional noise. This can be done by, for example, studying eigenvalues of PCs or by cross-validation (Wold et al. 1987). When using the software SIMCA, the number of significant PCs is automatically generated, either with the eigenvalue or the cross validation method (Anon 1998). The first PC in X -space, with the corresponding score vector t_1 , and the first PC in Y -space, with the corresponding score vector u_1 , are achieved with the PLS algorithm which maximises the correlation between t_1 and u_1 . This correlation between t_1 and u_1 plays an important role in PLS regression and is called the inner relation. The inner relation is often expressed as a linear model (Geladi and Kowalski 1986):

$$u_h = b_h t_h$$

where b_h is a regression coefficient and h is an index for the corresponding PC. The inner relation is found with least squares approximation. Since the relation between t_1 and u_1 is described as linear, the observations in the score plots with t_1/u_1 , t_2/u_2 , t_3/u_3 , and so on, should preferably be as close as possible to the linear regression fit in order to explain a maximum of information. However, data points in score plots with t_1/t_2 , u_1/u_2 , t_1/u_2 , and so on, where the scores correspond to different PCs, should scatter in the plots, since these scores are orthogonal and describe different information in the data set, and they are not connected with inner relations. Still, these plots are useful for data classification when searching for patterns and groups of related observations. Geladi and Kowalski (1986) explain the inner relation used in the Nonlinear Iterative Partial Least Squares (NIPALS) algorithm and also give a tutorial on PLS. PLS regression yields a lot of different graphs and data that can be used for evaluating the prediction modeling. As for PCA, score and loading plots are presented. Also, plots for variable importance, model coefficients, residuals, distance to model plots and validation plots are presented. Some areas of usage for this information are described in the next section, General modeling method.

Validation is of outmost importance for modeling. This is to ensure that as much of the information in the data set and as little of the noise are explained as possible. Cross-validation is a test where first one part of the observations is excluded from the data set and a modified model is made with the remaining observations. This model is used to predict the excluded observations. The same procedure is repeated for the remaining parts of the observations until all observations have been excluded once. Then the Prediction Error Sum of Squares (PRESS) is calculated by adding the squares of the differences between predicted, y_n^* , and observed, y_n for each observation.

$$PRESS = \sum_{n=1}^N (y_n^* - y_n)^2$$

This is then used in combination with the Sum of Squares for y , SS_{yy} , to calculate the prediction ability, called predicted variance, Q^2 .

$$SS_{yy} = \sum_{i=1}^N (\bar{y} - y_i)^2$$

$$Q^2 = 1 - \frac{PRESS}{SS_{yy}}$$

Q^2 can be compared with the explained variance, R^2 , which is a measure of how well the data set is explained, but it does not consider the predictability of new data.

$$SSE = \sum_{i=1}^N (y_i^* - y_i)^2$$

$$R^2 = 1 - \frac{SSE}{SS_{yy}}$$

where SSE is Sum of Squared Errors calculated as the squared difference between modeled observation, y_i^* , (based on all data) and the actual observation, y_i .

The study of Q^2 is important in order to avoid overfitting of the model, with too many variables, expanded terms and PCs. If only R^2 is studied, a model can be developed for almost any data set and get a good R^2 , but also most possibly a poor prediction ability, Q^2 .

Permutation testing evaluates the stability of the developed model by examining whether the model is based on actual relations between model variables and responses, and not only on random relations. In permutation testing, the observations in the Y-matrix are moved around randomly and a new prediction model is made to fit these "new" observations. This is done a certain number of times, recommended 10–25 times (Eriksson et al. 1996). If the original model is based on actual relations, the new models show low R^2 and Q^2 , but if there are a lot of random relations between variables, the new models, or some of them, show high R^2 and Q^2 . Eriksson et al. (1996) recommend interception limits of $Q^2 < 0.05$ and $R^2 < 0.30$ in the validate plots (Fig. 2) to be able to conclude that the achieved model is valid. The interception lines are linear regressions of the Q^2 and R^2 points in the plot. These suggested limits are based on the data analysed in that particular study and may therefore not be applicable to all other studies. In this work the suggested limits are considered as a good rule of thumb. Permutation testing is used for generating validation plots in SIMCA-P 7.01 by Umetrics AB. External testing is another validation test method where an external test set is excluded during modeling, and thereafter the achieved model is applied to predict the values in the test set and the predictability is evaluated.

The choice of methods suitable for validation is highly dependent on the structure of the studied data, which is emphasized by Esbensen and Huang (1999). They also emphasize the importance of external validation in comparison to other validation methods.

2.3

General modeling method

Here follows a brief description of the modeling procedure used in this study in combination with the SIMCA-P 7.01 software. For further information refer to Anon. (1998).

First, it is important to have a good knowledge of the experimental procedure and the expected results for easier analysis and understanding of the data.

Variables that are important for explaining the variance in Y can be identified in the Variable Importance Plot (VIP) where the influence of each variable on the model is shown. The VIP-values are generated from scaled and centred variables' coefficients. In this way the VIP-values corresponding to the variables can be compared in the same plot. The limit for excluding less important variables can be chosen by the user, but if too many variables are excluded, important explanatory information may be lost. There is always a risk that important variables will be excluded, since they might appear as weak variables in a specific model.

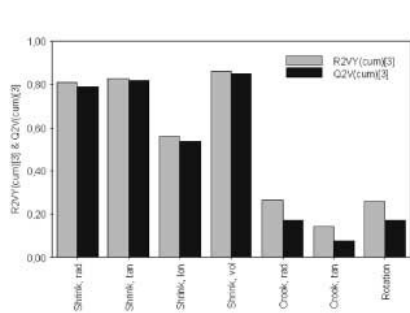


Fig. 2. Left: R^2 and Q^2 for each response showed that shrinkage was well modeled, but crook and rotation were poorly modeled. Right: Validation plot for tangential shrinkage, first model with all observations and variables. “Shrink, tan” proved to be valid, since all prediction models fitted during ten permutations have low R^2 and Q^2 . Thereby it could be concluded that this model predicted mostly information, and not noise. The interception limits of the y-axis were below 0,30 for R^2 and 0,05 for Q^2 , which was preferred by Eriksson et al. (1996). “Shrink, rad”, “Shrink, vol” and “Shrink, lon” showed similar appearance in their validation plots and were therefore also considered valid

Exclude observations prior to the exclusion of variables, since one extreme outlier might severely influence important variables to appear unimportant, so called leverage (Wold et al. 1987). When adding variables, it is of importance to ensure that the model is still valid and predicts information, and not random variations.

Explained variance, R^2 , and predicted variance, Q^2 , are evaluated. They should both be as high as possible, <1 . The difference between Q^2 and R^2 should be as low as possible. Also carry out permutation testing and plot validation plots to ensure that the model is valid (refer to Section 2.2 for suggested interception limits). If needed, perform external testing.

Residuals contain unexplained variance in the data set and are not described by the model. Look for deviating observations in plots of the residuals, Distance to Model plots (DMODX and DMODY), and score and loading plots. Check whether these can be related to experimental errors or any other known reason. If so, consider excluding these observations and creating a new model. Also look for patterns in the residuals and if there are patterns try to change the data set by, for example, expanding some of the variables or crossing them. If the changes do not improve the model, return to the old model. Remember that when observations have been excluded, it is recommended that the new model contain all the original variables, since they might have had low influence on the original model, due to the distorting effect that the outliers could have had on the model.

If the observations are close to the regression line in score plots, $t1/u1$, $t2/u2$ and so on, Fig. 3, the model is well fitted. Look for outliers and examine possible reasons why these are outliers and exclude them from the model, if possible. Examine nonlinearities and clusters of observations in score plots; consider modeling each group sepa-

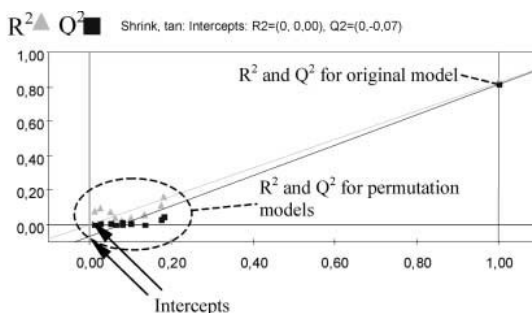


Bild 2. Links: R^2 und Q^2 jeder Korrelation zeigten, daß das Schwinden gut modelliert werden konnte, nur Längskrümmung und Verdrehung waren schwach modelliert. Rechts: Verifikations-Graph für tangenciales Schwinden; erstes Modell mit allen Variablen. “Shrink, tan” erwies sich als gültig, da alle Vorhersage-Modelle in zehn Permutationen jeweils geringe R^2 und Q^2 hatten. Daraus kann gefolgert werden, daß dieses Modell überwiegend Information und nicht Rauschen vorhersagt. Die Schnittgrenzen mit der y-Achse waren $<0,3$ für R^2 und $<0,05$ für Q^2 , wie es von Eriksson et al. (1996) bevorzugt wurde. “Shrink, rad”, “Shrink, vol” und “Shrink, lon” zeigten ähnliches Verhalten und wurden daher ebenfalls als gültig betrachtet

rately. Keep in mind that PCA finds groupings that are independent of the Y-space; therefore there is a risk in only performing PLS, since the patterns found with PCA might not be detected. Therefore it is preferable to do both.

Loading plots (Fig. 4) show relations between factors and responses. Consider modeling possible groups of observations separately, for example, only shrinkage responses and not deformation.

Histogram plots show the distribution of observations for different variables in an easy way (Fig. 9). They are useful for displaying patterns in sample data that may be of influence when modeling.

3 Modeling

The following responses and factors were included in the data set in this study:

Responses	Factors
Shrink, rad	Distance from pith
Shrink, tan	Moisture Content, MC
Shrink, lon	Time
Shrink, vol	Density (kg/m^3)
Crook, rad	Ring No.
Crook, tan	No. of rings
Rotation	Transit time (ms)
	MOE (GPa)

The deformation responses crook and rotation are further described in Danvind (1999). Index “rad”, “tan”, “lon” and “vol” are abbreviations for radial, tangential, longitudinal and volume. Distance from pith is the same as the sample number, i.e. the third sample on the east or the west side of the pith had “Distance to the pith”

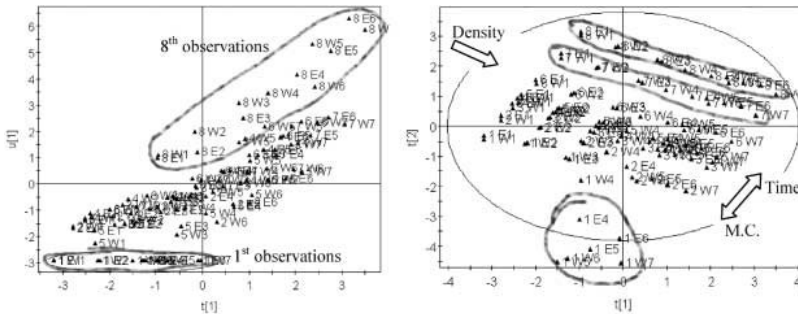


Fig. 3. *Left:* Patterns found in the t_1/u_1 score plot of the first PLS model (with all variables and observations). Observations from first and eighth measuring occasions (observation name starting with “1” and “8”) deviated. *Right:* Groups of observations in the t_1/t_2 score plot, also from the first PLS model. These groups were probably related to the variables “Time” and “MC”, since they were found to be important in both the first and second PC direction (see Fig. 4), and therefore also for the corresponding score vectors t_1 and t_2 . The separation of samples within groups was correlated to density-related factors, with lower density on the upper left side of each group. Compare with the position of density-related factors in the loading plot, (Fig. 4)

Bild 3. *Links:* Muster im t_1/u_1 -Graph des ersten PLS-Modells (mit allen Variablen und Beobachtungen). Beobachtungen (1–8) abgeleitet von der ersten und achten Messung. Rechts: Beobachtungsgruppen im t_1/t_2 -Graph, ebenfalls vom ersten Modell. Diese Gruppen sind wahrscheinlich mit den Variablen “Time” und “MC” und mit den Vektoren t_1 und t_2 korreliert, denn sie erwiesen sich als wichtige Faktoren in der ersten und zweiten PC-Richtung (Bild 4). Die Trennung der Proben in Gruppen korrelierte mit Dichte-bezogenen Faktoren (geringe Dichten auf der oberen linken Seite jeder Gruppe). Siehe auch die Position der Dichte-bezogenen Faktoren in Bild 4

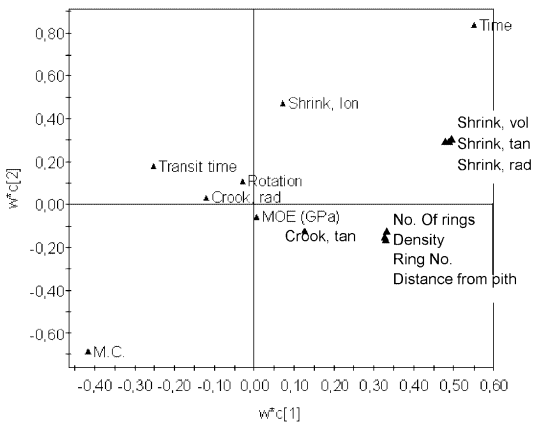


Fig. 4. Loading plot for first PLS model with all variables kept, displaying combined weights, w^*c , for the first two dimensions (Anon. 1998). Two groups were found, one with density related factors and another with volume-, tangential- and radial shrinkage. Crook and rotation responses were poorly explained (close to the origin of coordinates) and “MOE” was a weak factor. “Time” and moisture content, “MC”, were strongly negatively correlated (positioned opposite in the plot), i.e. when a short time had elapsed, the moisture content was high

Bild 4. Schema des ersten PLS-Modells mit allen Variablen und ihren kombinierten Gewichtungen, w^*c , für die ersten beiden Dimensionen (Anon. 1998). Zwei Gruppen lassen sich unterscheiden: eine Gruppe von Variablen mit Bezug zur Dichte, die andere zum Schwinden (Volumen, tangential und radial). Längskrümmung und Verdrehung sind schwach erklärt (nahe an den Ursprungskordinaten) und “MOE” war ein schwacher Faktor. “Time” und “MC” waren stark negativ korreliert (an gegenüberliegenden Plätzen des Graphs)

equal to three. “Time” is the time elapsed since the samples began drying, starting from the first measuring occasion. “Ring No.” denotes the annual ring in the middle of that specimen, starting from the pith. “No. of rings” is the number of annual rings within the sample. “Transit time” is the duration for sending a sound wave through the length of a green specimen. “MOE” is the Modulus of Elasticity in the longitudinal direction.

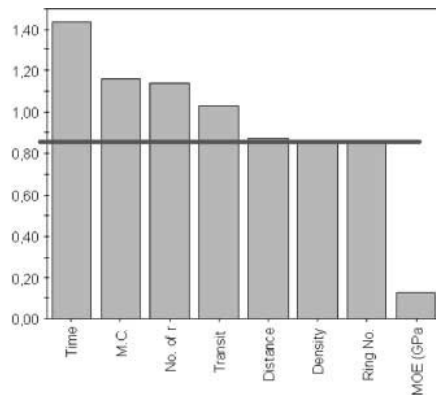


Fig. 5. Variable Importance Plot (VIP) shows the importance of factors on the prediction model. Here the VIP for the first model with all variables is shown. “MOE” was found to be a weak factor **Bild 5.** Der VIP zeigt die Bedeutung der einzelnen Variablen für die Vorhersage des Modells. Hier gezeigt ist der VIP des ersten Modells. “MOE” stellte sich als schwache Variable heraus

3.2 Excluding observations

Outliers in the DMODX plot for the first model showed high moisture content (see Fig. 7). The higher the moisture content, the higher the risk to have moisture gradients in the square samples due to quick drying of the surface. The surface might have had a much lower moisture content than the inside, and since shrinkage is known to appear mostly below fiber saturation point, the surface might have started to shrink at very high inner moisture levels. Therefore, observations with measured moisture content higher than 32% were excluded from the data set, which improved the model.

Observations from the fifth measuring occasion were grouped in the score plot for t_1/u_1 (see Fig. 8). It was also known from the collection of data that almost all of these measurements differed unexpectedly from the other readings (see Fig. 8). Possible reasons could be extreme moisture content in the samples, measuring error or perhaps some changes in external conditions, such as a failure of the air conditioning system leading to more humid air and thereby swelling of the samples. It could also have been the appearance of cracks that affected the behavior, since it was known that small cracks were developed during the drying cycle, but it was not known when they were developed. More information on the collected data is found in Danvind (1999). Consequently, observations from the fifth measuring occasion were excluded from the data set and a new model was created.

If “Time” as a variable was included in the model, then the exclusion of the fifth measurements did not improve the model. But when modeling without “Time”, which was desired (refer to next section), the model was clearly improved. This also showed that there might have been some time-dependent variables of the wood that were not

measured in this study. The influence of moisture gradients could be such a variable.

3.3 Excluding variables

“Time” was not considered to be a desired variable when modeling shrinkage in this investigation. Therefore, this variable was excluded, although it had a high VIP-value. The importance of “Time” showed that there were time-dependent characteristics of the wood not included in this study, as mentioned in the previous section.

“MOE” was excluded due to its low VIP-value. “Ring No.” was also excluded, although its VIP-value was almost equal to those for “Density” and “Distance from pith”. Since “Ring No.” and “Distance to pith” measure almost the same characteristic, “Ring No.” was excluded, and it was apparent that excluding it did not influence the model.

3.4 Modeling of deformation

It was found that no model for deformation could be made. SIMCA could not find any Principal Component for a data set with only deformation responses using PLS regression.

3.5 Modeling of shrinkage

After variables and observations, stated in Section 3.3, had been excluded, the remaining data set had 77 observations. In addition, deformation responses were also excluded in the shrinkage models. The distribution of moisture content in these observations was not uniform, as seen in Fig. 9.

Three groups were found in the score plots, and these proved to match the groups in the moisture content dis-

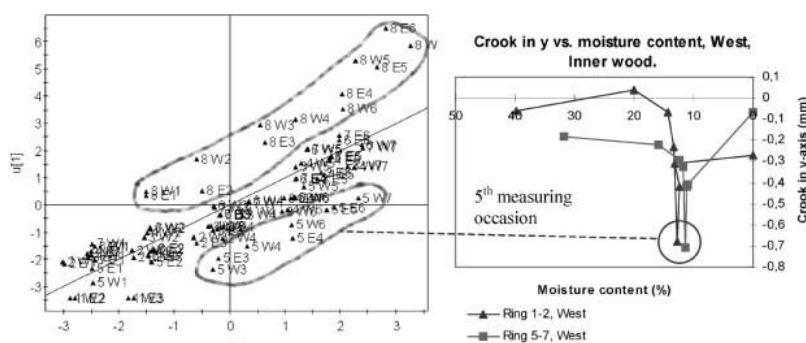


Fig. 8. Score plot and sample data, model with “Time”, “Ring.No.”, “MOE” and observations above 32% moisture content excluded. The t_1/u_1 plot showed groups of observations from measuring occasions five and eight (observation names starting with “5” and “8”). The “Crook in y” plot from the experimental data collection showed the crook measurements of two samples during drying, where the fifth clearly deviated. Similar behavior was found for shrinkage responses. Observations from the fifth measuring occasion were therefore excluded from further modeling

Bild 8. Bewertungs-Graph und Probandaten. Modell unter Ausschluß der Variablen “Time”, “Ring.No.”, “MOE” und Beobachtungen oberhalb 32% Feuchte. Der t_1/u_1 -Graph zeigt Beobachtungsgruppen der Messungen fünf und acht (Bezeichnungen “5” und “8”). Der Graph “Krümmung in y” aus den gesammelten Daten zeigt Krümmungsmessungen an zwei Proben während des Trocknens, wobei die fünfte Messung stark abweicht. Ähnliches ergab sich für das Schwinden. Die Beobachtungen der fünften Messung wurden deshalb ausgeschlossen

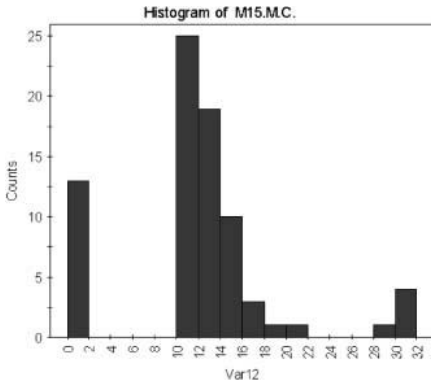


Fig. 9. Moisture content distribution of 77 observations. Observations above 32% moisture content and observations from the fifth measuring occasion are excluded. The histogram shows three separate groups, where most of the observed moisture contents in samples are between 10% and 22%.

Bild 9. Feuchteverteilung von 77 Beobachtungen. Beobachtungen oberhalb 32% Feuchte und der fünften Messung wurden weggelassen. Das Histogramm zeigt drei getrennte Gruppen mit starker Häufung der Feuchtwerte zwischen 10 und 22%

tribution histogram. To check whether the model explained the difference between the groups or if it was valid also within the main group, between 10% and 22% moisture content, two new models were made.

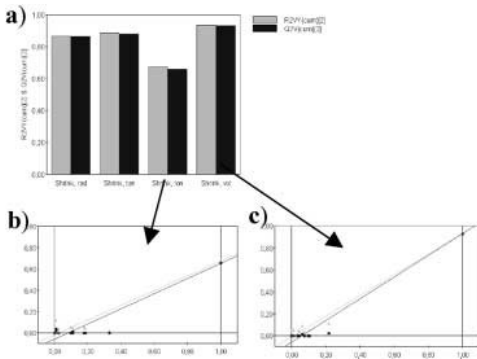


Fig. 10a, b, c. PLS prediction model for 0–22% moisture content. *Left:* R^2 and Q^2 for each shrinkage response (a) and validation plots for longitudinal (b) and volume shrinkage (c). R^2 and Q^2 had good values and the validation plots proved that the prediction models were valid. *Right:* The loading plot showed that longitudinal shrinkage was almost independent of density related factors (perpendicular in plot). “Shrink, lon” was explained almost only by the second PC, which was influenced mostly by “Transit time” and “MC”. Density related factors, on the other hand, were strongly correlated to the first PC and thereby also to tangential, radial and volumetric shrinkage

3.5.1

Shrinkage model, interval 0% to 22% MC

This model was based on 72 observations and 2 Principal Components. Q^2 and R^2 showed good values for modeling the shrinkage responses and validation plots proved the model to be reliable (Fig. 10).

The loading plot indicated that the variables “Density”, “No. Of rings” and “Distance from pith” vaguely influenced longitudinal shrinkage, since they were almost orthogonal along the axis of the loading plot (Fig. 10).

The explained variance and the predicted variance were $R^2 = 0.67$ and $Q^2 = 0.65$ for longitudinal shrinkage and Q^2 and R^2 both approximately 0.9 for the other shrinkage responses (refer to Table 1). The model between 0% and 22% moisture content for predicting shrinkage values had, therefore, good predictive power and was valid (refer to Fig. 10). The regression coefficients for this model are presented in Table 1.

3.5.2

Shrinkage model, interval 10% to 22% MC

This model was based on 59 observations and 2 Principal Components. Longitudinal shrinkage has much lower Q^2 and R^2 than the model from 0% to 22%, but the other shrinkage responses are still well modeled. This proves that the model for longitudinal shrinkage explains the variation between the two moisture content groups better than the variation within the region from 10% to 22% moisture content. This could mean that the amount of change in longitudinal shrinkage within this group is small in relation to the measuring error.

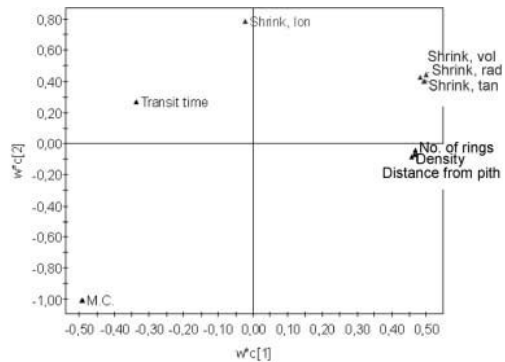


Bild 10a, b, c. PLS-Vorhersagemodell für Holzfeuchten zwischen 0 und 22%. *Links:* R_2 und Q_2 für jedes gemessene Schwinden (a) sowie Validierung für longitudinales (b) und Volumen-schwinden (c). R_2 und Q_2 wiesen gute Werte auf und die Validierung erwies das Vorhersagemodell als gültig. *Rechts:* Der Bewertungs-Graph zeigt, daß longitudinales Schwinden fast unabhängig von den Dichte-bezogenen Faktoren ist (senkrecht im Graph). “Shrink, lon” war fast ausschließlich durch die zweiten PC (Principle Components) erklärt, d.h. überwiegend beeinflusst durch “Transit time” und “MC”. Dichte-bezogene Faktoren waren andererseits stark korreliert mit den ersten PC, d.h. mit tangentialem, radialen und Volumen-Schwinden

4 Discussion

Patterns were found in the DMODX plots, where each sample formed groups of its DMODX-values (Fig. 11). This indicates that there was some unmeasured factor that influenced the specimens. No strong patterns were found in the N-probability plot over the Y-residuals, which showed that the residuals were nearly normally distributed.

Expanded variables were also tested, but that did not improve the model and therefore they are not presented here.

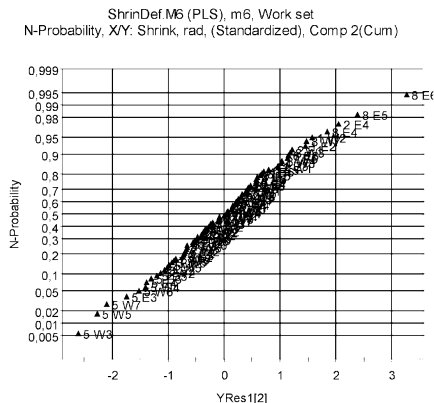
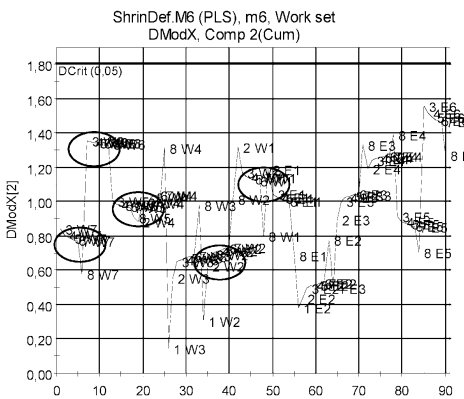
Longitudinal shrinkage was also modeled separately from the other shrinkage responses, but no significant improvement of the model was achieved.

It was interesting to find that longitudinal shrinkage was almost independent of the density of studied samples. Considering this, the measuring accuracy of longitudinal shrinkage could be questioned. However, the measuring method using the StickMaster DD was found to be accurate for the sample sizes used (Danvind 1999). Therefore it was probably the samples' true responses that were measured.

Table 1. R², Q² and coefficients for shrinkage prediction model between 0% and 22% moisture content. The response is a linear combination of the coefficients. For example: Shrink, rad = 1.6865 - 0.00874703*(Transit time) + 0.0037914*(Density) - 0.142256*(M.C) + 0.112405*(Distance from pith) + 0.217513*(No. of rings)

Tabelle 1. R², Q² und Koeffizienten des Modells zur Vorhersage des Schwindens zwischen 0% und 22% Feuchte. Das Modell erfordert eine lineare Kombination der Koeffizienten, z.B.: Shrink, rad = 1.6865 - 0.00874703*(Transit time) + 0.0037914*(Density) - 0.142256*(M.C) + 0.112405*(Distance from pith) + 0.217513*(No. of rings)

Y	R ²	Q ²		
Shrink, rad	0.867	0.856		
Shrink, tan	0.878	0.868		
Shrink, lon	0.674	0.649		
Shrink, vol	0.931	0.926		
Coefficient	Shrink, rad(%)	Shrink, tan(%)	Shrink, lon(%)	Shrink, vol(%)
Constant	1.6865	2.70692	0.208958	4.52734
Transit time (ms)	-0.00874703	-0.0142319	0.00238886	-0.0202903
Density (kg/m ³)	0.0037914	0.00583206	-0.000157909	0.00919087
MC (%)	-0.142256	-0.210658	-0.0153544	-0.354452
Distance from pith	0.112405	0.172795	-0.0043954	0.272613
No. of rings	0.217513	0.331857	-0.0019475	0.53049



Dcrit [2] = 1,8061, Normalized distances, Non weighted residuals
 Simca-P7.01 by Umetri AB 1998-12-09 00:03

Simca-P7.01 by Umetri AB 1998-12-09 00:03

Fig. 11. DMODX and N-probability over Y-residuals from prediction model where observations above 32% moisture content had been excluded. Groups of observations were found where each group consisted of observations from one sample. These groups show that there was something characterising each individual sample that was not measured. The right plot shows nearly normal distribution of residuals

Bild 11. DMODX und N-Wahrscheinlichkeit in Abhängigkeit von den Restabweichungen der Vorhersagen, wobei alle Beobachtungen über 32% Feuchte ausgeschlossen waren. Beobachtungsgruppen wurden gefunden, die nur aus Beobachtungen an einer Probe bestanden. Diese Gruppen zeigen, daß jede einzelne Gruppe etwas Charakteristisches aufweist, das nicht gemessen wurde. Der rechte Graph zeigt eine annähernd Normalverteilung der Restabweichungen

No results of the PCA analysis are presented here, because these results did not add any more information important for modeling than the PLS data description and classification.

It would have been interesting to do a similar study of samples with proven equilibrium moisture distribution throughout the samples on each measuring occasion. To more easily achieve equilibrium moisture distribution, the dimensions of the samples should have been chosen differently, but then the measuring methods also have to be changed.

The measuring accuracy of MOE was not satisfactory (Danvind 1999), and therefore it was not unexpected that this variable had a low influence on the model. This was also one reason why MOE was set as a factor, and not as a response. Of course, MOE could have been set as a response instead, but most probably no prediction model would have been achieved for MOE.

Perhaps it was wrong to exclude the 5th measurements, if the measured responses were the wood samples' true behaviour. This is a particular example where unexpected behavior appeared during experiments, and it would be interesting to perform a similar study in order to verify this behavior and study the factors causing it. Such a survey could possibly be a contribution to further fundamental understanding of wood characteristics.

External test sets for validation were not used in this study. This complementary test method would have been very useful for further validation of obtained models.

The material selection in this study was too poor for stating any general conclusions on shrinkage and deformation behaviour of *Pinus radiata*. However, the study was mainly a method study presenting an example of PLS prediction modeling of wood properties.

To achieve the greatest possible amount of information from a study, it is of importance to have good experiment planning. There are several methods and tools for experiment planning that can be used in order to control variables within appropriate levels and choose a sufficient number of observations at each level. However, these methods will not be presented here, and also, this work is not a good example of experiment planning.

5

Conclusions

This study showed that using SIMCA-P 7.01 by Umetrics AB for PLS prediction modeling of shrinkage and deformation in studied wood samples was an effective and easy-to-use tool for untangling relationships between variables and generating information from data. The method proved to yield a good understanding of where information and noise were found in the data set, for example, understanding of the importance of variables, patterns in variables, patterns in residuals, patterns in observations, validity of models and prediction ability of models.

Radial, tangential and volume shrinkage were highly related to moisture content and density-related variables in the studied wood. Longitudinal shrinkage had low correlation with density related variables. No model with good prediction ability of deformation was found.

References

- Andersson C (1997) PLS-modeller för sortering av friskkvisttimmer. (In Swedish.) Master Thesis. Luleå University of Technology
- Anon. (1998) User's guide to SIMCA-P Version 7.0. Umetrics AB, Umeå
- Danvind J (1999) Systems to dynamically measure shape changes in wooden sample sticks to determine shrinkage, twist, crook, bow, MOE and Poisson's ratio. Master Thesis. Luleå University of Technology
- Eriksson L, Johansson E, Wold S (1996). QSAR Model Validation. Proceedings of the 7th International Workshop on QSARs in Environmental Science, Elsinore, Denmark, June 24–28
- Esbensen K, Huang J (1999) Principles of Proper Validation (PPV). Poster. 6th Scandinavian Symposium on Chemometrics, August 15–19 1999, Porsgrunn, Norway
- Geladi P, Kowalski BR (1986) Partial Least-Squares Regression: A Tutorial. *Analytica Chimica Acta* 185: 1–17
- Lindgren F (1994) Third generation PLS. Some Elements and Applications. Thesis. Umeå University
- Marklund A, Hauksson JB, Edlund U, Sjöström M (1998) Prediction of strength parameters for softwood kraft pulps. *Nordic Pulp and Paper Res J* 13: 211–219
- Nyström J, Hagman O (1999) Real-time spectral classification of compression wood in *Picea abies*. *J Wood Sci* 45: 30–37
- Wold S, Esbensen K, Geladi P (1987) Principal Component Analysis. *Chemometrics and Intelligent Laboratory Systems* 2(1987): 37–52
- Wold S, Nordvedt R (1996) Anvendelsen av kjemometri innom forskning og industri. John Grieg AS, Bergen, Norway, pp. 33–51

